

Metal Leaching and Performance of Supported Copper and Palladium Catalysts during Liquid-Phase Hydrogenation and CC-Coupling Reactions

Andrea Abram

Vollständiger Abdruck der von der TUM School of Natural Sciences der Technischen Universität München zur Erlangung einer

Doktorin der Naturwissenschaften (Dr. rer. nat.)

genehmigten Dissertation.

Vorsitz: Prof. Dr. Lukas Hintermann

Prüfer*innen der Dissertation:

1. Prof. Dr. Klaus Köhler
2. Prof. Dr. Ulrich K. Heiz

Die Dissertation wurde am 19.07.2023 bei der Technischen Universität München eingereicht und durch die TUM School of Natural Sciences am 08.08.2023 angenommen.

Die vorliegende Arbeit entstand im Zeitraum vom November 2017 bis Juli 2023 an der Fakultät für Chemie und am Zentralinstitut für Katalysatorforschung (CRC) der Technischen Universität München.

Mein besonderer Dank gilt meinem akademischen Lehrer

Prof. Dr. Klaus Köhler

für die freundliche Aufnahme in seinem Arbeitskreis,
seine uneingeschränkte Unterstützung,
sein Vertrauen und die damit verbundenen Freiräume in der
Gestaltung und Bearbeitung der Aufgabenstellung
sowie sein großes Interesse am Gelingen der Arbeit.

ACKNOWLEDGEMENT

First and foremost, I wish to thank **Prof. Dr. Klaus Köhler** for giving me the opportunity to work in his research group. As a lateral entrant from the field of geological sciences I am deeply grateful for his trust and the opportunity to continue my academic studies in the field of chemistry. Without his support, near-endless patience, and understanding I would not have been able to accomplish the work presented here.

I would especially like to thank my former and present colleagues for welcoming me into the research group and for the help, advice, and fun we had. Namely, they are: **Dr. Hannah Augenstein, Franz Bannert, Dr. Florian Boch, Dr. Patrick Bretzler, Dr. Tobias Bruhm, Dr. Christoph Dörfelt, Dr. Christoph Gnad, Dr. Carmen Haeßner, Jasper Lingdi Kong, Lea Kopietz, Dr. Max Hiller, Patrick Schlachta, Jinjin Tie, Dr. Oliver Thomys, and Dr. Xiaoqiao Zhang.**

Special thanks to **Dr. Hannah Augenstein** for all her help and advice, especially in my first months in the lab. Thank you for answering and explaining even the most basic questions coming from an (ex)-geologist without batting an eye. Also, your help with any kind of computer problem was highly appreciated. **Dr. Christoph Gnad** is thanked for the synthesis of the grafted catalysts and the good collaboration. **Dr. Patrick Bretzler** for guiding me how to use the autoclave set-up and the related analytical steps. **Dr. Max Hiller** for his help with TPR and chemisorption measurements. **Dr. Tobias Bruhm** for his introductions to sample work-up and all the nice discussions from science to football and biathlon. **Lea Kopietz** for all the hours spent tirelessly fixing the glove box and pumps and sharing quantities of coffee during discussions about science, life and everything else. And, of course, **Dr. Florian Boch** and **Dr. Oliver Thomys** for all their knowledge and a treasure trove of stories over many, many years. Last, but not least, I thank the masters of the group finances **Dr. Hannah Augenstein, Dr. Patrick Bretzler** and **Dr. Max Hiller** for the reliable supply of coffee and milk, without which functionality of certain students would be severely diminished.

I thank **Dr. Christoph Dörfelt** for his work on Cu-Al spinels and the good collaboration in our short time together in the group. Clariant and MuniCat are also acknowledged. **Prof. Dr. Notker Rösch, Dr. Alexander Genest, Assoc. Prof. Chun-Ran Chang** and **Prof. Dr. Jun Li** are thanked for the DFT calculations. **Max Koch** and **Prof. Tom Nilges** are thanked for the opportunity to measure ICP-OES samples on their instrument.

The students who worked with me in the lab also deserve my gratitude. They are **Andreas Hochholzer** and **Matthias Jacob**. It was a pleasure to work together with both of you.

Prof. Dr. Thomas Baumann, Prof. Dr. Christoph Haisch and **Dr. David Bauer** have my gratitude for giving me the opportunity to learn and familiarize myself with the process of measuring Raman using their instruments in Großhadern in the first weeks of my PhD. I also thank David for sharing his initial MatLab code for automated plotting with me, which has been a great help and starting point for developing my own codes. **Dr. Anna Vogel** is thanked for her

*initial introduction to the InVia Raman system, which helped a great deal in familiarizing myself with the set-up. My gratitude goes also to both Renishaw contacts **Dr. Patrick Kubryk** and **Hans Kienzler** for their quick and competent help with any arising problem. **PD Dr. Natalia Ivleva** is thanked for her insights and help with Raman questions.*

*In addition, special thanks goes to the group members of lab 2019 of **Prof. Dr. Ulrich Heiz** group, especially **Clara Aletsee**, for their cooperation and acceptance of the many Raman users in their lab. Especially in difficult Covid times your understanding and willingness for cooperation was highly appreciated.*

*I'd like to thank all the people from the central analytics laboratory of the CRC, especially **Dr. Eliza Gemel** for maintenance of the analytical devices and her help with the Booking System.*

*In addition, I would like to thank **Dr. Gabriele Raudaschl-Sieber**, **Rodica Dumitrescu** and **Richard Wetzel** for organizing and managing the lab course for geology students. It was a pleasure to work with you in those lab courses every year.*

*Most importantly, I need to thank **my family**. It would not have been possible to finish this work without my parents. They supported me at any time and probably gained a few additional gray hairs on my account in the process. A special thanks goes to my aunt for offering me a place to stay which turned into many years living together here in Munich. I also want to thank my sister for all the time we spent together, be it in the stable, inside an ice rink or in front of one of countless sport broadcasts.*

ABSTRACT

Leaching of catalyst species is an important cause for the deactivation of solid catalysts, especially in liquid phase reactions. The dissolution of metals was investigated for the copper aluminate spinel catalyzed hydrogenation of aldehydes and carbon-carbon couplings by supported palladium catalysts. For a better understanding of the complex leaching processes at solid-liquid interfaces, the content of dissolved metal species was determined during the reactions as function of the reaction time and temperature, dependent on the nature of the solid catalyst, solvent, substrates and additives. Copper aluminate spinel leaching is influenced by most of the named parameters, especially carboxylic acid additives increase leaching considerably. Without available carboxylate ligands copper leaching is low overall due to strongly reducing conditions. Aluminum leaching is more relevant due to stability concerns. Ethanol addition suppresses most of the metal leaching but has some influence on catalyst selectivity (acetal formation). In *Heck* reactions palladium leaching is a prerequisite for catalytic activity. Depending on the substrate and the pre-catalyst, differing leaching mechanisms have been revealed for supported palladium oxide catalysts and for isolated palladium surface complexes. Relevant parameters for the leaching of palladium atoms from small Pd clusters during *Heck* reactions of bromobenzene and styrene have been explored computationally and experimentally. Pd dissolution and re-deposition experiments agree well with DFT calculations.

KURZZUSAMMENFASSUNG

Ein wichtiger Aspekt der Desaktivierung von Festkörperkatalysatoren ist der Verlust an aktiver Spezies durch Leaching, besonders in Flüssigphasenreaktionen. Das Herauslösen von Metallspezies aus Festkörperkatalysatoren wurde für die Hydrierung von Aldehyden mittels eines Kupferaluminat-Spinells sowie die *Heck*-Reaktion an einem geträgerten Palladiumkatalysator untersucht. Um die komplexen Leachingprozesse nachzuvollziehen wurde die gelöste Metallspezieskonzentration als Funktion gegen die Reaktionszeit und Temperatur und in Abhängigkeit von Katalysortyp, Lösemittel, Substrat und Additiven betrachtet. Leaching aus dem Kupferaluminat-spinell wird durch die meisten der genannten Parameter beeinflusst, insbesondere durch die Beimischung von Carbonsäuren, welche das Leaching verstärken. Ohne Carbonsäuren bleibt das Kupferleaching durch die stark reduzierenden Bedingungen niedrig. Aluminiumleaching erfolgt konstant und ist im Bezug auf die Katalysatorstabilität relevant. Beimischung von Ethanol kann das Metallleaching verringern, aber beeinflusst zum Teil die Selektivität (Acetalbildung). In *Heck*-Reaktionen ist Palladiumleaching eine Voraussetzung für die Katalysatoraktivität. Abhängig von Substrat und Präkatalysatorspezies konnten unterschiedliche Leachingmechanismen für geträgerte PdO-Katalysatoren und für Katalysatoren mit isolierten Pd-Oberflächenkomplexen vorgeschlagen werden. Die relevanten Parameter zum Lösen von Palladium aus kleinen Pd-Clustern während der *Heck*-Reaktion von Brombenzol und Styrol wurden experimentell und anhand von DFT-Berechnungen betrachtet. Die Ergebnisse stimmten gut überein.

LIST OF ABBREVIATIONS

2 θ	Bragg angle
a.u.	Arbitrary unit
BET	Brunauer-Emmett-Teller
cm ⁻¹	wavenumber (Raman shift)
CuO-spinel	Adkins analogue spinel CuO · CuAl ₂ O ₄
DMF	<i>N,N</i> -Dimethylformamide
G _r	Gibbs free (reaction) energy
GC	Gas chromatography
H ₂ -TPD	H ₂ -Temperature programmed desorption
H ₂ -TPR	H ₂ -Temperature programmed reduction
ICP-OES	Inductively coupled plasma – optical emission spectrometry
ICP-MS	Inductively coupled plasma – mass spectrometry
IR	Infrared
mol-%	molar percentage
NMP	<i>N</i> -methyl-2-pyrrolidone
NMR	Nuclear magnetic resonance
ORR/OER	Oxygen reduction/evolution reaction
P-Sp	phase-pure spinel CuAl ₂ O ₄
RPM	rounds per minute
S-Sp	stoichiometric spinel (CuO) · CuAl ₂ O ₄
SVHC	'substances with very high concern'
TBAB	tetra- <i>n</i> -butylammonium bromide
TGA	Thermogravimetric analysis
tmeda	<i>N,N,N',N'</i> -tetramethyl ethylenediamine
TPR	Temperature programmed reduction
wt.-%	Weight percentage
(p-)XRD	(powder) X-Ray diffraction

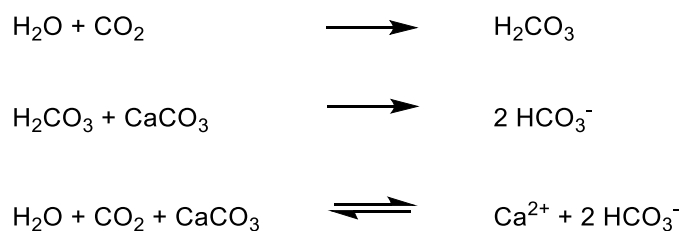
TABLE OF CONTENTS

1 Introduction and Objectives	1
2 Leaching in Cu-Al spinel catalyzed liquid phase hydrogenation	5
2.1 <i>Introduction</i>	6
2.2 <i>Theoretical background</i>	8
2.2.1 CuAl ₂ O ₄ spinel – Synthesis and Application	8
2.2.2 Hydrogenation reactions	10
2.3 <i>Motivation</i>	12
2.4 <i>Results and Discussion</i>	13
2.4.1 Leaching and catalytic performance in the hydrogenation reaction	14
2.4.2 Leaching behavior depending on the copper/aluminum ratio of Cu-Al spinels	19
2.4.3 Variation of carboxylic acids as additive in Cu-Al spinel standard leaching experiments ...	23
2.4.4 Variation of the solvent.....	28
2.4.5 Solvent mixtures.....	38
2.4.6 Long term experiments – stability investigation	48
2.4.7 Synthesis and characterization of the catalysts.....	56
2.5 <i>Conclusion</i>	72
3 Leaching of palladium atoms from small cluster models during Heck reactions	77
3.1 <i>Introduction and Motivation</i>	78
3.2 <i>Theoretical background</i>	79
3.3 <i>Results and discussion</i>	81
3.3.1 Synthesis and characterization of the catalysts.....	81
3.3.2 Targeted variation of parameters concerning Pd leaching during <i>Heck</i> reactions.....	81
3.3.3 Leaching of supported Pd-complexes in <i>Heck</i> Reactions of Aryl Bromides and Chlorides	86
3.4 <i>Conclusion</i>	88
4 Summary	90
5 Zusammenfassung	93
6 Experimental	96
6.1 <i>Experimental to chapter 2 – Leaching in Cu-Al spinel catalyzed liquid phase hydrogenation</i>	97
6.2 <i>Experimental to chapter 3 – Leaching of palladium atoms from small cluster models during Heck reactions</i>	103
Literature	106
7 Appendix	116
7.1 <i>Additional data</i>	117
7.2 <i>List of Publications</i>	120
7.3 <i>Conference contributions</i>	121

**Introduction and
Objectives**

The term “Leaching” describes the removal of a soluble species from its surrounding by way of a solvents. This very general description of the process gives a first idea of its omnipresence in our lives, with or without realizing it. Leaching is of substantial relevance in nature as well as in industry.

Leaching is a naturally occurring process which can be found in very different scales and time-frames. Slow dissolution and reprecipitation of carbonate species are the basis of the formation of carbonaceous mountain regions built from mostly limestone, dolomite or gypsum.^[1, 2] A prominent example is the “Karst” region in middle Europe, stretching from the Alps along the Mediterranean. It is characterized by its many dissolution features like sinkholes and caves with impressive stalagmites and stalactites, which are built from the precipitates of the previously leached species. In this case rain water functions as the solvent, which reacts with CO₂ present in the surrounding air and soil to a weak carbonic acid which in turn dissolves the carbonaceous rock (Equation 1).



Equation 1: Dissolution of carbonate material

Another prominent but less desirable leaching occurrence is the leaching of nutrients from soil in agriculture.^[3] This loss of nutrients due to leaching leads to a less productive harvest and can in turn affect the surrounding water bodies and groundwater quality. Once again, like in most natural leaching processes, water is acting as the solvent and transports the leached species along its path. In case of over-fertilization or leached pesticides^[4], a large quantity of leached species can lead to diminished ground water quality and negatively affect surrounding rivers and lakes (algal bloom, fish die-off).

Focusing on topics more relevant to chemical industry, leaching is an important process to remove and enrich valuable metals from mined ores.^[5, 6] The same is true in waste recycling, where valuable metal components are leached to reuse them and reduce the amount of waste product.^[7] This is especially important in the case of rare and noble metals with a limited number of available natural deposits and high production costs.^[8, 9] Copper is also a good material to recover through leaching processes. Especially copper oxides have a low leaching tolerance

in regards to acidic leaching. Due to the leaching potential of many metals present in industrial and mining waste, special care must be taken when storing them or placing them in landfills (tailings, sludge).^[10] When not isolated properly, there is an increased risk of contaminating the surrounding area and especially nearby groundwater sources.^[11-13] Research projects have investigated potential phase transformations to a more leaching-resistant product before storage as well as improved leaching protocols^[14] to regain more of the incorporated metal resources for later use and enable a further use for the remaining material (cement production, soil stabilization, ...).^[15-17]

In large scale chemical conversions, the leaching phenomenon also cannot be ignored, especially for heterogeneously catalyzed liquid-phase reactions.^[18] Catalyzed liquid-phase reactions are especially important for chemical reactions with low thermal stability which are difficult to handle in the gas phase. One example is the catalytic conversion of biomass.^[19] The presence of a liquid phase is inherently a factor favoring leaching from solid catalyst components into solution. A result of increased catalyst leaching can be the deactivation of the catalyst due to a loss of active species. Especially in continuous flow reactors the leached species cannot be recovered due to the continuous transport of the liquid phase along the catalyst bed.^[20] This results in a deactivated catalyst and impurities within the product stream. Depending on the type and amount of leached species, the product stream must be further processed to remove the unwanted components to not hinder or affect its further use (impurities or poisoning of the product stream). Apart from deactivation, the stability of the catalyst itself can also be affected by increased leaching. Industrial processes often use shaped catalysts for an easier separation of catalyst and product. If the shaped catalysts lose their integrity this easy separation is no longer possible and the catalyst bed must be renewed in addition to possible feed impurities due to catalyst residue.

In some cases, leaching can be a crucial step of the catalytic cycle itself instead of an unwanted side-effect. One such example is C-C coupling using supported palladium catalysts, e.g. *Heck* coupling. Especially in the case of the *Heck* reaction^[21], the matter of how the reaction is catalyzed starting from solids drew much attention.^[22-24] In principle, the two discussed possibilities were that either the reaction is catalyzed by a “truly heterogeneous” surface mechanism or that dissolved palladium, which is generated by metal leaching, catalyzes the reaction following the homogeneous reaction mechanism. The general conclusion is that though the possibility of a surface mechanism cannot be excluded completely, the homogeneous pathway is evident for several systems such as palladium nanoparticles as well as supported palladium oxide catalysts and that the active species are at least temporary coordinately unsaturated dissolved Pd(0) species.^[25, 26]

In the following chapters both the deactivation of a catalyst by metal leaching (chapter 2) as well as the incorporation of the metal leaching into the catalytic cycle (chapter 3) will be explored and its underlying parameters and principles investigated in detail for the chosen reaction system.

**Leaching in Cu-Al spinel
catalyzed liquid phase
hydrogenation**

2.1 Introduction

The process of leaching can be found in a large variety of processes, reaching from the large-scale process in nature to the microscale leaching in chemical reactions. The term 'leaching' itself describes broadly speaking the process of a soluble species being removed from its original substance by way of a solvent. The substance transfers from its original solid phase to the liquid phase of the solvent. This process can be intentionally used to separate and remove unwanted elements from a product phase or to get valuable subspecies during waste treatment (enrichment of valuable metals, metal leachates) to be used in further production processes. Especially in the case of noble metals or rare earth metals where the resources are limited this is an important factor. The leaching of species can also be a negative effect e.g. in the case of unwanted leaching during production processes. Material corrosion can lead to unwanted impurities in the product feed or negatively impair the ongoing reaction if the leached species affect the ongoing reaction. This is mainly a problem in liquid phase reactions due to its constant presence of a liquid phase, in contrast to gas phase reactions where leaching is less of a problem. In particular, when catalysts are used in the production process those catalysts are of course also affected by leaching in liquid phase reactions. Depending on the catalyst and reaction the leaching process itself can be part of the catalytic cycle and the leached species formed is the catalytically active phase. In these cases, it is important that the catalytic cycle is complete and the leached phase redeposited at the end so that no catalytically active phase is lost during the process (see Chapter 3). The leaching of catalyst species into the liquid reaction phase can also negatively impact the process if it is unwanted. The loss of catalytically active phase leads to the deactivation of the catalyst and the catalyst needs to be exchanged for a new batch. In this case the catalyst cannot be reactivated because the catalytically active sites are not (reversibly) blocked but the active species itself has been lost. Depending on the leached amount and the leached species this can also impair the purity of the product or negatively impair further production steps. If the leaching process proceeds over a longer amount of time the catalyst structure itself can become unstable due to the missing leached component(s)

Reaction parameters that can influence leaching of active components during catalytic reactions can be manifold and are in fact very rarely reported in detail in the literature. This does not only concern the intrinsic parameters like the nature of the reaction itself (reduction, oxidation, acid-base etc.), temperature, pressure, concentrations and solvent. Also, additives, ligands and impurities even at low concentrations may influence the phenomenon substantially. This chapter focusses on the investigation of leaching phenomena in a metal (copper) catalysed hydrogenation reaction (butyraldehyde to butanol), where - to first approximation - leach-

ing is not expected due to the strongly reducing conditions (elevated hydrogen pressure, increased temperature keeping the metal in reduced, insoluble state). In a former study however leaching of active components and of the support was surprisingly observed.^[27] The influence of reaction parameters and components – the subjects of the present study - were however not yet investigated and the consequences of leaching for catalytic cycle, activity and catalyst stability remained untouched.

2.2 Theoretical background

In this chapter, hydrogenation reactions using copper-based catalysts are shortly summarized. In addition, a closer look is taken on the use of spinels as catalysts and their synthesis.

2.2.1 CuAl_2O_4 spinel – Synthesis and Application

Spinel-type compounds are available in a wide variety of chemical composition. The spinel species found in nature are classified as a mineral, in contrast to synthetically produced spinel-types, and classified according to the nomenclature of the International Mineralogical Association (IMA). Bosi et al. report on the new classification scheme of the spinel-supergroup.^[28] The spinel-type structure (Figure 1) is identified by a cation-to-anion ratio of 3:4 and typically crystallizes in the general formula AB_2X_4 (A and B representing cations and X anions). The distribution of the cations leads to so-called “normal spinel”, where the divalent cations are situated in the tetrahedral and the trivalent cations in the octahedral position, or “inverse” spinel where the tetrahedral position is occupied by a trivalent cation and the octahedral positions by both divalent and trivalent cations. This distribution leads to a flexible degree of inversion depending on the number of cations found in which lattice position, with normal and inverse spinel being the endmembers. Most spinel minerals belong to the oxyspinel subgroup, containing O^{2-} as an anion which can be further subdivided by the valence state of its cations into “sub-group 2-3” ($\text{A}^{2+}\text{B}_2^{3+}\text{O}_4$) and “ulvöspinel subgroup” ($\text{A}^{4+}\text{B}_2^{2+}\text{O}_4$).^[28]

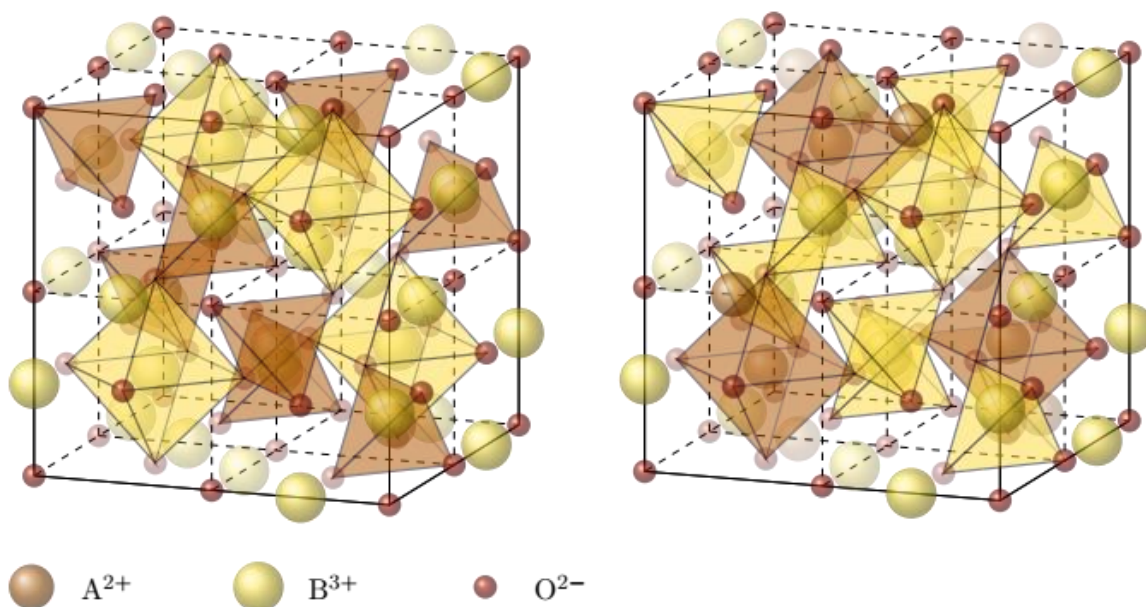


Figure 1: Spinel structure of a normal spinel (left) and inverse spinel (right).

The spinel supergroup itself is named after the mineral “spinel” (MgAl_2O_4), which is a normal spinel. Magnetite (Fe_3O_4) is an example of an inverse spinel with the additional feature that both cations are the same chemical element (Fe), but of different valence (+2 and +3).

Due to their varied chemical composition spinel type compounds can be used in a variety of chemical processes. Zhao et al. reviewed the different synthesis methods for obtaining spinel compounds and their application in 2017 with a special focus on their application in the oxygen reduction/evolution reaction (ORR/OER).^[29] Other areas include oxygenation^[30], hydrogenation^[27, 31] and electrochemistry^[32] in liquid and gas phase reactions.^[33]

In 2018, Pekov et al. published the discovery of the Cu-bearing spinel CuAl_2O_4 in nature, found in fumaroles of the Tolbachik volcano in Kamchatka, Russia.^[34] The mineral was named Thermaerogenite and forms a continuous isomorphous series with gahnite (ZnAl_2O_4). Their occurrence is very limited and coupled to very harsh and specific environmental conditions. Thus, any CuAl_2O_4 species used in chemical processes or catalytic reactions are produced synthetically.

There are a number of different synthetical routes described in literature to synthesize copper aluminate spinel, e.g. solid-state reactions^[33, 35, 36], combustion methods^[37] as well as precipitation and impregnation reactions^[36, 38, 39]. To obtain the spinel lattice the precursor must be heated at least to 600-800 °C, often up to 1000 °C. The specific amount of obtained spinel species and its distribution and surface area is dependent on the chosen synthesis route and tailored towards the final application of the produced spinel compound. The use of carbonate or oxalate precursors leads to an increase of pore volume in the resulting spinel due to the release of carbon dioxide during the calcination process.^[29]

Literature often describes the presence of identifiable copper oxide phases within the synthesized spinel, even at elevated temperatures.^[33, 35, 37, 39-41] Hu et al. describe that to gain a spinel end product without a detectable CuO signal, they calcined the sample for 20 days at 950 °C.^[35] Liu et al. caution that the CuO signal in XRD patterns vanishes at temperatures of 950 °C and above but that H_2 -TPR data still identify non-spinel CuO at this stage.^[33]

An increase in calcination temperature above 1000°C favors the formation of delafossite-type CuAlO_2 by decomposition of CuAl_2O_4 .^[40, 41] On the other hand, calcination temperatures below 600 °C result in CuO supported on Al_2O_3 , which is itself widely used as a catalyst in a number of reactions (Equation 2).



Equation 2: Phase composition with increasing calcination temperature

The high-temperature Cu-Al spinel phase shows a distinctly better acid leaching resistance compared to Cu(I) or^[42] Cu(II) copper oxide phases. This characteristic leads to a number of studies utilizing CuAl_2O_4 formation to decrease copper leaching from metal-laden sludges by thermal treatment.^[35, 40, 43] Its decreased copper leaching makes CuAl_2O_4 also a candidate as an antibacterial-agent in wastewater treatment or corrosion protection, avoiding the danger of metal- and environmental pollution while inhibiting bacterial growth.^[38]

The use of CuAl_2O_4 as a catalyst involves in most cases the activation of the catalyst pre-reaction to create the catalytically active phase driving the reaction. This can be a separate step independently of the main reaction or a part of the targeted reaction path itself.^[33, 44] The activation of Cu-Al spinel involves the reduction of the present Cu(II) and Cu(I) species to Cu(0). Most Temperature-programmed reduction (TPR)-profiles show two reduction peaks corresponding to the reduction of Cu^{2+} to Cu^0 .^[33, 45-47] Since most synthesized CuAl_2O_4 includes a copper(II)oxide phase, the first reduction peak is assumed to be the reduction of the CuO phase at temperatures around 200-250°C. Depending on the amount of CuO the first reduction step can be more pronounced and shifted to lower temperatures around 150-200 °C. The second reduction step takes place at higher temperatures and is ascribed to the reduction of the copper in the spinel phase. Plyasova et al. describe a migration of copper from within the spinel lattice to the surface as copper metal upon reaction with hydrogen, resulting in a copper-deficient spinel lattice.^[48] The copper ions in tetrahedral sites show an earlier migration to the surface compared to those in octahedral sites. The remaining protons are stabilizing the structure, forming OH⁻ groups within the spinel lattice.

2.2.2 Hydrogenation reactions

Catalytic hydrogenation reactions are a cornerstone of the chemical industry. They cover a wide range of applications, from petrochemical, fine chemical industries to the food industry and conversion of biomass.^[49-53] Hydrogenation itself describes the reaction of (molecular) hydrogen with another compound. It is a very useful reaction to transform unsaturated organic compounds to their saturated derivatives. The related hydrogenolysis reaction is the addition of hydrogen to an organic compound resulting in the cleavage of the compound into smaller fragments, severing either a C-C or a C-heteroatom bond.

Heterogeneously catalyzed hydrogenation reactions can be conducted both in the liquid and the gas-phase. These reactions mostly occur at elevated temperatures and pressures, which can be optimized by use of a suitable catalyst. Most of the hydrogenation reactions are catalyzed by late transition metals, e.g. platinum, palladium, nickel. The catalytically active metals are often finely dispersed on a suitable substrate to decrease cost. Other metals such as copper are also suitable hydrogenation catalysts, often promoted by a secondary metal to improve

catalyst stability and selectivity.^[52, 54] Cu-Ni-Zn-Al and Cu-Co-Al catalysts are used in cinnamaldehyde hydrogenation. Cu-chromite catalysts were applied in a number of hydrogenation reactions e.g. furfural hydrogenation^[55, 56] and fatty alcohols production^[53] before the regulation of “substances with very high concern” by the European Union.^[57]

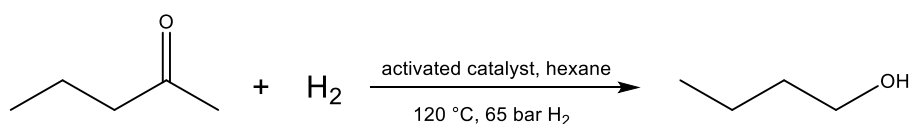
Butanals are produced on an industrial scale by hydroformylation of propylene, a process discovered in 1938.^[42] The global butyraldehyde market is estimated with a market value of 220 million US\$ in 2022 and an expected Compound Annual Growth Rate (CAGR) of 6%.^[58] During hydroformylation olefins react with a mixture of carbon monoxide and hydrogen (syn gas) in the presence of (nowadays mostly) rhodium catalysts to form aldehydes containing one more carbon atom than the starting olefin. Butanals are highly reactive intermediates that serve as building blocks for other C₄ and C₈ compounds such as alcohols, carboxylic acids, and amines. Downstream products range from paints to flavors and pharmaceuticals. The reactivity of the carbonyl group can lead to unwanted consecutive intermolecular reactions. In the presence of atmospheric oxygen butyraldehyde can slowly oxidize to the corresponding carboxylic acid which leads to feed impurities (in the industrial and laboratory scale). The hydrogenation of *n*-butanal with a suitable catalyst produces *n*-butanol. *n*-Butanol is together with 2-ethylhexanol production the largest consumer of butyraldehyde, accounting for about 80% of the global *n*-butyraldehyde production.^[59]

Cu-aluminate spinels are a possible alternative hydrogenation catalyst for the hydrogenation of aldehydes, but suffer from stability losses in liquid reactions.^[31] In the gas-phase application they show good stability for the hydrogenation of butyraldehyde.^[47]

2.3 Motivation

The hydrogenation of aldehydes and the hydrogenolysis of esters to corresponding alcohols have been described above as large-scale industrial processes of high interest. Historically they can be catalysed by the Adkins catalyst (copper chromite, $\text{CuO} \cdot \text{CuCr}_2\text{O}_4$), which had to be substituted by chromium-free systems due to toxic chromate (Cr^{6+} , (CrO_3)) species occurring during the production process. The catalyst has been practically banned by regulations of the European Union on 'substances with very high concern (SVHC)' by 2017.^[57] Copper aluminate spinel catalysts ($\text{CuO} \cdot \text{CuAl}_2\text{O}_4$) were found to be a possible non-toxic alternative with comparable activity and selectivity, however they suffer from stability losses during reactions in the liquid phase.

In a former study on the hydrogenation of butyraldehyde to butanol, leaching of active and of support components was observed.^[27] The influence of reaction parameters and components were however not yet investigated and the consequences of leaching for catalytic cycle, activity and catalyst stability remained untouched. These aspects being important for a detailed understanding of leaching and catalyst deactivation are the subject of the following study and thesis chapter. In extension to former investigations, the species dissolved into solution are not only determined at the end of the reaction as single points, but progression of leaching was quantitatively determined as function of reaction time and parallel to conversion of the substrate and catalytic performance. A corresponding suitable experimental set-up has been developed and optimized involving autoclave reactor, continuous sampling unit, catalyst transfer, product analysis and metal trace analysis. This set-up has been proven to guaranty sampling as function of time within a closed system with very good comparability and reproducibility. In order to get a comprehensive picture of the leaching processes and the relations to catalytic properties, a large variety of parameters has been investigated within an extensive and elaborate experimental series: For the test reaction hydrogenation of butyraldehyde to butanol,



Equation 3: Hydrogenation of butyraldehyde to butanol

the concentration of dissolved components (Cu, Al) and products were determined as function of reaction time and of parameters like catalyst preparation and composition, solvent, solvent mixtures, additives (carboxylic acids) and impurities, both as separated parameter or in combination. This integrative approach allowed the conclusive interpretation and also generalization of leaching phenomena in correlation to catalytic performance.

2.4 Results and Discussion

The main focus of the leaching investigation is the behavior of the (so-called) phase-pure CuAl_2O_4 spinel which had been previously established in the doctoral thesis of C. Dörfelt.^[27] He noticed the not insignificant leaching tendencies of the spinel catalyst during hydrogenation reactions, which led to the more detailed exploration of the leaching trends and behaviors in this thesis.

The leaching progression is documented by regular sampling in established time intervals of an otherwise closed reaction system. It is an improvement to previous leaching results due to the sampling opportunity without major interference. Due to the necessary reduction of Cu(II) to form the active species Cu^0 , an open system during sampling massively affects the leached amounts in solution. This new procedure allows for a reproducible observation of the leaching behavior of the chosen spinel catalyst. It further allows the modification of individual aspects of the reaction system and the influence those have on the leaching behavior.

In order to understand the role of preparation and composition of the copper aluminate spinel catalysts on leaching behavior, three different types of catalysts were prepared and compared:

- (i) the “phase-pure” spinel CuAl_2O_4 , where CuO residues remaining on the surface of copper aluminate spinel after calcination were removed by an optimized copper leaching procedure,
- (ii) the “original” spinel forming during synthesis, the so-called “stoichiometric” spinel $(\text{CuO}) \cdot \text{CuAl}_2\text{O}_4$ (slight excess of CuO on the spinel surface) after calcination, and
- (iii) the copper oxide-copper aluminate spinel, $\text{CuO} \cdot \text{CuAl}_2\text{O}_4$, analog to the previously established Cu-Cr Adkins catalyst, $\text{CuO} \cdot \text{CuCr}_2\text{O}_4$, which contained a stoichiometric excess of CuO , practically supported on copper aluminate.

Due to that, different Cu:Al ratios in related spinel structures can be compared and the possible influence of the (non)-existent surface copper(II)oxide layer can be studied as well. For details regarding catalyst synthesis and characterization, please see chapter 2.4.7.

The liquid samples were investigated by ICP-OES to determine the leached copper and aluminum, the catalysts activity was tested by GC measurements. This allows a correlation between catalyst activity and leaching behavior. The catalysts themselves were characterized by elemental analysis, XRD and Raman before and after use in the hydrogenation reaction.

2.4.1 Leaching and catalytic performance in the hydrogenation reaction

The leaching behavior of the Cu-Al spinel catalysts are tested in the liquid-phase hydrogenation of *n*-butyraldehyde to *n*-butanol (Equation 3). The catalytic reaction takes place in a closed system under hydrogen pressure. The reaction parameters established previously by C. Dörfelt^[27] were used as the initial starting parameters to establish a “baseline behavior” of catalyst activity and leaching progression. The catalyst is activated under hydrogen in a separate step before use. This requires inert handling of the catalyst after activation to avoid re-oxidation and thus deactivation of the catalyst.

Experimental set-up

The experiments were performed as batch experiments in a closed system, using a stainless-steel autoclave (Figure 2). All experiments used the same set-up to ensure a good comparability and reproducibility of the obtained data.



Figure 2: Experimental set-up of the autoclave. Left: fully assembled autoclave, including heater. Top right: pipe and 2-way valve used for sampling. Bottom right: stirring, thermocouple and sampling pipe attached to autoclave head.

The stainless-steel autoclave is equipped with a 300 mL glass liner which contains the chemicals. The removable head is equipped with gas in- and outlets with valves, a thermocouple,

an analog barometer, stirrer and a thin metal pipe used for sampling. The piping can be opened and closed using a two-way valve, to enable quick and easy sampling. Heating is accomplished by a removable heater which fully enclosed the autoclave, apart from the head. Heating ramps and stirring can be programmed by an external controller.

The transfer of the catalyst into the reaction vessel was performed under pseudo-inert conditions to minimize the danger of reoxidizing the activated copper catalyst. The autoclave vessel and the liquid educts were flushed with Ar to minimize the available oxygen as well. A detailed description of the autoclave assembly can be found in the Experimental section. A high number of experiments and repetitions of the transfer procedure ensure a comparable effectiveness of the assembly of the autoclave. Repeat experiments of the same batch composition ensured the reproducibility of the identified leaching trends.

Phase-pure catalyst stability and performance in hexane

To establish a “baseline” for the catalyst stability and performance, the CuAl_2O_4 catalyst was first tested in hexane. Figure 3 shows the leaching behavior and catalytic performance of the phase-pure catalyst. The initial copper leaching is a lot higher than the average copper leaching over time. It decreases quickly until no leached copper remains in solution. Aluminum leaching in hexane is very low but slowly increases with the ongoing reaction. The hydrogenation of butyraldehyde progresses steadily and reaches full conversion after 4-5 hours. The *n*-butanol yield increases parallel to the substrate conversion, the catalyst shows a medium selectivity to butanol of around 52 %. This is a lower selectivity compared to the corresponding gas phase reaction using the same catalyst. Experiments using a fixed bed continuous gas-phase hydrogenation set-up showed a selectivity to *n*-butanol of 99 %.^[47] The difference in selectivity is most likely related to the more complex activation of a spinel catalyst, where apart from copper(0) sites the presence of copper(I) sites is possible. It is also feasible that not all copper within the spinel lattice has been completely reduced to Cu^0 . Cu^0 has been reported as the main active site for the hydrogenation of butyraldehyde, activating the C-O bond. Copper(I) sites could catalyze unwanted side reactions, resulting in a decrease in selectivity compared to the gas phase reaction. For the gas phase reaction, only the formation of $\text{Cu}(0)$ during activation has been reported using the Cu-Al spinel catalyst.^[47] Since the focus of this thesis is not the improved selectivity of the catalyst but its leaching behavior, the formation of side products has not been investigated in detail.

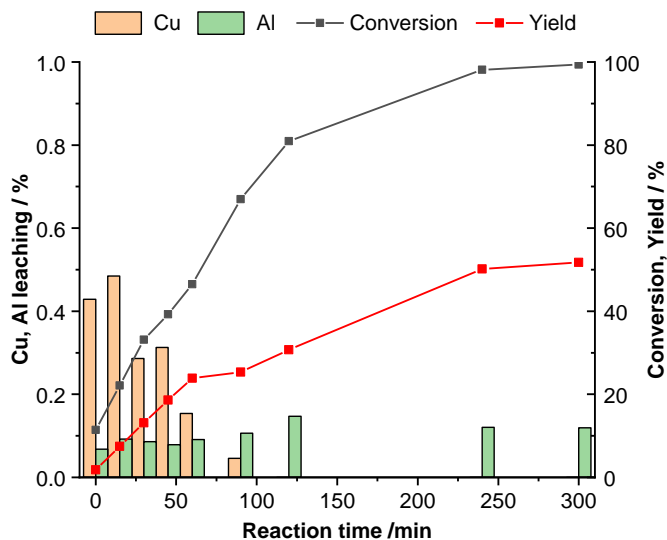


Figure 3: **Spinel catalyst performance in hexane.** The leached amounts are very low overall. Copper (brown bars) leaches primarily at the start of the reaction, whereas aluminum (green bars) shows a steady low leaching overall.

Repeat experiments shows a fluctuation in initial copper leaching ranging from 0.2 to 1.1 %, even if all experimental parameters remain the same. It is most likely related to the efficiency of the transfer of the activated catalyst to the reaction vessel. Since the previously reduced copper (Cu^0) has to be oxidized to Cu(II) to leach into the liquid phase, a non-ideal transfer to the autoclave might result in a partially (re)oxidized catalyst surface due to prolonged contact with air (Equation 4).



Equation 4: (I) Reduction of Cu(II) oxide ; (II) (Re)oxidation of elemental copper to copper(II)

To illustrate: the two highest initial leached copper values in Figure 4 were the first two experiments done in an experimental grouping. An experiment done at a later time of the lab work (when the steps of the catalyst transfer and assembly of the autoclave were more familiar) shows 0.5 % Cu leaching, so about half of the other two experiments.

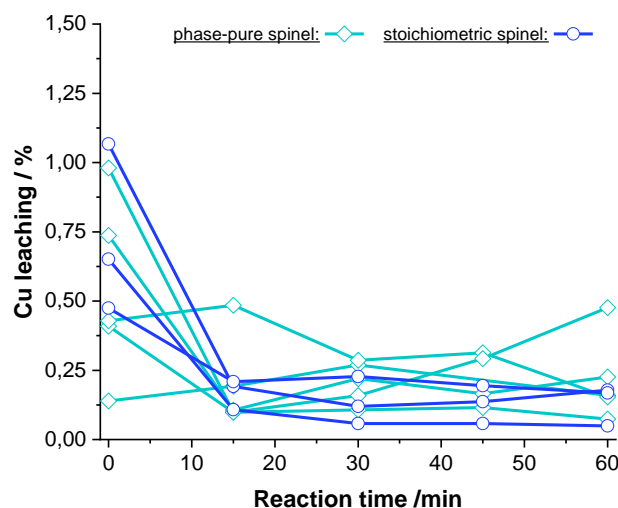


Figure 4: Initial leached copper in solution at the start of the hydrogenation reaction. The initial leached copper varies, even under the same reaction conditions, but converges quickly to similar values.

Regardless of the initially higher or lower Cu leaching, all observed leaching trends in Figure 4 result in comparable low leaching values within 30 min of reaction time. A further optimization of the transfer process might be able to eliminate this fluctuation of the initially leached copper and give a clearer picture of the “true” initial leached amount. But since all of the experiment batches show similar values after 15-30 min of reaction time, independent of the initial value, this is not a major concern for the investigation of leaching trends using this method of catalyst transfer. The results also indicate that residual copper(II) species are (at least nearly) completely reduced to metallic copper under the chosen “standard” reaction conditions (see also chapter 2.4.7, Characterization of the catalysts).

In contrast to copper leaching, the aluminum leaching is more relevant long-term. There is no aluminum leaching at the start of the reaction but it increases steadily over reaction time. The presence of carboxylic acids leads to a noticeable increase of leached species (Figure 5). The continuous leaching of aluminum from the spinel lattice may be a problem concerning lattice stability. In contrast to copper, there is no aluminum leaching previous to the formation of *n*-butanol (heating phase). Regardless of experimental batch composition, none show aluminum in solution before reaching the reaction temperature of 120 °C. The blind test (batch experiment without butanal) and a test batch under Ar pressure (no hydrogen) show no aluminum leaching at all. This implies that the mobility of aluminum from the catalyst is related to the (active) hydrogenation reaction itself.

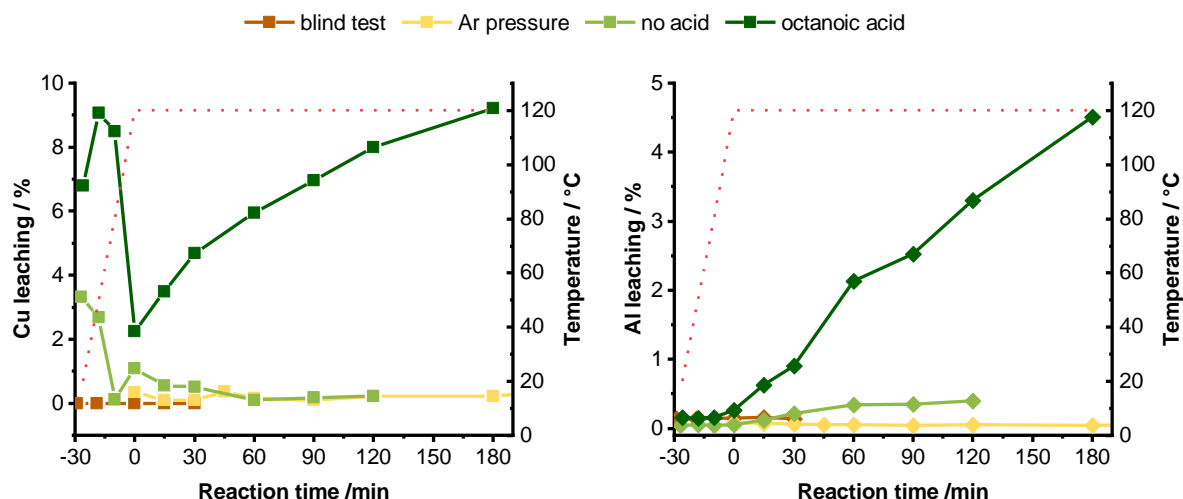


Figure 5: **Leaching behavior of CuAl_2O_4 catalyst in hexane.** The red dotted line shows the heating ramp. There is no relevant leaching under inert gas (yellow line) or with a blind test (no butyraldehyde present). An active hydrogenation process leads to small-scale Al leaching over time. Carboxylic acid additives lead to increased leaching of copper and aluminum.

In the subsequent chapters a number of experiments with varying catalyst composition, solvents and additives will be described and discussed. All batch experiments discussed are listed in the Appendix in Table S2, subdivided by figure. To simplify and differentiate between the individual experiments, each has a distinct shortened description given in brackets to allow a quick understanding of the main components involved in the individual experiment. The short description informs about the type of spinel used, the solvent, the addition of (which) carboxylic acid as well as the length of the reaction time (see Table S1).

2.4.2 Leaching behavior depending on the copper/aluminum ratio of Cu-Al spinels

This section shows the main leaching trends of the three spinel catalysts with different Cu:Al ratios as well as their activity and stability behavior in the first five hours of reaction time under “standard” conditions. It illustrates principle trends comparing at the same time the different catalysts, i.e. copper amounts and dispersions available on the catalyst surface. The previous section focused on the CuAl_2O_4 catalyst without copper(II) oxide on its surface. Here, its leaching behavior is compared to two other Cu-Al spinel catalysts where the surface CuO is not removed or purposefully formed from the start.

The leaching progression of the three Cu-Al spinel catalysts during the hydrogenation reaction of butyraldehyde to butanol in hexane is shown in Figure 6 together with the catalytic performance of the catalysts (activity and selectivity).

Hydrogenation reaction in hexane:

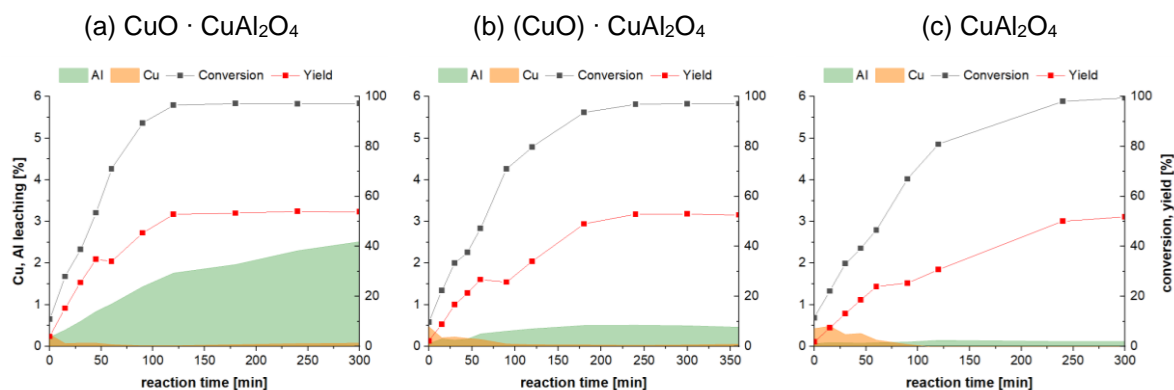


Figure 6. Progression of leaching (left axis) and catalyst performance (right axis) over reaction time for three Cu-Al spinel catalyst with different surface CuO: (a) $\text{CuO} \cdot \text{CuAl}_2\text{O}_4$, (b) $(\text{CuO}) \cdot \text{CuAl}_2\text{O}_4$, (c) CuAl_2O_4 . Reaction conditions: $T = 120\text{ }^\circ\text{C}$, $p = 65\text{ bar}$, 0.1 mol butyraldehyde in 100 mL hexane.

The experimental results in Figure 6 show clear differences in the leaching behavior and catalytic performance of the three catalysts, in particular in aluminum leaching. In detail: (a) $\text{CuO} \cdot \text{CuAl}_2\text{O}_4$ (Adkins analogue): the hydrogenation reaction progresses fast and reaches full conversion after about 2 hours with a yield of 55 %. There is negligible Cu leaching at the start of the reaction, which reduces quickly to trace amounts only. In contrast, there is constant Al leaching during the hydrogenation reaction, which increases slightly slower after full conversion is achieved. At the end of reaction, around 2.5 % of total Al of the catalyst has leached into the reaction mixture. (b) $(\text{CuO}) \cdot \text{CuAl}_2\text{O}_4$ (stoichiometric spinel): the hydrogenation reaction progresses slightly slower than in (a) and reaches full conversion after about 3 hours with a yield of 52 %. There is small-scale Cu leaching during the first 2 hours which does not rise above 0.5 % of the overall Cu content. There is Al leaching present during the hydrogenation reaction but it is limited to around 0.5 % of the overall Al and does not increase further after

2 hours of reaction time. (c) CuAl_2O_4 (phase-pure spinel): the hydrogenation reaction progresses slower than (a) and (b) and reaches full conversion after about 5 hours with a yield of 51 %. There is small-scale Cu leaching during the first 2 hours, comparable with (b). The Al leaching is negligible at 0.1-0.2 % overall Al and does not increase over reaction time. In the following, leaching of copper and aluminum and catalytic properties shall be discussed separately:

The copper leaching in hexane is negligible for all three tested catalysts, being well below 1 % of the overall copper amount. There is slightly higher leaching in the beginning of the reaction but the dissolved copper concentration decreases quickly to a background level within the first hour. The difference in initial copper leaching (right at the start of the reaction) is less dependent on the type of spinel catalyst and rather related to the more or less inert transfer of the activated catalyst to the reaction vessel, as discussed in the previous section 2.4.1.

Figure 6 suggests that the stability of the copper species during the liquid hydrogenation reaction is dependent on the amount of surface CuO /reduced Cu^0 , since CuO-Sp (Figure 6a) shows the least and P-Sp (Figure 6c) shows the highest amount of copper in solution. This might be due to the easier accessibility of the CuO surface phase during activation, resulting in a protection for the Cu deeper within the spinel phase which might not have been completely reduced during the activation procedure.

Aluminum leaching. In contrast to the copper leaching, the aluminum leaching is less uniform and more relevant. There is no aluminum leaching at the start of the reaction but it increases steadily over reaction time. The three tested spinels show the opposite behavior compared to copper leaching: the phase-pure spinel catalyst shows the lowest and the CuO-spinel the highest amount of aluminum leached into solution (up to 2 % of total Al in the catalyst after 5 hours). The highest increase in Al leaching occurs during the first two hours of reaction time, compared to the rest of the observed time frame. This coincides with the highest rate of the hydrogenation reaction, i.e. when most of the substrate is converted into *n*-butanol, as shown by the slope of the Al leaching and conversion curve in Figure 6. This implies that the aluminum leaching is related to the (active) hydrogenation reaction itself and not a “passive” secondary reaction. The Al leaching does not completely stop after the main conversion has passed, but the slope flattens prominently.

All three spinel catalysts reach full conversion of the available butanal in the observed time frame. The fastest conversion occurs with CuO-Sp with full conversion within 2 hours. The conversion rate in this series of experiments decreases along with the amount of copper available on the surface of the catalyst. The slowest conversion belongs to the phase-pure spinel

catalyst with full conversion after about 5 hours. The achieved product yield is comparable for all three catalysts and is about 50-55 % of the initial butyraldehyde deployed.

At this point of investigation, it is surprising that there seems to be a correlation of aluminum leaching and the reaction progress. This may however be a chance to understand later the mechanism of aluminum leaching, which is surprising at all. On the other hand, the rather constant leaching of only traces of copper under hydrogen pressure and increased temperature with continuous progress of the reaction can rationally be explained.

Addition of carboxylic acid as leaching parameter for different copper-aluminum ratios.

A final leaching experiment comparing the three catalysts with varying Cu/Al ratio has been performed to estimate the influence of a carboxylic acid as additive on the potential dissolution of catalyst components into solution in general. Carboxylic acids can be regarded as well coordinating ligands via the carboxylic group for the metal ions bound in the catalyst lattice, i.e. Cu^{2+} , and Al^{3+} (possibly Cu^+). In addition, their influence on catalyst leaching and stability is of very practical relevance for industrial hydrogenation of aldehydes, because carboxylic acids are often typical impurities of the raw materials. Their concentration can reach up to 2 % (due to partial oxidation of the aldehydes during handling), thus being potentially a relevant factor for additional leaching. Heptanoic acid has been chosen due to several reasons, in particular because the solubility of the product of complex formation (carboxylate complexes) will depend on the carbon chain length (hydrophobicity). For hexane as solvent, heptanoic acid appeared as a good compromise to us. For these experiments, the same reaction conditions have been applied, only 8 mol-% of heptanoic acid were added to the reaction mixture. The results are shown in Figure 7 for the experiments with all three copper-alumina catalysts.

Hydrogenation reaction in hexane with addition of 8 mol-% heptanoic acid:

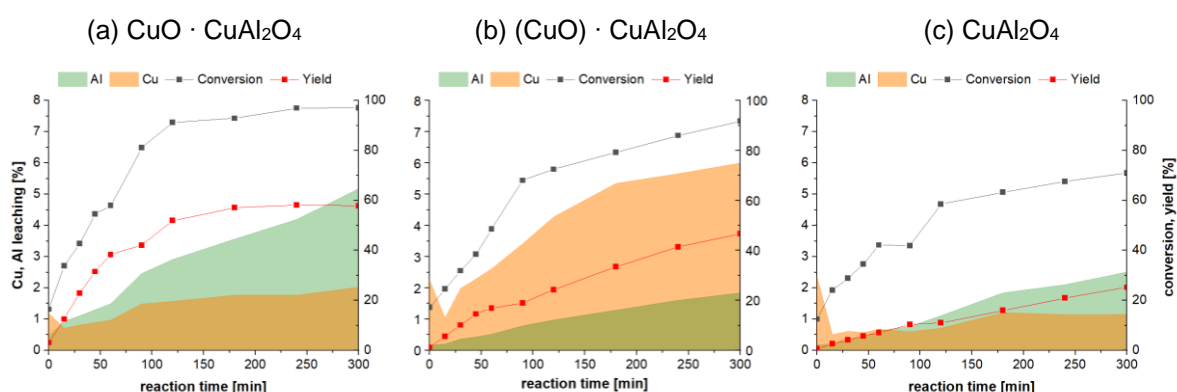


Figure 7. Progression of leaching (left axis) and catalyst performance (right axis) with addition of heptanoic acid. (a) $\text{CuO} \cdot \text{CuAl}_2\text{O}_4$, (b) $(\text{CuO}) \cdot \text{CuAl}_2\text{O}_4$, (c) CuAl_2O_4 . Reaction conditions: $T=120\text{ }^\circ\text{C}$, $p=65\text{ bar}$, 100 mmol butyraldehyde in 100 mL hexane, 8 mol-% heptanoic acid

Figure 7 illustrates the influence of the presence of a carboxylic acid on leaching but also on catalytic performance of the three catalysts: (a) $\text{CuO} \cdot \text{CuAl}_2\text{O}_4$: the hydrogenation reaction still progresses fast and reaches full conversion after about 2 hours with a yield of 58 %. There is increased Cu leaching over reaction time. More significantly, there is a noticeable increase in Al leaching, which still progresses after full conversion is reached. At the end of reaction time around 5 % of the overall present Al in the catalyst has leached into the reaction mixture. (b) $(\text{CuO}) \cdot \text{CuAl}_2\text{O}_4$: the hydrogenation reaction progresses noticeably slower than in Figure 6 and does not reach full conversion in 5 hours reaction time. There is a drastic increase in Cu concentration in solution reaching 6 % overall Cu content. Al leaching is also higher in the presence of carboxylic acids with 1.5 % Al leaching into the liquid phase. (c) CuAl_2O_4 : the hydrogenation reaction is considerably slower than in (a) and (b) and the reaction does not reach full conversion. There is an increase in Cu leaching compared to Figure 6, but it shows the lowest Cu leaching compared to (a) and (b) in the presence of heptanoic acid. The Al leaching is no longer negligible but does increase over reaction time to about 2 % overall Al content. An important difference to the leaching behavior without carboxylic acids present in the system (see Figure 6) is that no constant metal amounts in solution (“leaching equilibrium”) is reached in the observed reaction time. The stoichiometric spinel in Figure 7b is the only system where the leaching of copper into the liquid phase is considerably higher than the leaching of Al.

The addition of heptanoic acid to the batch results in a marked increase in leaching of both copper and aluminum into solution for all three catalyst variations. The previously mentioned factor of high initial copper leaching at the start of the reaction is still observed, but the “base level” of copper leaching after the initial peak decreases considerably stronger compared to the batch without the addition of heptanoic acid. The copper leaching stabilizes in the case of CuO-spinel and phase-pure spinel at about 1-1.5 % overall copper.

The stoichiometric spinel does not follow this trend or the behavior of its counterparts (Figure 7b). Here, the Cu leaching does not stabilize over reaction time but keeps consistently increasing, reaching up to 6 % overall Cu content in the observed reaction time. This amount of leaching is expected to be a potentially decisive factor concerning long-term catalyst activity as well as catalyst stability. The increased amount of copper in solution can also lead to unwanted side reactions which may contaminate the desired product. The explanation of this particular effect, if it can be correlated to specific properties of this catalyst ($(\text{CuO}) \cdot \text{CuAl}_2\text{O}_4$) or if it is related to specific experimental conditions (reproducibility) will be subject of the more detailed investigations of the next sub-chapters.

The $\text{CuO} \cdot \text{CuAl}_2\text{O}_4$ catalyst shows more or less the same copper and aluminum leaching trend as found in pure hexane (Figure 7a), but the overall leached amounts are considerably higher with the addition of heptanoic acid. Cu leaching increases to about 1 % and Al leaching up to 5 %. The slope of the aluminum leaching again correlates to the slope of the butyraldehyde

conversion, but the resulting slope after full conversion is reached is steeper than in the batch containing hexane.

The conversion rate of the reaction is considerably slower in the system containing heptanoic acid, only one catalyst (CuO-spinel) reaches full conversion in the observed time frame. This is a clear difference to the reaction in pure hexane, where all three catalysts reached full conversion within the observed 5 hours. The conversion rate of the stoichiometric and phase-pure spinel declines to 95 % and 75 % respectively (see Figure 7b and c). The resulting yield can only be extrapolated in these cases but appears to be comparable to the previous results (see Figure 6b and c). $\text{CuO} \cdot \text{CuAl}_2\text{O}_4$ shows a comparable yield and conversion as the acid-free system. At this state of investigations, the most probable explanation for the difference in activity is the substantial loss of active copper species into solution, where the ligand stabilized Cu^{2+} is stable and cannot be re-reduced under reaction conditions. This loss is substantial for the stoichiometric and phase-pure spinel catalysts, whereas the Adkins analog has a large excess of CuO (metallic copper in activated form) partially compensating this loss.

2.4.3 Variation of carboxylic acids as additive in Cu-Al spinel standard leaching experiments

The next section concentrates on the two catalysts with a copper to aluminum ratio of 1:2, which results in catalysts primarily composed of spinel phase, without a deliberate copper oxide layer on top of the catalyst surface.

The phase-pure spinel catalyst CuAl_2O_4 consists exclusively of Cu-Al spinel material. Any built-up CuO on the surface during synthesis has been removed before catalyst activation and use in an experimental set-up. The stoichiometric spinel catalyst $(\text{CuO}) \cdot \text{CuAl}_2\text{O}_4$ is synthesized from the same precursor as the phase-pure spinel catalyst but the CuO which develops on the spinel surface during calcination is left unchanged. This leads to a larger initially available Cu^0 surface area after activation compared to the phase-pure spinel catalyst. A more detailed characterization of both catalysts can be found in chapter 2.4.7.

The figures illustrating the leaching trends are grouped by catalyst and subdivided into leaching (copper and aluminum in solution) and catalyst activity (educt conversion and product yield). All subplots contain the same color coding for the different experiment batches. To distinguish them more easily, the stoichiometric spinel plots contain strong colors and the phase-pure spinel plots the corresponding softer colors.

The previously established standard parameters for a leaching batch experiment are 350 mg of activated catalyst, 0.1 mol butanal as substrate in 100 mL of hexane as a solvent, heated to 120 °C under 65 bar H_2 pressure. To test the effect of different carboxylic acids in the reaction

system 8 mol-% (in regard to butanal) were added to different batches. The resulting leaching trends and product yields are shown in Figure 8 for a stoichiometric spinel and in Figure 9 for a phase-pure spinel catalyst.

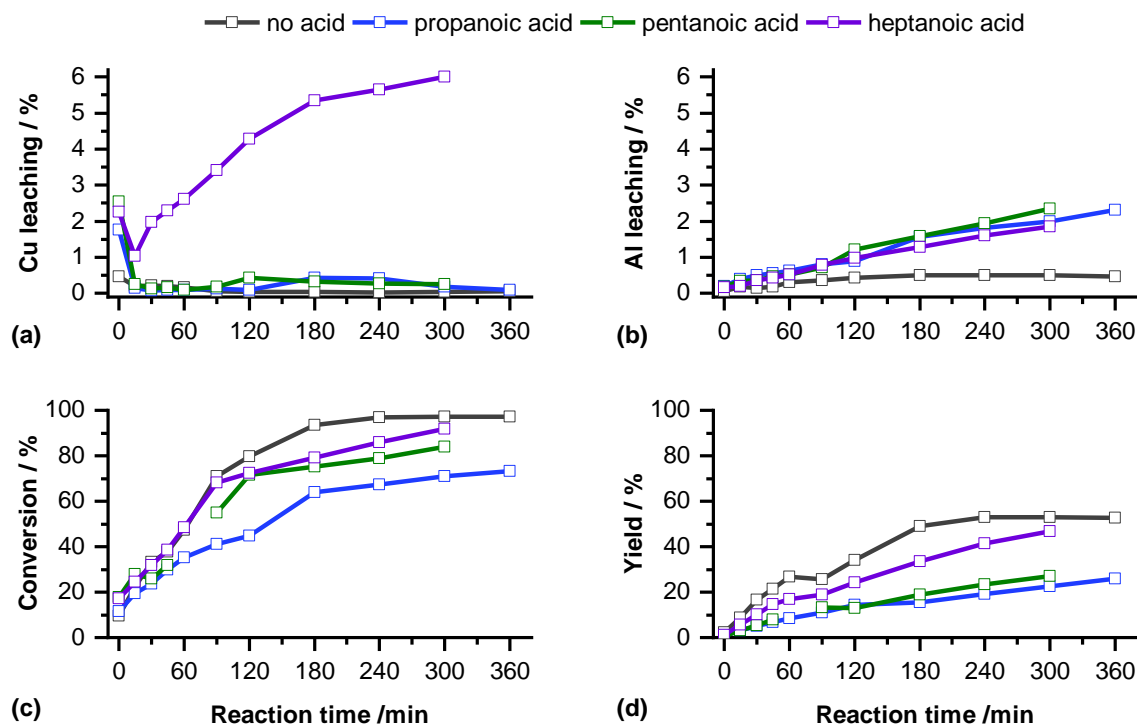


Figure 8: **Stoichiometric spinel catalyst - Leaching progression in hexane with three different carboxylic acids as additives (8 mol-%):** (a) Cu leaching, (b) Al leaching, (c) conversion of butyraldehyde, (d) butanol yield in %-overall during the hydrogenation of butanal.

As expected from the preliminary tests in the previous chapters, the presence of carboxylic acids in the system leads to an increase of leached species in the liquid phase. The effect is primarily focussed on aluminum and only sporadically includes copper. Under standard conditions a significant amount of copper leaching merely occurs using the stoichiometric spinel with the addition of a longer chainlength carboxylic acid (heptanoic acid). Heptanoic acid addition leads to a slight increase of leached copper using a phase-pure spinel as well (Figure 9), but it is significantly lower than using a stoichiometric spinel and does not increase over reaction time (compare Figure 8a and Figure 9a). All other experimental batches show the same low level of copper leaching with or without addition of carboxylic acids for both catalyst species, remaining below 0.5 % of total copper amount.

Unlike copper leaching, aluminum leaching is more affected by the addition of carboxylic acids. The leached aluminum amount increases over time using either of the spinel catalysts without a clear differentiation concerning chain length. Neither of the catalysts show significant Al leaching in hexane (below 0.5 %) but as soon as carboxylic acids are introduced into the

system the aluminum leaching increases steadily throughout the reaction (Figure 8b and Figure 9b). Both spinel catalysts show 2-4 % of aluminum leaching after 5 hours of reaction time, mostly without a clear distinction between the acids. The phase-pure spinel catalyst exhibits higher aluminum leaching compared to its stoichiometric spinel counterpart (see Table 1). It also shows a slight favoring in aluminum leaching with shorter chain length acids, the stoichiometric spinel shows no such distinction. Neither batch shows a stabilization of the observed leaching, the process is still ongoing without the curve nearing an equilibrium.

The increase of aluminum leaching is a concerning factor regarding catalyst stability due to the underlying spinel structure of the catalyst. Aluminum is an important component of the spinel lattice, especially since the other present copper cations are more mobile and involved in the underlying catalytic mechanism. Due to the copper mobility and its substitution by protons in the lattice, the spinel structure is not as stable anyway and an additional removal of aluminum cations will further weaken the spinel lattice. Worst case, this process will lead over time to a collapse of the spinel structure and significantly impair the integrity lifetime of the catalyst. Since long-term stability is an important factor for the economic viability of a catalyst species, this increased aluminum leaching must be alleviated.

In particular, dissolution of aluminum can have drastic consequences for the stability of shaped catalyst (grains), when aluminum represents a component of the binder material, what is in fact often the case in the corresponding industrial catalyst. This can be critical especially in continuous processes with fixed bed flow reactors (e.g. trickle bed) for the long term stability of the catalyst bed and the reactant flow.

Due to the fact that copper is migrating through the spinel lattice during activation, an increase in copper leaching is not necessarily a stability risk from the outset, but it may lead to a loss in catalyst activity if the leached species does not catalyze the same target reaction as the Cu^0 residing on the catalyst surface (which can in fact be assumed). A first quick check is the correlation between conversion as well as product yield and copper leaching. If they show an inverse correlation that is a clear sign that the copper leaching negatively affects the butanal conversion and butanol production.

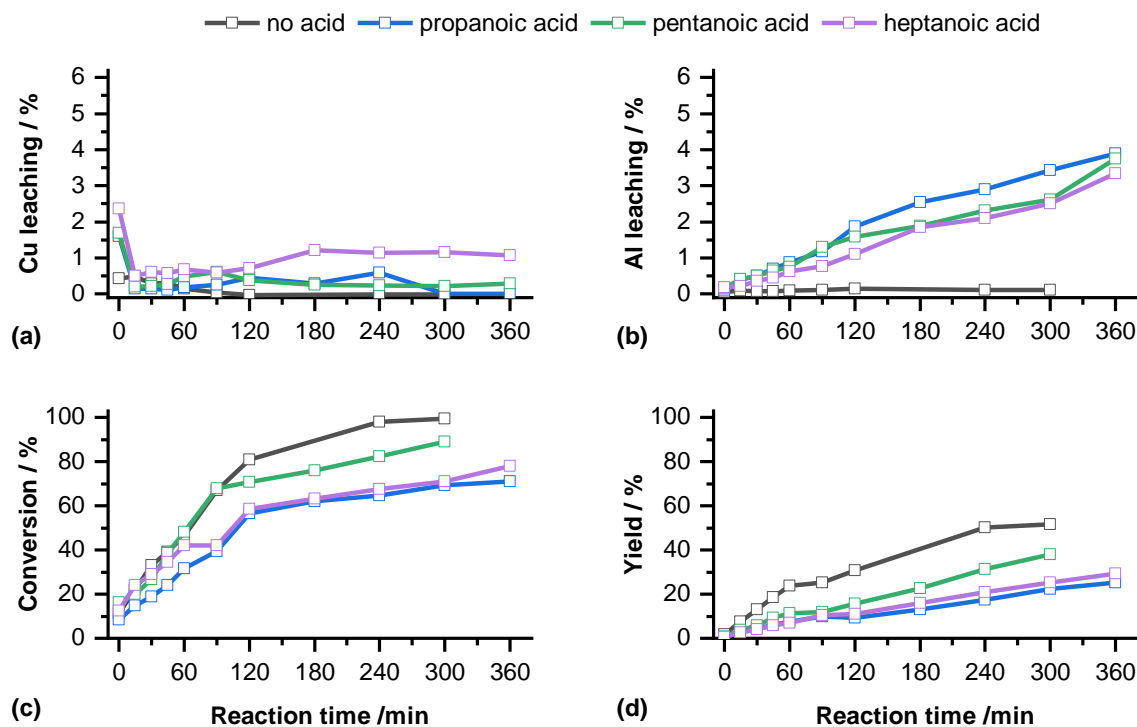


Figure 9: **Phase-pure spinel catalyst - Leaching progression in hexane with three different carboxylic acids as additives (8 mol-%):** (a) Cu leaching, (b) Al leaching, (c) conversion of butyraldehyde, (d) butanol yield in %-overall during the hydrogenation of butanal.

In the observed timeframe of 5 hours of reaction time, none of the batches containing carboxylic acids reach full conversion, neither stoichiometric nor phase-pure spinel. The only batches to reach full conversion are the initial batch of hexane without acid addition. The butanol yield of this batch using stoichiometric spinel is 53 % (corresponding to a selectivity of 54.5 %) after about three hours. The phase-pure spinel batch also reaches full conversion but needs 4-5 hours of reaction time. The yield (and selectivity) of the batch is similar to its S-Sp equivalent with 52 % butanol yield and selectivity. The small difference might be due to the difference in surface copper which increases the speed of the conversion.

The addition of carboxylic acid leads in all cases to a decrease in catalyst activity, the rate of conversion decreases. Since none of the batches reach full conversion in the observed time frame it is not quite clear if the addition of carboxylic acid also leads to decreased yield of butanol or if it only affects the conversion time. This will be checked with longer running experiments (chapter 2.4.6).

The decrease in conversion does not correlate with the copper leaching behavior in all experiments. Interestingly, the only batch with considerably higher copper leaching (S-Sp, H, C7) shows a conversion trend like the standard batch. The first 90 min have more or less the same conversion values (around 75 % at this point) whereas the copper(II) in solution of the heptanoic acid batch is already at 3.5 % (compared to below 0.5 % in the standard batch). This is an indicator that the catalyst activity in regards to the hydrogenation reaction is not solely

dependent on the loss of copper into solution as long as enough active copper(0) remains available on the spinel “support” and that copper(II) complexes in solution do not influence the butanal conversion. The copper(II) in solution does however also not considerably catalyze competing reactions: the final butanol yield in the presence of heptanoic acid is with 46.6 % (at 92 % conversion resulting in 50.9 % selectivity to butanol) close to the results of the standard batch without heptanoic acid. The batch with the short-chain propanoic acid shows the slowest conversion progression with 73 % butyraldehyde conversion after 6 hours and 26 % butanol yield (Figure 8, blue line). It must be taken into account that the shorter chain carboxylic acid can temporarily dissolve copper, but re-deposits as sparingly soluble Cu(II) carboxylate onto the support and/or is thus separated with the solid by the leaching experiment. Thus, copper would be continuously lost during the experiment or are even deposited onto and blocking active sites explaining the reduced activity.

Table 1: Batch composition in hexane, after 5 or 6 hours of reaction time. The table shows the results of the last sample taken from each experimental batch in %-overall.

% overall	Sample after X min	leached Cu*	leached Al*	Conversion Butanal ⁺	Yield Butanol ⁺
Stoichiometric spinel (CuO) · CuAl ₂ O ₄					
No acid	360	0.05	0.46	97.13	52.60
Propanoic acid	360	0.10	2.31	73.13	26.00
Pentanoic acid	300	0.26	2.35	83.88	27.16
Heptanoic acid	300	6.00	1.84	91.73	46.65
Phase-pure spinel CuAl ₂ O ₄					
No acid	300	0	0.12	99.39	51.77
Propanoic acid	360	0	3.90	89.12	25.38
Pentanoic acid	300	0.29	3.75	71.09	37.95
Heptanoic acid	360	1.08	3.34	78.17	29.26

* analyzed by ICP-OES (if the value is given as 0 it was below the limit of quantitation of the instrument)

+ analyzed by gas chromatography

To summarize: the presence of carboxylic acids noticeable increases the leaching of aluminum from the spinel lattice into solution. Copper leaching is only affected with heptanoic acid. The formed copper carboxylates are better soluble in the non-polar hexane compared to copper carboxylates with shorter carbon chains. All experiments with any carboxylic acids applied show a decreased conversion rate and product yield. It is possible that the formation of the

particularly sparingly soluble copper carboxylates re-deposit as solid and are lost as active species and / or even block active copper sites, resulting in a less active catalyst.

2.4.4 Variation of the solvent

The previously established hydrogenation test reaction of butyraldehyde to *n*-butanol uses hexane as a solvent. The subsequent leaching and catalyst behavior has been documented in the previous subchapter. Next the solvent of the batch reaction is changed from the nonpolar hexane to different solvents with increased polarity to see if and how the polarity of the solvent influences both the leaching and the catalyst activity. In these experiments not all carboxylic acid batches were tested again. In most cases a batch without acid addition is compared to a batch with pentanoic acid addition, the mid-length of the investigated carboxylic acids, because the previous experiments showed a big enough variation between the non-acid and acid batches. Occasionally, one of the other acids was tested as well to gain further insights.

The chosen solvents are in order of increasing polarity:

- (100 mL hexane)
- 100 mL toluene
- 100 mL 1,4-dioxane
- 100 mL ethanol

Toluene

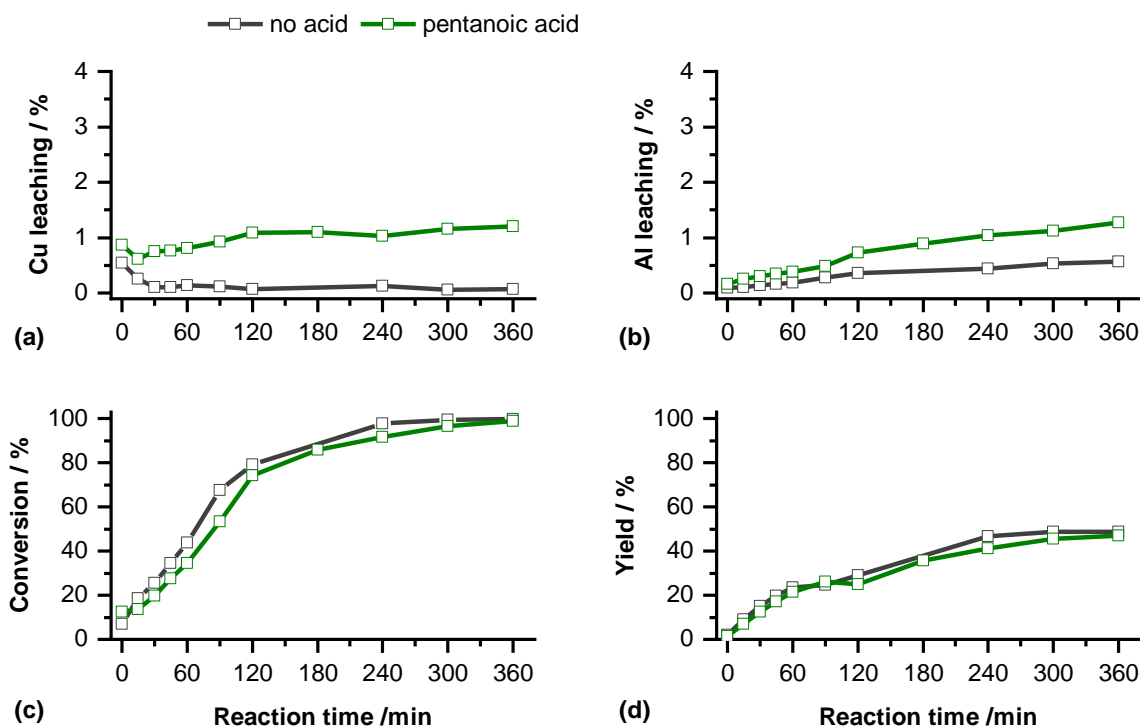


Figure 10 **Stoichiometric spinel catalyst - Leaching progression in toluene with pentanoic acid as additive (8 mol-%):** (a) Cu leaching, (b) Al leaching, (c) conversion of butyraldehyde, (d) butanol yield

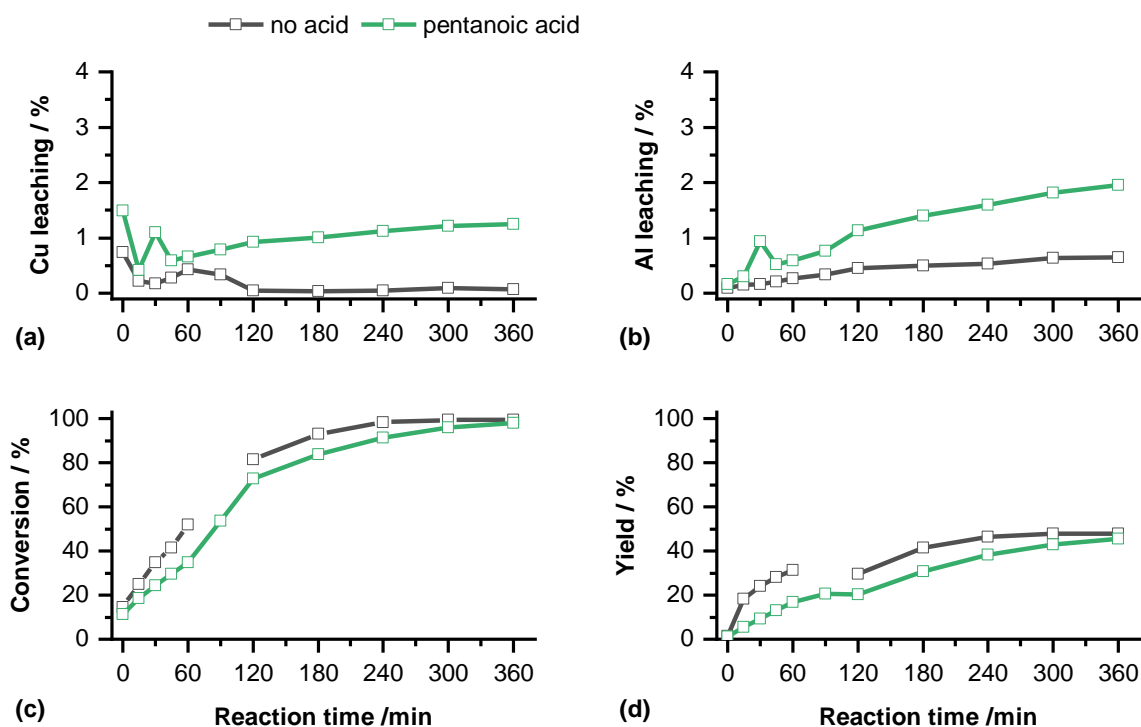


Figure 11: **Phase-pure spinel catalyst - Leaching progression in toluene with pentanoic acid as additive (8 mol-%):** (a) Cu leaching, (b) Al leaching, (c) conversion of butyraldehyde, (d) butanol yield

The experiments in toluene without acid addition show comparable result with its equivalent in hexane for either of the spinel catalysts. Looking at the batches containing pentanoic acid, they show an improvement in conversion and yield compared to their hexane counterparts. Both batches reach full conversion in a similar timeframe to the experiments without acid (about 4-5 hours). The yield decreases slightly compared to the hexane batches (around 47% yield vs. 53 % yield), but reaches the same level as the toluene batch without acid addition. Especially the S-Sp catalyst shows no significant difference in yield between the non-acid batch and the pentanoic acid batch (Figure 10). The phase-pure spinel batch shows slightly slower conversion and yield but reaches the same amounts as the corresponding non-acid batch.

Both copper and aluminum leach once again stronger into solution when the batch contains small amounts of acid in comparison to pure toluene. However, the increase in aluminum leaching is less prominent compared to its hexane counterpart (Figure 8b and Figure 9b, pentanoic acid). This is true for both spinel variations. The aluminum leaching after 5 hours of reaction time decreases compared to experiments in pure hexane from 2.3 % to 1.1 % (stoichiometric spinel) and from 2.6 % to 1.8 % for the phase-pure spinel.

In contrast, copper shows increased leaching of about 1% compared to the pure solvent as well as its hexane counterpart for both stoichiometric and phase-pure spinel. The copper leaching does not increase but remains steady through the whole experiment.

Table 2: Leached Cu and Al in solution, conversion of butyraldehyde and butanol yield in %-overall after 5 or 6 hours of reaction time in toluene as a solvent.

% overall	Sample [min]	leached Cu*	leached Al*	Conversion Butanal ⁺	Yield Butanol ⁺
Stoichiometric spinel (CuO) · CuAl ₂ O ₄					
No acid	360	0.08	0.57	99.72	48.69
Propanoic acid	-	-	-	-	-
Pentanoic acid	360	1.20	1.28	99.02	47.00
Heptanoic acid	-	-	-	-	-
Phase-pure spinel CuAl ₂ O ₄					
No acid	360	0.08	0.65	99.65	48.00
Propanoic acid	-	-	-	-	-
Pentanoic acid	360	1.25	1.96	98.09	45.50
Heptanoic acid	-	-	-	-	-

* analyzed by ICP-OES; ⁺ analyzed by gas chromatography

1,4-Dioxane

Experiments in 100 mL 1,4-dioxane were only tested for a batch containing pentanoic acid, for a stoichiometric and a phase-pure spinel respectively. Due to problems with overlap of the gas chromatography peaks, a reliable estimation of the butanol yield was not possible. Since the main question remains the leaching behavior, the product analysis was disregarded in this case and further experiments in pure 1,4-dioxane set aside for now. Further experiments using 1,4-dioxane as sole solvent must create a new GC analysis method to separate the relevant reaction product peaks.

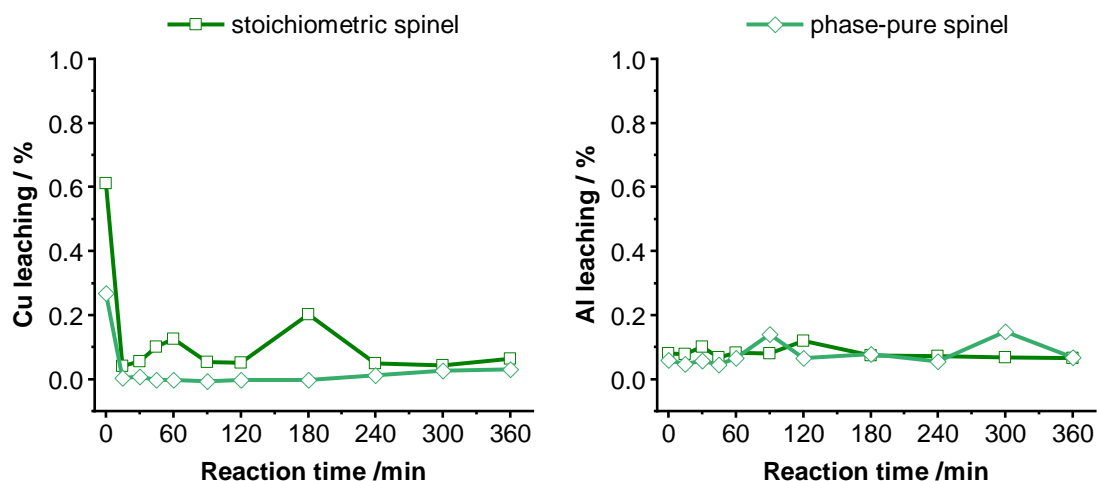


Figure 12: **Leaching progression in 1,4-dioxane for pentanoic acid as additive.** There is no significant difference in the leaching behavior of the stoichiometric and the phase-pure spinel. Both show no relevant Al leaching and only moderate Cu leaching in the beginning of the reaction.

Both spinel variations show the same trend: no significant copper or aluminum leaching (Figure 12). The Al leaching can be seen as non-existent over reaction time and does not change between phase-pure and stoichiometric spinel. Copper leaching shows the previously established slightly higher leaching at the start of the reaction, but remains well below 1%. The subsequent copper leaching is practically non-existent with values close to 0 % and only a small fluctuation in case of stoichiometric spinel.

Table 3: Leached Cu and Al in solution in %-overall after 6 hours of reaction time in 1,4-dioxane as a solvent. Due to problems with overlapping peaks in the GC results there are no conversion or yield rates.

% overall	Sample [min]	leached Cu*	leached Al*	Conversion Butanal ⁺	Yield Butanol ⁺
Stoichiometric spinel (CuO) · CuAl ₂ O ₄					
Pentanoic acid	360	0.06	0.07	-	-
Phase-pure spinel CuAl ₂ O ₄					
Pentanoic acid	360	0.03	0.07	-	-

* analyzed by ICP-OES; ⁺ analyzed by gas chromatography

Ethanol

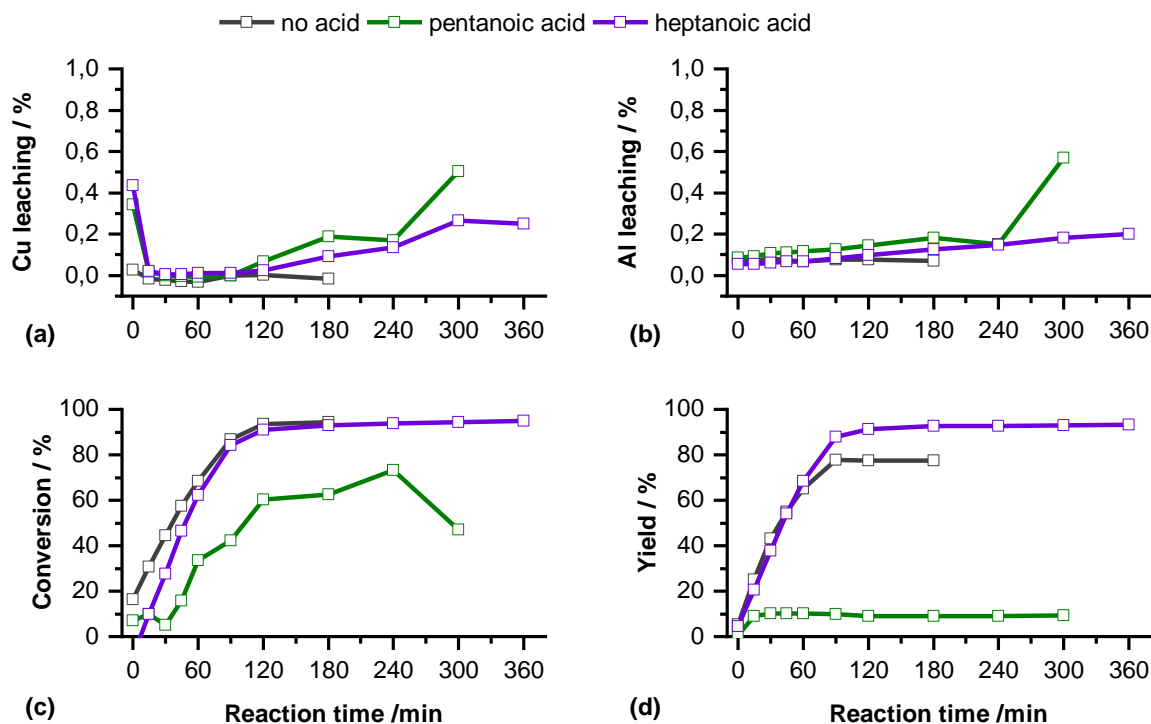


Figure 13: **Stoichiometric spinel catalyst - Leaching progression in ethanol with two different carboxylic acids as additives (8 mol-%):** (a) Cu leaching, (b) Al leaching, (c) conversion of butyraldehyde, (d) butanol yield in %-overall during the hydrogenation of butanal.

The experiments with ethanol further underline the trend that leaching of both aluminum and copper is distinctly decreased in more polar solvents. There are small deviations depending on chain-length but non lead to significant differences in the leaching behavior. In case of ethanol, there is also a significant increase in conversion rate and product yield compared to previous experiments.

The stoichiometric spinel does not show significant copper leaching in the observed time frame for either batch. The batches show a tendency towards increased copper leaching in the later hours of reaction time. The experiment using a stoichiometric spinel in ethanol with heptanoic acid addition (purple line in Figure 13) is shown separately in Figure 14 to illustrate the aluminum and copper behavior in solution a bit more clearly.

The start of the copper increase fits quite well with the end of conversion. As long as conversion is still ongoing, the copper leaching remains constant compared to its start value.

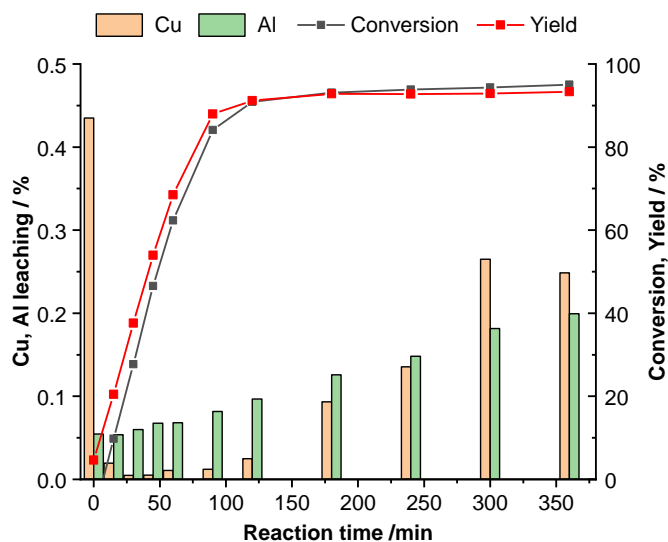


Figure 14: **Stoichiometric spinel catalyst performance in ethanol with heptanoic acid as additive** (purple curve in Figure 13). The leached amounts are very low overall but start to increase once the conversion of the educt has finished, especially copper (brown bars).

The same trend can be found for aluminum leaching but less pronounced. There is close to no aluminum leaching in the first two hours of reaction time. When conversion is finished after those two hours, aluminum concentration starts to increase. Overall, both the aluminum and copper leaching is negligible in the observed time frame. Depending on their long-term development they might still pose a problem for longer runtimes.

Conversion and yield are not affected in the last hours of reaction time. Both reach their maximum values after 90 min to 2 hours and remain constant afterwards. There is no secondary reaction of the desired end product. The yield is considerably higher than in previous experiments, it increases from around 50% to 80-90 % yield depending on the batch.

The copper leaching behavior of the phase-pure spinel catalyst (Figure 15a) in ethanol shows a similar trend to its stoichiometric spinel counterpart (Figure 13a). There is no copper leaching in the first two hours of reaction time while the substrate conversion is ongoing. After two hours the copper content in solution increases slowly once more for carboxylic acid experiments. There is no significant difference in behavior concerning the alkyl-chain length of the carboxylic acid used. The copper amounts remain significantly lower than in hexane or toluene.

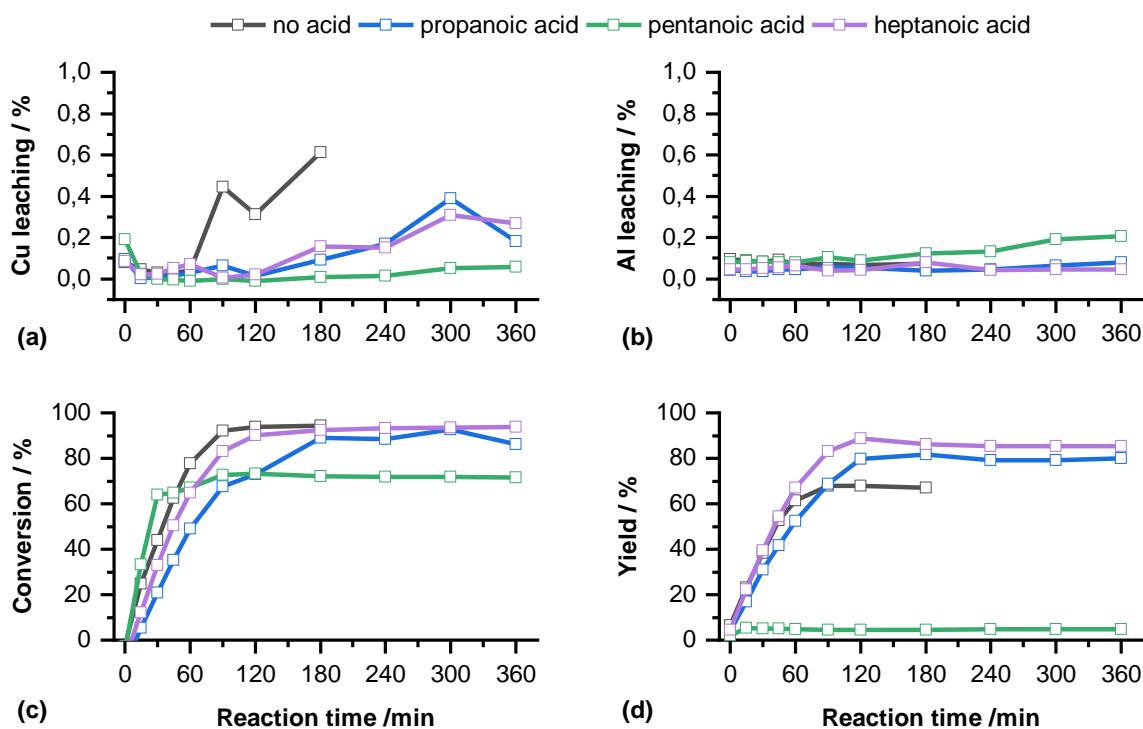


Figure 15: **Phase-pure spinel catalyst - Leaching progression in ethanol with three different carboxylic acids as additives (8 mol-%):** (a) Cu leaching, (b) Al leaching, (c) conversion of butyraldehyde, (d) butanol yield in %-overall during the hydrogenation of butanal.

The non-acid batch shows a slightly different copper leaching behavior, the Cu amount starts increasing in solution after 60 min of reaction time. There is no correlation to the conversion curve which keeps following its previously established trend until full conversion around 90 min, but there is a corresponding trend in yield. The yield in butanol steadily increases until 60 min of reaction time and then stops at around 65 % yield and does not change after that. There is no decrease either, but the achieved yield is about 10 % lower than its stoichiometric spinel counterpart. A competing second reaction occurs in the next hour of reaction time which uses up the remaining butyraldehyde and also leads to an increase of copper concentration in solution.

In contrast to the stoichiometric spinel in ethanol, the phase-pure catalyst shows no aluminum leaching during the observed reaction time for neither of the experiments. There is no difference between non-acid and acid batches.

The trends of butyraldehyde conversion and butanol yield show the same progression and final amounts as the stoichiometric spinel. The pentanoic acid experiment fails to produce butanol and also has a lower conversion rate, as seen in its stoichiometric spinel counterpart.

Table 4: Leached Cu and Al in solution, conversion of butyraldehyde and butanol yield in %-overall after 5 or 6 hours of reaction time in ethanol as a solvent. Additionally, the yield of acetal is shown due to its influence, especially in the batches containing pentanoic acid (see Figure 16).

% overall	Sample [min]	leached Cu*	leached Al*	Conversion Butanal ⁺	Yield Butanol ⁺	Yield Acetal ⁺
Stoichiometric spinel (CuO) · CuAl ₂ O ₄						
No acid	180	0	0.07	94.42	77.56	0.18
Propanoic acid	-	-	-	-	-	-
Pentanoic acid	300	0.51	0.57	47.11	9.38	47.93
Heptanoic acid	360	0.29	0.20	95.04	93.35	0.12
Phase-pure spinel CuAl ₂ O ₄						
No acid	180	0.61	0.07	94.50	66.96	2.34
Propanoic acid	360	0.18	0.08	86.16	80.03	0.2
Pentanoic acid	360	0.06	0.21	71.43	4.82	55.43
Heptanoic acid	360	0.27	0.04	93.94	85.22	0.18

* analyzed by ICP-OES (if the value is given as 0 it was below the limit of quantitation of the instrument)

+ analyzed by gas chromatography

The increased stability in the presence of carboxylic acids and often increased yield of butanol in ethanol as solvent is a positive factor. On the other hand, there are some problems with unwanted side-reactions, especially in certain batch mixtures.

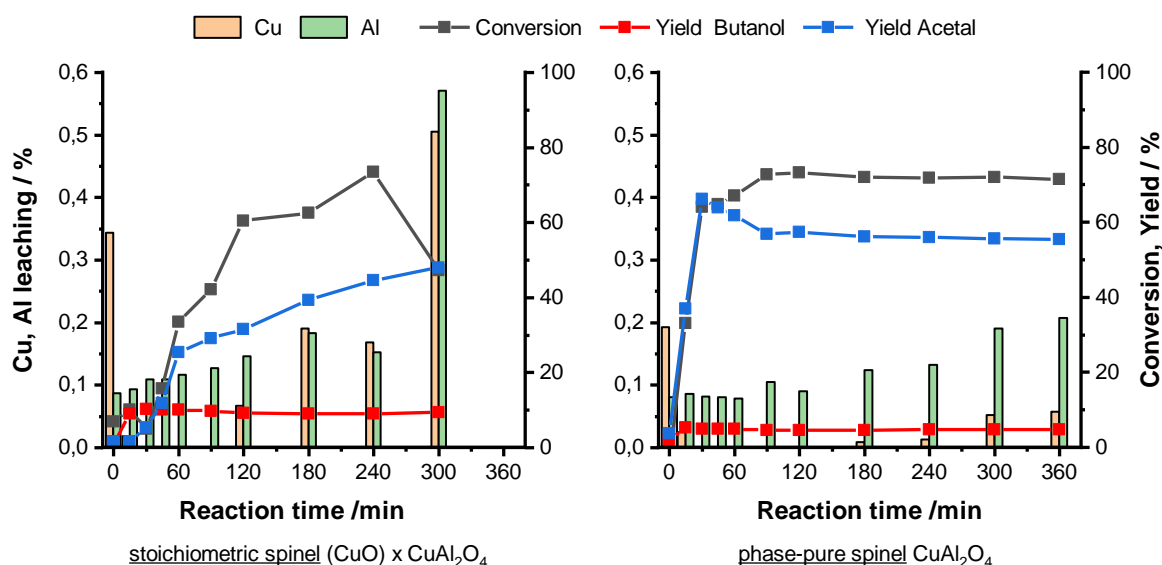
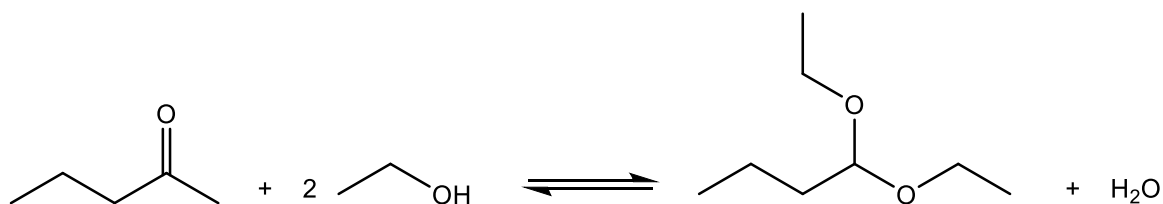


Figure 16: **Increased acetal formation in ethanol.** Both, stoichiometric and phase-pure spinel catalyst, show very low butanol yield when pentanoic acid is present in the solvent. The acetal formation (blue curve) notably impedes the desired formation of butanol, the majority of the butyraldehyde educt is transformed into acetal.

Figure 16 shows an example of a stoichiometric spinel catalyst in ethanol with pentanoic acid as an additive (left side). There is close to no butanol yield and conversion of butyraldehyde to butanol only occurs in the first 15 to 30 min of reaction time. A look at the gas chromatography results shows an enormous spike in acetal formation which increases throughout. The available ethanol reacts with the aldehyde educt instead of the desired hydrogenation of butyraldehyde to butanol (Equation 5). In the beginning of the reaction a small amount of butanol is formed by hydrogenation but after that only the acetal yield increases. Since the acetal formation is often catalyzed by acidic conditions the batches with carboxylic acid addition are more susceptible. The same is true for the phase-pure spinel experiment. Interestingly, this is not the case for every experimental batch using ethanol as a solvent. It mostly happens in the presence of pentanoic acid, the other tested carboxylic acid additions did not show pronounced acetal formation with both catalysts. All experiments in ethanol show a low amount of acetal formation, but not to the extent that it severely impairs the formation of butanol. On the other hand, some experimental batches without carboxylic acid addition did also fail due to excessive acetal formation. The butyraldehyde feed contains small impurities of butyric acid, especially in already opened bottles, which can be found in the GC results. In some cases, this seems to be enough to kick-start the acetal formation even without any extra acid additive.



Equation 5: Butyraldehyde diethyl acetal formation in acidic medium.

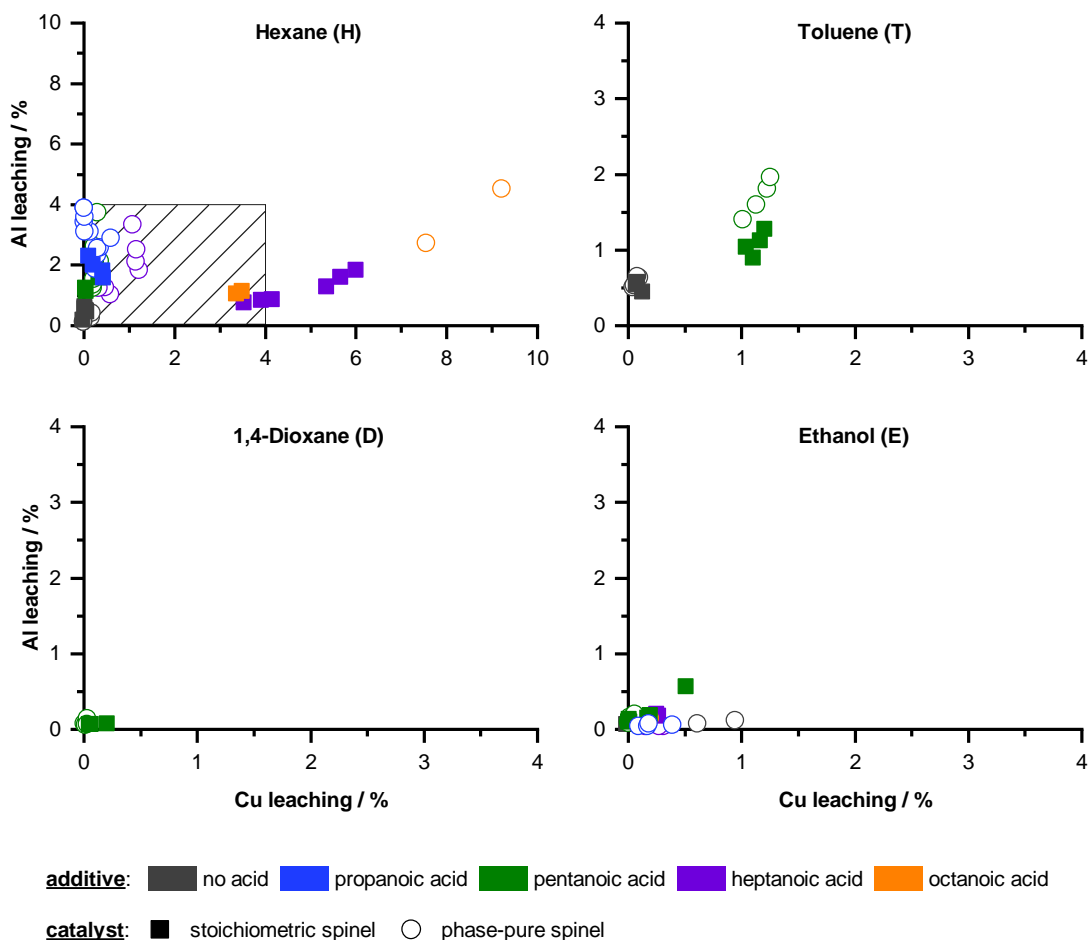


Figure 17: **Scatter plot of Cu and Al leaching in pure solvents** (≥ 3 hours of reaction time) The scatter plot clearly shows the decrease in leached species when the solvent is switched from hexane to a more polar solvent. For easier comparability the range of the other three subplots is marked by the hatched rectangle in the hexane subplot (top left). The acid additives are color coded the same as in previous plots. Full symbols signify stoichiometric spinel, empty symbols phase-pure spinel batches.

2.4.5 Solvent mixtures

Since the switch to more polar solvents showed a reduced copper and aluminum leaching and in the case of ethanol also an increase in butanol yield, other experimental batches were tested with a solvent mixture of 100 mL hexane and 10 mL of the other tested solvents (toluene, 1,4-dioxane and ethanol). The question was if the effects observed can also be replicated with less amounts of e.g. ethanol to avoid the excessive formation of acetal and other negative side effects.

The chosen solvent mixtures are in order of increasing polarity:

- 100 mL hexane
- 100 mL hexane + 10 mL toluene
- 100 mL hexane + 10 mL 1,4-dioxane
- 100 mL hexane + 10 mL ethanol

Hexane + 10 mL toluene

The batches tested in a hexane/toluene mixture show a similar copper leaching behavior to their pure toluene counterparts in the presence of pentanoic acid with a mean value of 1 % Cu leaching (S-Sp) and no significant increase after a few hours of reaction time (Figure 18a). The phase-pure catalyst batch even shows a slightly lower copper leaching of around 0.5 % which is half of the value in pure toluene (Figure 19a). The non-acid batches show no copper leaching after a few hours of reaction time for both spinel variations, the same behavior as the toluene batches. Table 5 gives the results (leaching, product analysis) of the last sample taken from each experimental batch using a hexane/toluene mixture.

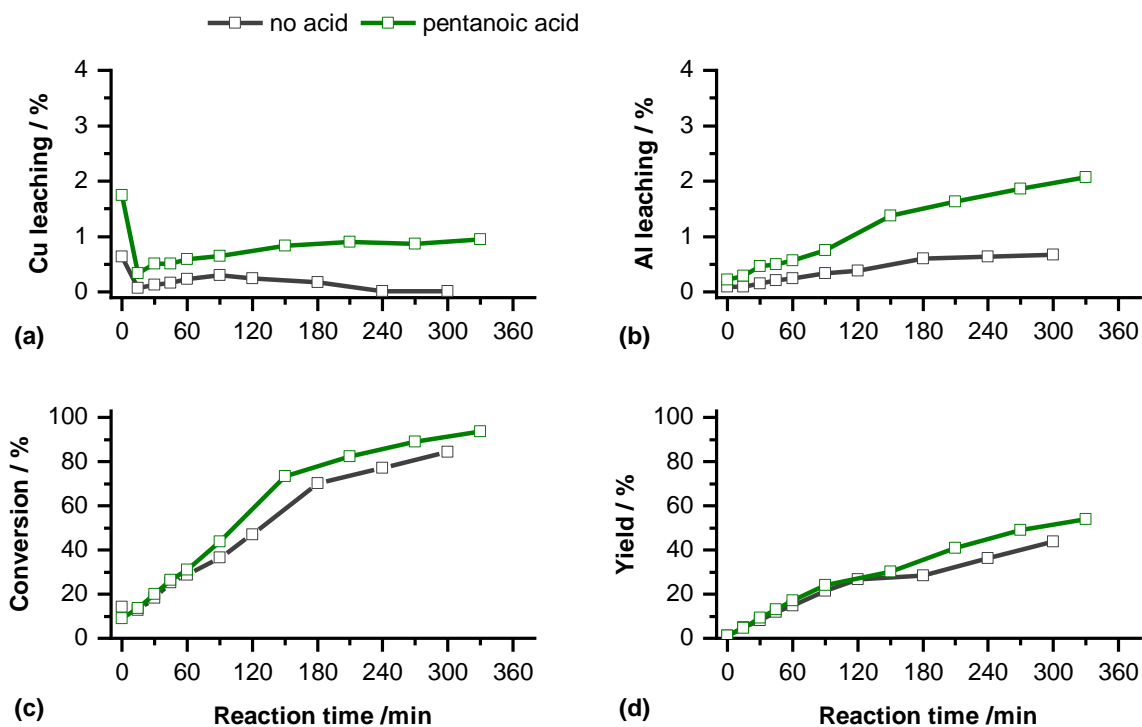


Figure 18: **Stoichiometric spinel catalyst - Leaching progression in hexane/toluene mixture with pentanoic acid as additive (8 mol-%):** (a) Cu leaching, (b) Al leaching, (c) conversion of butyraldehyde, (d) butanol yield.

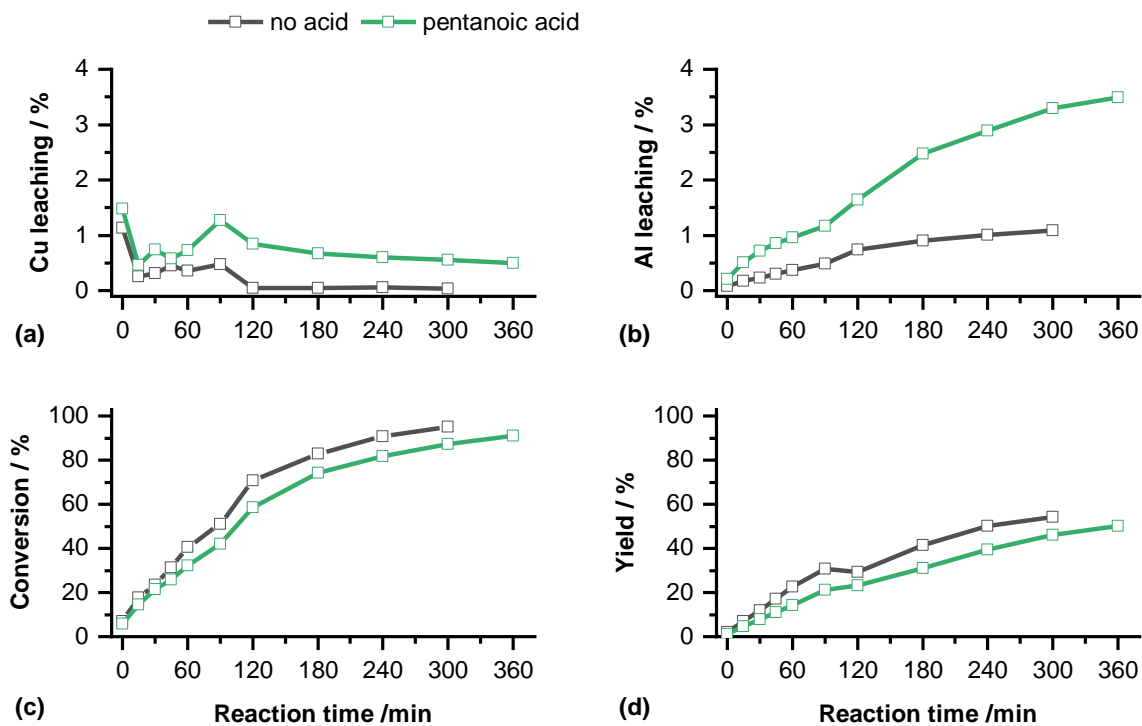


Figure 19: **Phase-pure spinel catalyst - Leaching progression in hexane/toluene mixture with pentanoic acid as additive (8 mol-%):** (a) Cu leaching, (b) Al leaching, (c) conversion of butyraldehyde, (d) butanol yield

Contrary to copper leaching, the aluminum leaching keeps increasing over reaction time and in many cases doubles compared to the pure toluene batches for both catalyst variations with or without pentanoic acid addition (Figure 10b and Figure 11b). A comparison with the pure hexane experiments also shows no “improvement” due to the addition of toluene: 2 % and 2.3 % (stoichiometric spinel, 5 hours), 3.5 % and 3.7 % (phase-pure spinel, 6 hours). Another trend which can be seen in the curve progression of aluminum leaching is the increased slope after about 2 hours of reaction time which coincides with a decrease in conversion rate.

The conversion of butyraldehyde progresses faster than in hexane, but not as fast as in pure toluene. The yield of butanol is in most cases 4-5 % higher than in pure toluene (compare Table 2 and Table 5)

Overall, it seems that toluene addition has a positive effect on the copper leaching but a stronger negative effect on the stability of aluminum in the catalyst spinel lattice.

Table 5: Leached Cu and Al in solution, conversion of butyraldehyde and butanol yield in %-overall after 5 or 6 hours of reaction time in a 10:1 mixture of hexane and toluene as a solvent.

% overall	Sample [min]	leached Cu*	leached Al*	Conversion Butanal ⁺	Yield Butanol ⁺
Stoichiometric spinel (CuO) · CuAl ₂ O ₄					
No acid	300	0.02	0.68	84.52	43.80
Propanoic acid	-	-	-	-	-
Pentanoic acid	270	0.87	1.86	88.97	49.12
Pentanoic acid	330	0.95	2.07	93.77	53.84
Heptanoic acid	-	-	-	-	-
Phase-pure spinel CuAl ₂ O ₄					
No acid	300	0.04	1.1	95.14	54.12
Propanoic acid	-	-	-	-	-
Pentanoic acid	300	0.55	3.30	87.45	46.06
Pentanoic acid	360	0.50	3.49	91.16	50.12
Heptanoic acid	-	-	-	-	-

* analyzed by ICP-OES; ⁺ analyzed by gas chromatography

Hexane + 10 mL 1,4-dioxane

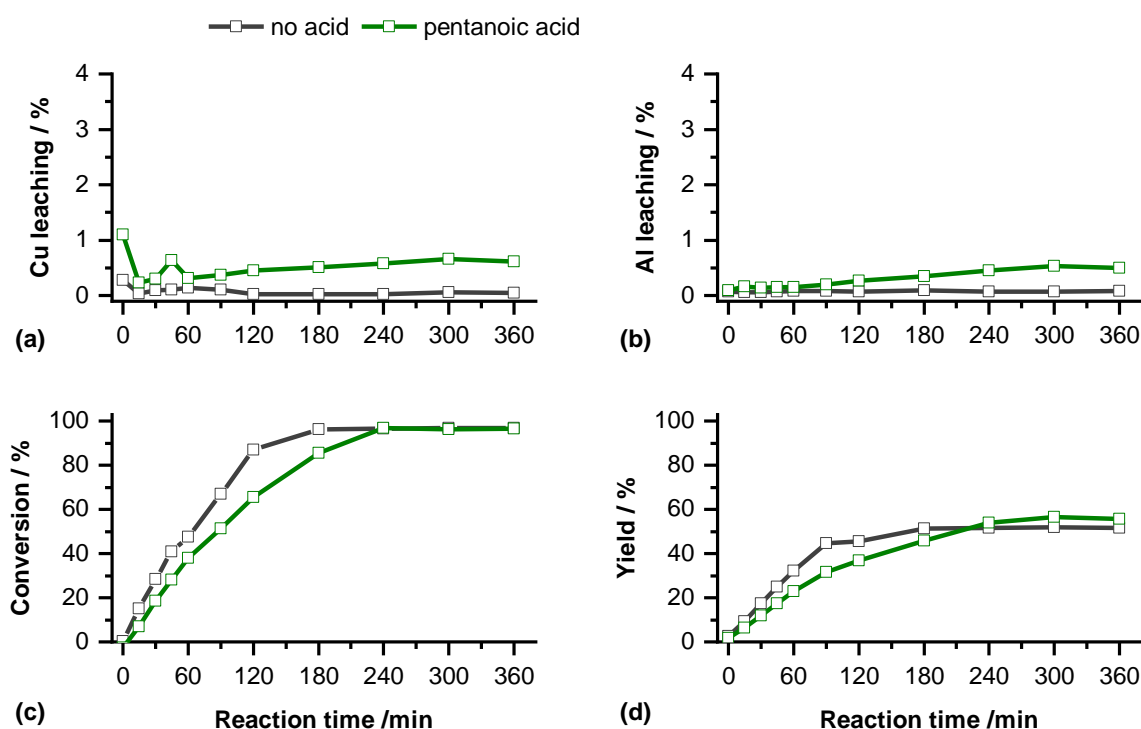


Figure 20: **Stoichiometric spinel catalyst - Leaching progression in hexane/1,4-dioxane mixture with pentanoic acid as additive (8 mol-%):** (a) Cu leaching, (b) Al leaching, (c) conversion of butyraldehyde, (d) butanol yield.

The mixture of hexane and 1,4-dioxane results in more leached copper and aluminum compared to the pure 1,4-dioxane. On the other hand, those values were very low to non-existing and the leaching observed in the samples in this section is still comparatively low. In contrast to the experiments using pure 1,4-dioxane as a solvent, the mixture of hexane and 1,4-dioxane once again allows product analysis via GC measurements due to the reduced peak width of 1,4-dioxane, which allows a good enough distinction of the neighboring peaks.

The stoichiometric spinel batch without acid does not show copper or aluminum leaching (Figure 20). The pentanoic acid addition leads to a slight increase of leaching around 0.5 % (Table 6), but there is no significant increase over reaction time which would affect the long-term stability of the catalyst. Both batches shown in Figure 20 reach similar conversion rates and yields after 6 hours. The non-acid batch has a quicker butyraldehyde conversion and reaches full conversion after 2-3 hours with a yield of 52 % butanol. The pentanoic acid batch (S-Sp) needs around 4 hours for full conversion of the educt, in turn it shows a slightly higher butanol yield (56 %). Compared to the corresponding pure hexane experiments the pentanoic acid batch shows a vast improvement in conversion rate and yield (see Table 1), the yield nearly doubles. The aluminum leaching is also decreased from over 2 % to around 0.5 %.

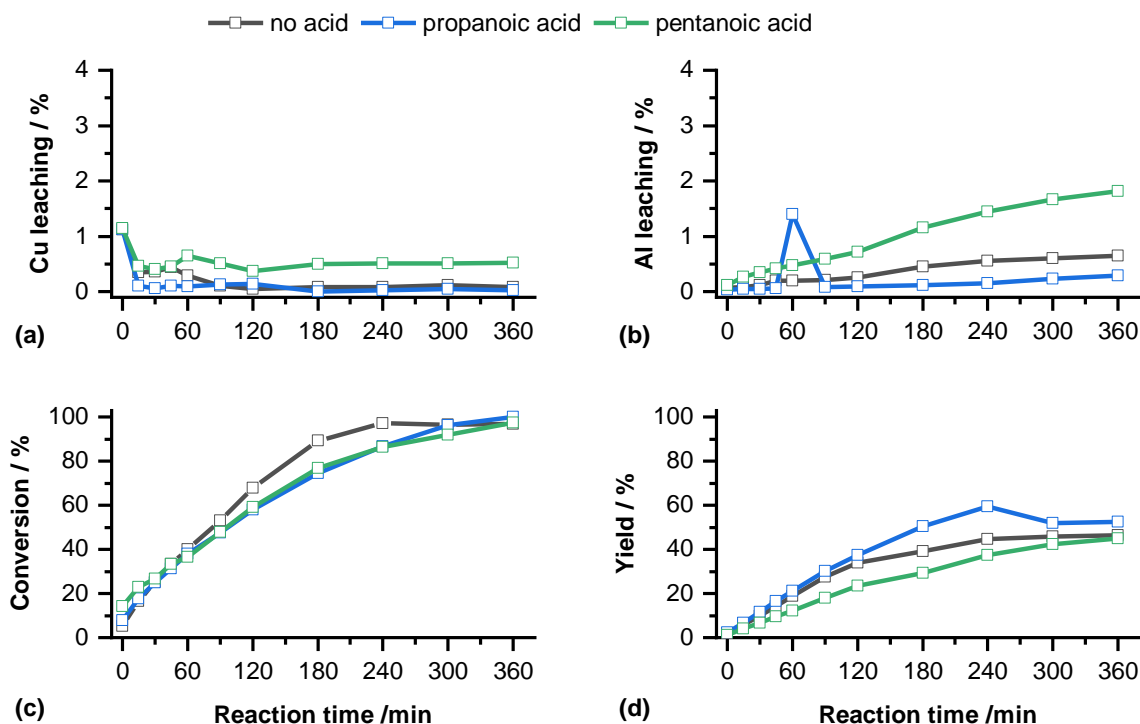


Figure 21: **Phase-pure spinel catalyst - Leaching progression in hexane/1,4-dioxane mixture with two different carboxylic acids as additives (8 mol-%):** (a) Cu leaching, (b) Al leaching, (c) conversion of butyraldehyde, (d) butanol yield in %-overall during the hydrogenation of butanal.

The phase-pure catalyst batches containing no acid addition or propanoic acid show no copper leaching after a few hours of reaction time (Figure 21a). The pentanoic acid batch shows a similar constant value of 0.5 % as the stoichiometric batches containing the hexane/1,4-dioxane mixture.

In contrast to its stoichiometric spinel counterpart, this pentanoic acid batch shows increased aluminum leaching which progresses steadily during the 6 hours of reaction time. After 6 hours it is close to 2 % aluminum in solution, but is still only half of the leached Al in pure hexane (P-Sp). The addition of 1,4-dioxane leads to an improvement concerning aluminum leaching, but does not repress or stabilize it completely as is the case for the stoichiometric spinel.

The three tested phase-pure spinel batches show very similar results for conversion and yield after 6 hours. The non-acid batch again shows the fastest conversion rate but is slightly slower compared to the stoichiometric spinel (4 hours vs 3 hours to full conversion). The experiments containing carboxylic acid additions need 5-6 hours to reach full conversion. The resulting yield after 6 hours is lower than using a stoichiometric spinel. Especially in the case of pentanoic acid addition the yield is 10 % lower (Table 6). The highest yield of 53 % is achieved with the additive of propanoic acid. Interestingly, the yield is close to 60 % after 4 hours but decreases in the following two hours. None of the other batches show this behavior. A secondary reaction consuming butanol seems to take place in the presence of propanoic acid.

Table 6: Leached Cu and Al in solution, conversion of butyraldehyde and butanol yield in %-overall after 6 hours of reaction time in a 10:1 mixture of hexane and 1,4-dioxane as a solvent.

% overall	Sample [min]	leached Cu*	leached Al*	Conversion Butanal ⁺	Yield Butanol ⁺
Stoichiometric spinel (CuO) · CuAl ₂ O ₄					
No acid	360	0.05	0.08	96.86	51.78
Propanoic acid	-	-	-	-	-
Pentanoic acid	360	0.61	0.50	96.68	55.69
Heptanoic acid	-	-	-	-	-
Phase-pure spinel CuAl ₂ O ₄					
No acid	360	0.08	0.65	96.80	46.46
Propanoic acid	360	0.02	0.29	99.98	52.61
Pentanoic acid	360	0.53	1.82	97.48	44.94
Heptanoic acid	-	-	-	-	-

* analyzed by ICP-OES; + analyzed by gas chromatography

Hexane + 10 mL ethanol

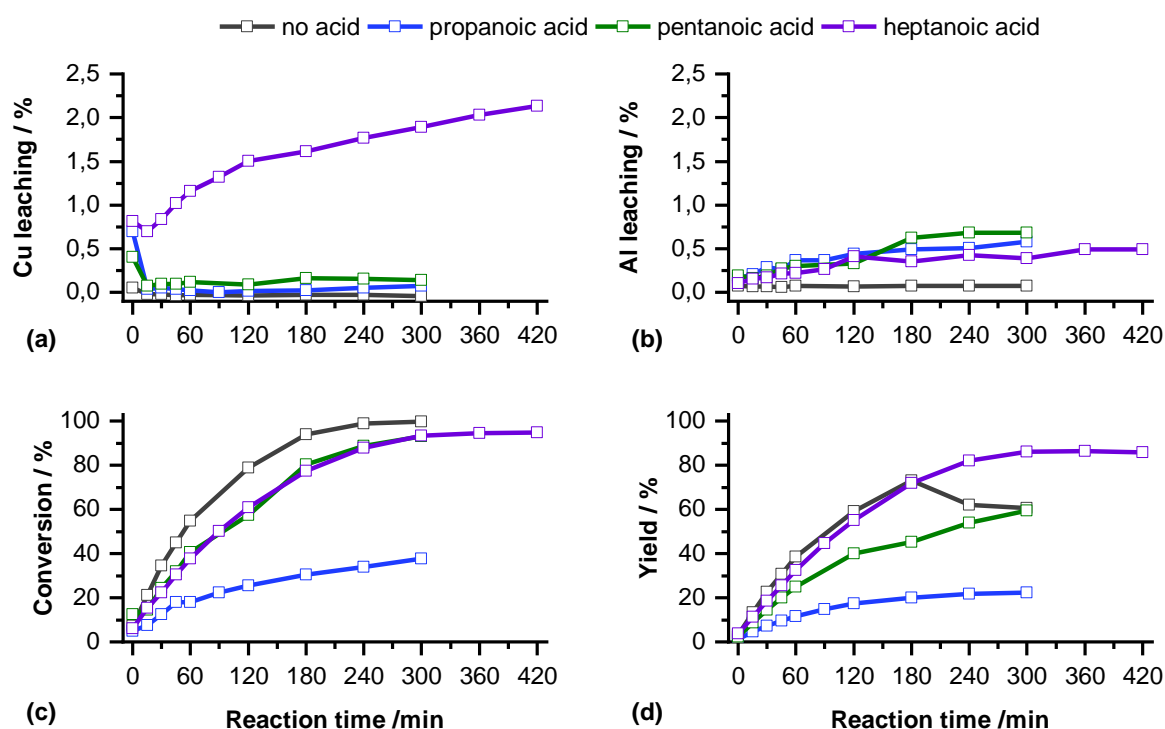


Figure 22: **Stoichiometric spinel catalyst - Leaching progression in hexane/ethanol mixture with three different carboxylic acids as additives (8 mol-%):** (a) Cu leaching, (b) Al leaching, (c) conversion of butyraldehyde, (d) butanol yield.

Apart from the heptanoic acid experiment, the addition of ethanol to the hexane solvent inhibits copper leaching as well as pure ethanol as a solvent (Figure 22a). The measured values using a stoichiometric spinel are well below 0.2 %. In addition, the previously observed trend of slowly increasing copper leaching after the educt conversion has finished is not present here (compare Figure 13a). The heptanoic acid batch (Figure 22a, purple line) does still show copper leaching in relevant amounts and keeps increasing during the ongoing reaction. After 7 hours the leached amount is over 2 % overall copper. The progression of the leaching curve is very similar to the one seen in pure hexane (Figure 8) but the overall leached amount is only one third compared to the hexane batch (6 % after 5 hours). The leached copper does not directly correlate with conversion rate or yield, which would be a sign towards catalyst deactivation due to a loss of active Cu^0 species to the solvent. On the contrary, the heptanoic acid batch shows a higher yield compared to all the other batches (86 % compared to 60% for pentanoic acid). The propanoic acid batch shows by far the lowest rates of conversion and yield. They only reach 38 % and 24.5 % respectively. Table 7 shows that the low rates in conversion and yield once again coincide with acetal formation. The propanoic acid batch is the only one of the stoichiometric spinel catalysts in hexane/ethanol solvent which shows a significant amount of acetal in the GC analysis (1.8 % after 5 hours). It increases more rapidly in the last two hours of the observed 5 hours reaction time which coincides with very little butanol

formation (Figure 23). The produced acetal is a lot less compared to the amount formed in some batches in pure ethanol (up to 50 % acetal formation in pentanoic acid batches) but even this small amount negatively impairs the hydrogenation reaction. But in this case here, not only the butanol yield but also the conversion rate of the educt is affected.

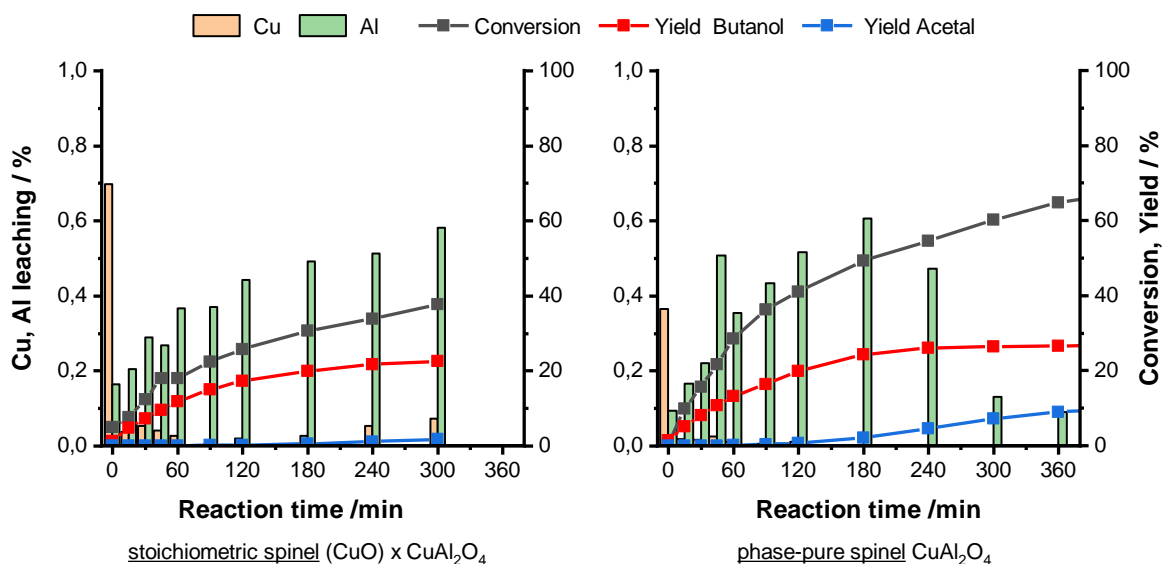


Figure 23: **Increased acetal formation in hexane/ethanol mixture.** Both, stoichiometric and phase-pure spinel catalyst, show very low butanol yield when propanoic acid is present in the solvent. The acetal formation (blue curve) notably impedes the desired formation of butanol, the majority of the butyraldehyde educt is transformed into acetal. The stoichiometric spinel batch produces less acetal, but the conversion rate and butanol yield remain low.

The aluminum leaching behavior is quite similar for the batches containing carboxylic acids, the acid-free batch shows no Al leaching at all (Figure 22). The results show a slight increase in leaching over reaction time with 0.6 % - 0.7 % after 5 hours. Those values are slightly higher than in pure ethanol or 1,4-dioxane (practically no aluminum leaching was found) but considerably lower than in toluene or hexane. The values are similar to those in the hexane/1,4-dioxane solvent mixture (Table 6).

The phase-pure spinel catalysts show a similar qualitative behavior to the stoichiometric ones in Figure 22 but there are also small differences (Figure 24). The heptanoic acid batch is again the only one that shows any quantifiable copper leaching. In contrast to its stoichiometric counterpart the copper leaching is only around 0.5 % and does not significantly increase during the reaction.

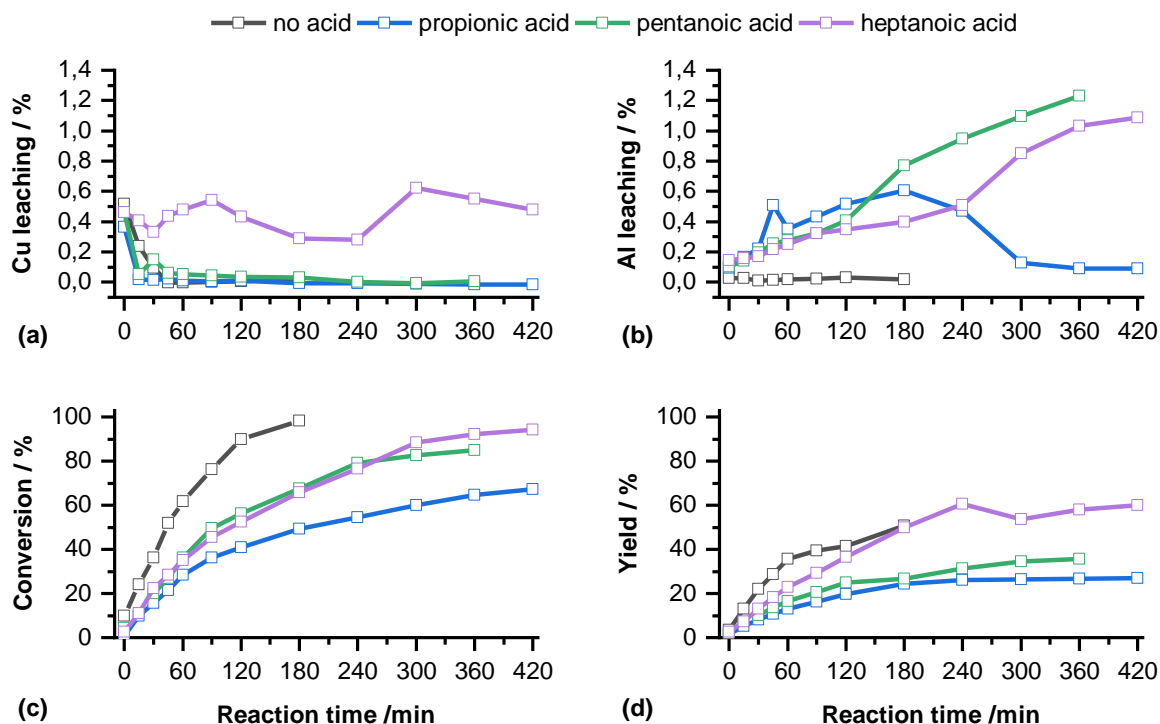


Figure 24: **Phase-pure spinel catalyst - Leaching progression in hexane/ethanol mixture with three different carboxylic acids as additives (8 mol-%):** (a) Cu leaching, (b) Al leaching, (c) conversion of butyraldehyde, (d) butanol yield.

The leached aluminum is slightly different compared to the stoichiometric spinel batches. The non-acid batch once again shows no aluminum leaching. The propanoic acid batch shows an intermediate increase in aluminum leaching (up to 0.6 % in the first three hours of reaction time) which decreases again to barely any Al leaching in the last three hours (0.1 %). In contrast to those two experiments, the batches containing pentanoic or heptanoic acid show continuous aluminum leaching which reaches about 1 % after 6 hours. Apart from pure ethanol or 1,4-dioxane, those are still the lowest observed aluminum values in solution for the leached spinel catalysts. They are a bit higher than the corresponding leached aluminum values of the stoichiometric spinel catalyst (Table 7).

The progression of conversion and yield are quite similar to its stoichiometric counterparts but the overall butanol yield is lower for all experiments in comparison to the stoichiometric spinel version. Propanoic acid once again shows the lowest yield but the pentanoic acid batch is in this case also severely lower in butanol yield. A look at Table 7 shows that those two batches have quantifiable acetal formation, in the case of propanoic acid up to 10 %. As seen before, even a small amount of acetal formation signals a negative effect on the desired butanol formation. In case of pentanoic acid addition only the butanol yield is affected whereas the butyraldehyde conversion progresses similarly to the heptanoic acid batch. The propanoic acid

batch with the highest acetal yield of 10 % is both affected in conversion speed and butanol yield (67 % and 27 % respectively, see Figure 23).

Table 7: Leached Cu and Al in solution, conversion of butyraldehyde and butanol yield in %-overall after 5-7 hours of reaction time in a 10:1 mixture of hexane and ethanol as a solvent.

% overall	Sample [min]	leached Cu*	leached Al*	Conversion Butanal ⁺	Yield Butanol ⁺	Yield Acetal ⁺
Stoichiometric spinel (CuO) · CuAl ₂ O ₄						
No acid	300	0	0.07	99.67	60.61	0.14
Propanoic acid	300	0.07	0.58	37.73	22.47	1.81
Pentanoic acid	300	0.14	0.69	93.14	59.47	0.25
Heptanoic acid	300	1.89	0.39	93.34	86.07	0.11
Heptanoic acid	420	2.14	0.49	94.93	85.74	0.12
Phase-pure spinel CuAl ₂ O ₄						
No acid	180	0.02	0.02	98.28	50.80	0.10
Propanoic acid	360	0	0.09	64.71	26.59	9.02
Propanoic acid	420	0	0.09	67.42	26.98	9.92
Pentanoic acid	360	0.00	1.23	84.97	35.61	1.30
Heptanoic acid	360	0.55	1.03	92.20	57.93	0.28
Heptanoic acid	420	0.48	1.09	94.38	60.14	0.29

* analyzed by ICP-OES (if the value is given as 0 it was below the limit of quantitation of the instrument)

+ analyzed by gas chromatography

The switch to a mixture of hexane and a second solvent (10:1) indicate improved catalytic performance and stability, when solvents of higher polarity are added. There is no real improvement in the case of toluene. 1,4-dioxane and ethanol addition both diminish the leaching of copper and aluminum compared to pure hexane significantly (Figure 25). In the case of ethanol addition there is also in many cases a positive effect on conversion rate and product yield, which was already observed in the pure ethanol experiments. On the other hand, the problem of acetal formation is again an observation for the addition of a small portion of ethanol. Here the samples containing propanoic acid were more vulnerable whereas in pure ethanol this was the case for experiments containing pentanoic acid. This trend needs to be further studied to avoid the formation of acetals instead of butanol.

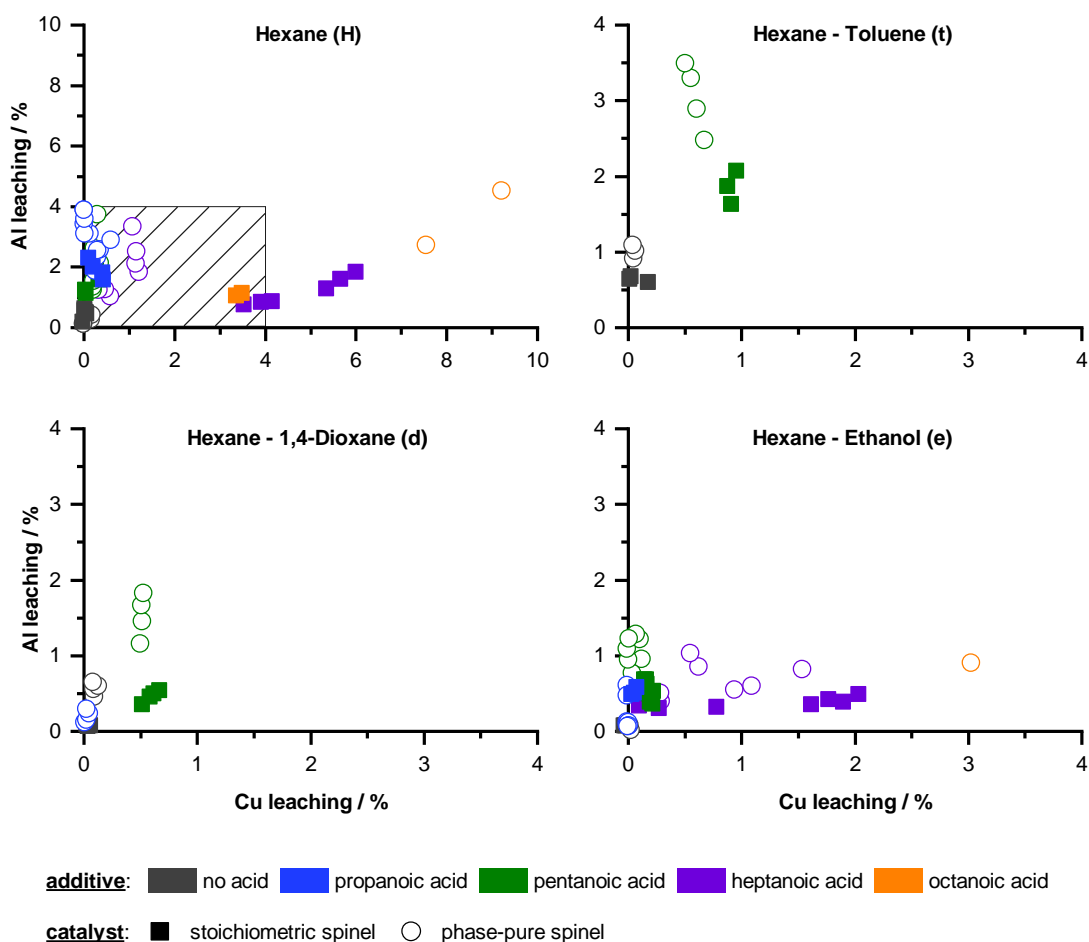


Figure 25: **Scatter plot of Cu and Al leaching in solvent mixtures** (≥ 3 hours of reaction time). For easier comparability the samples using pure hexane are plotted as well (top left), the range of the other three subplots is marked by the hatched rectangle. The acid additives are color coded the same as in previous plots. Full symbols signify stoichiometric spinel, empty symbols phase-pure spinel batches.

2.4.6 Long term experiments – stability investigation

To get a better notion of the long-term leaching behavior select experiments were studied over a longer reaction time. The sampling intervals at the start of the reaction were kept to get a conclusive curve progression which can also be compared to the other related experiments. Samples were taken during the first 4-5 hours of the reaction. The autoclave was then left under reaction conditions (increased hydrogen pressure, 120° C, stirred with 800 RPM) and additional samples were taken the next day. For these long-term experiments, the previously established standard condition batches in hexane and the solvent mixture of hexane and ethanol was tested for both stoichiometric and phase-pure spinel catalysts. Since the carboxylic acid batches were found to produce the most extreme changes in leaching or yield, only those were tested long-term. The corresponding (“short-term”) non-acid experiment is still shown in the plots as a visual reference.

Hexane

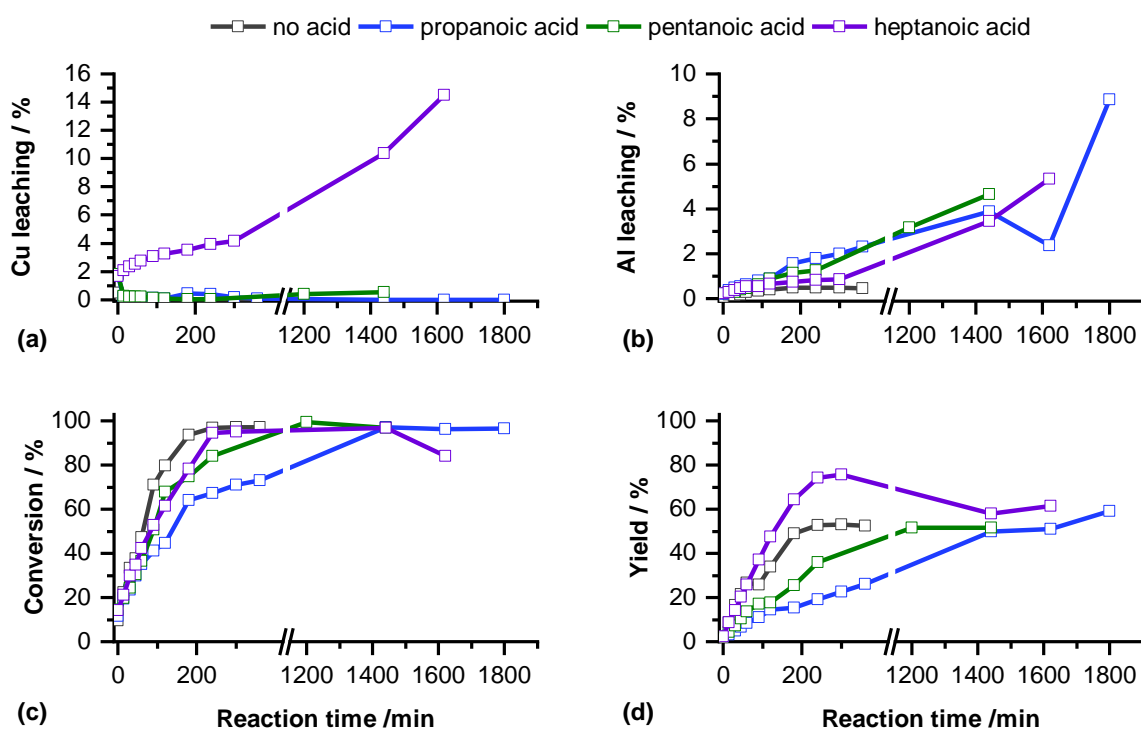


Figure 26: **Stoichiometric spinel catalyst - Leaching progression over 24h in hexane with three different carboxylic acids as additives (8 mol-%):** (a) Cu leaching, (b) Al leaching, (c) conversion of butyraldehyde, (d) butanol yield. during the hydrogenation of butanal. There is an axis break between 400 and 1150 min to simplify the depiction of the longer time frame. There were no samples taken during this time period.

The trends observed from previous experiments using the stoichiometric spinel catalyst in hexane in the presence of carboxylic acids were increased copper leaching only in the presence of heptanoic acid whereas all acid batches showed an increase in aluminum leaching over reaction time, without a distinction between alkyl chain length (Figure 8). The highest yield and conversion were obtained by the heptanoic acid batch. The pentanoic acid batch showed a similar conversion rate but only half the yield. Propanoic acid showed slow conversion and low yield.

Most of those trends can also be found in the longer experimental series (Figure 26). The heptanoic acid batch remains the only one with relevant copper leaching. Problematically, the previously anticipated stabilization of the leached copper does not occur. The copper leaching keeps progressing with reaction time and reaches the highest copper leaching yet observed with 15 %. A similar observation is true for the aluminum leaching. The carboxylic acid experiments all continue to leach aluminum into solution. They also show continuous increase (slope). Both of these trends are rather worrying concerning the stability of the catalyst. Especially the continuous leaching of aluminum from the spinel lattice cannot be compensated indefinitely. The product analysis of the solution shows that all experimental batches (with or

without acid additive) seem to reach a similar amount of butanol yield. Propanoic acid addition still shows the slowest conversion rate but also reaches 51 % butanol yield after longer time. Since the pentanoic acid experiment shows a very similar behavior in the first 5 hours of reaction, the same can be expected here. The heptanoic acid batch shows signs of a secondary reaction taking place after butyraldehyde conversion is finished. It reaches (close) to full conversion after 4-5 hours with a butanol yield at this time of 75 %. After 24 hours the butanol found in the GC analysis has diminished to 58 %. This value is closer to the other experiment done with an analogous batch composition.

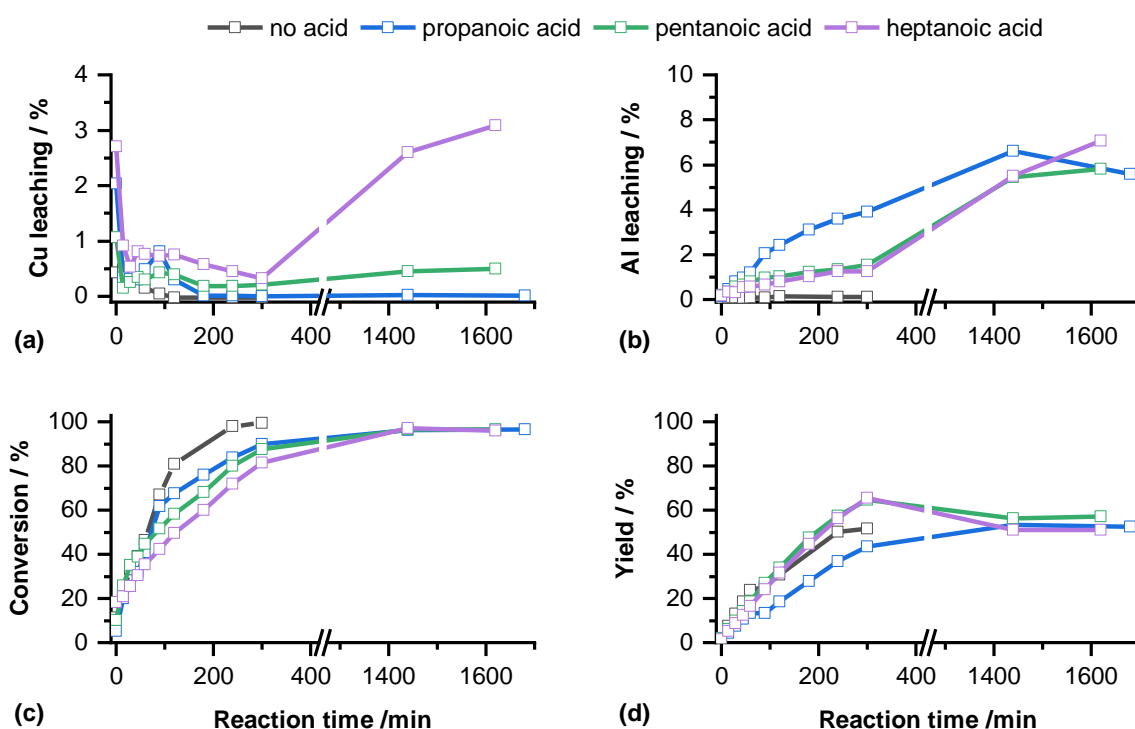


Figure 27: **Phase-pure spinel catalyst - Leaching progression over 24h in hexane with three different carboxylic acids as additives (8 mol-%):** (a) Cu leaching, (b) Al leaching, (c) conversion of butyraldehyde, (d) butanol yield. during the hydrogenation of butanal. There is an axis break between 400 and 1150 min to simplify the depiction of the longer time frame. There were no samples taken during this time period.

The long-term experiments using the phase-pure spinel show some trends which were not anticipated from the previous short-term experiments. Previously the carboxylic acid batches showed low (heptanoic acid, stable at 1%) or no copper leaching. The samples after 24 hours now show that only the propanoic acid batch does not show copper leaching. The pentanoic acid batch shows some increase but is still very low at 0.5 % whereas the heptanoic acid batch shows a strong increase up to 3%. The previously observed trend suggested a stable low copper leaching. The amount of leached copper is a lot lower than using a stoichiometric spinel

with a lot more surface copper available, but the trend of increased leaching might still be a problem for long-term catalyst stability.

The Al leaching also increases consistently over time for all three batches. In this case, there is some separation of the leaching behavior in the first hours of reaction: increasing for propanoic acid, stable for the other two batches (Figure 27). The previous experiments showed a very similar increase in aluminum leaching in the first few hours (Figure 9). Nonetheless, the three batches arrive at similar aluminum leaching amounts of 6 % after 24 hours of reaction time. This is slightly higher than the aluminum leaching of their stoichiometric counterpart. All experiments reach (close to) full conversion after 27 hours of reaction time (Table 8) and, regardless of conversion rate, a very similar butanol yield. Interestingly both the heptanoic and pentanoic acid addition show a higher butanol yield in the middle part of the reaction time and show the same lower final yield as the propanoic acid batch. The non-acid batch again shows the highest conversion rate and reaches full conversion within the first 5 hours of reaction time with a similar butanol yield as the other batches containing carboxylic acid additives. The phase-pure spinel reaches slightly lower but similar yields as the stoichiometric spinel (see Table 8).

Table 8: Leached Cu and Al in solution, conversion of butyraldehyde and butanol yield in %-overall after 24 hours or more of reaction time in hexane as a solvent.

% overall	Sample [min]	leached Cu*	leached Al*	Conversion Butanal ⁺	Yield Butanol ⁺
Stoichiometric spinel (CuO) · CuAl ₂ O ₄					
No acid	360 min	0.05	0.46	97.13	52.60
Propanoic acid	27 h	0.01	2.38	96.19	51.05
Propanoic acid	30 h	0	8.88	96.66	59.31
Pentanoic acid	24 h	0.55	4.64	96.82	51.53
Heptanoic acid	27 h	14.52	5.34	84.00	61.52
Phase-pure spinel CuAl ₂ O ₄					
No acid	300 min	0	0.12	99.39	51.77
Propanoic acid	28 h	0.02	5.58	96.71	52.48
Pentanoic acid	27 h	0.50	5.82	96.62	57.10
Heptanoic acid	27 h	3.09	7.06	96.17	51.00

* analyzed by ICP-OES (if the value is given as 0 it was below the limit of quantitation of the instrument)

+ analyzed by gas chromatography

Hexane + 10 mL ethanol

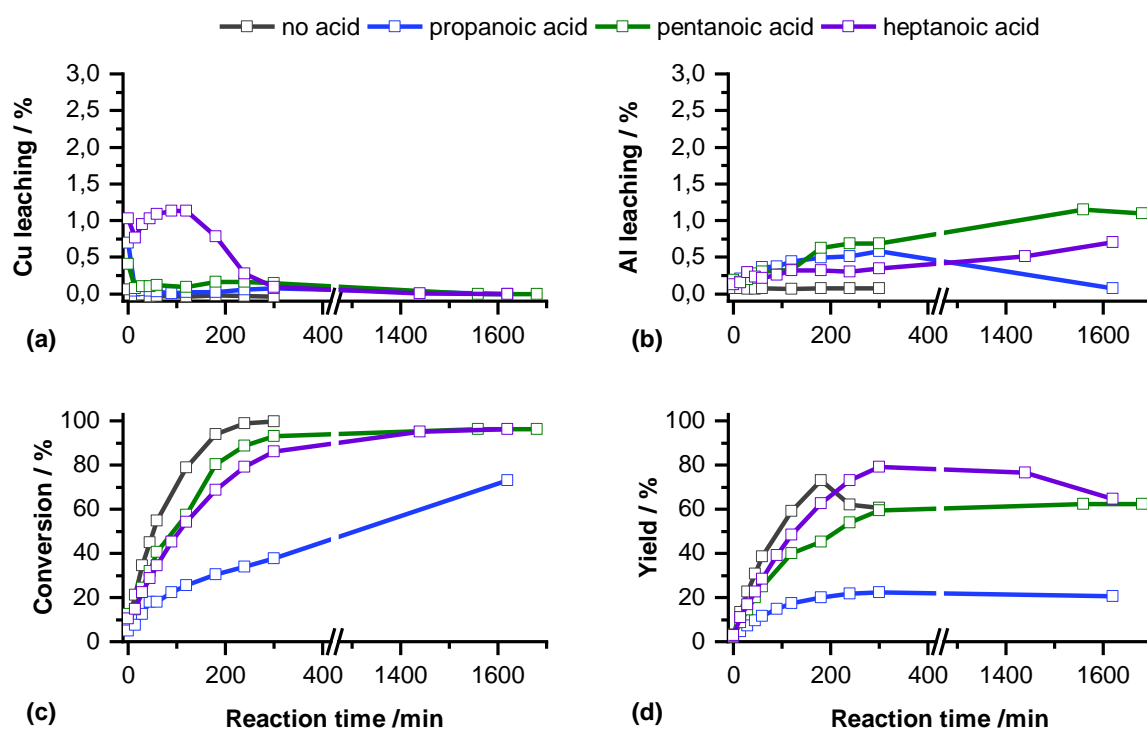


Figure 28: **Stoichiometric spinel catalyst - Leaching progression over 24h in hexane/ethanol mixture with three different carboxylic acids as additives (8 mol-%):** (a) Cu leaching, (b) Al leaching, (c) conversion of butyraldehyde, (d) butanol yield. during the hydrogenation of butanal. There is an axis break between 400 and 1150 min to simplify the depiction of the longer time frame. There were no samples taken during this time period

The long-term experiments of the stoichiometric spinel in the hexane/ethanol mixture mostly show the trends already established in the first few hours of reaction time. There is no increase in leaching for longer reaction times though there is some increase in aluminum leaching for selected batches. The overall aluminum leaching remains low compared to other solvent mixtures with around 1 % of aluminum leaching after 27-28 hours. The shorter chain length carboxylic acids additionally show a decreasing (propanoic) or at least stabilizing (pentanoic acid) trend. None of the experimental batches show copper leaching after 24 hours of reaction time. The only one showing some quantifiable copper leaching is the heptanoic acid batch during the first 3 hours of the reaction, maximum 1%. This is surprising for the heptanoic acid batch, the previous shorter experiments did not show a decrease in copper leaching with time. All other batches also had low to no copper leaching during the shorter reaction time period when using a hexane/ethanol mixture. The yield and conversion progression follow the trends established previously by the shorter reaction times. The propanoic acid batch again battles with a very slow conversion rate and low butanol yield due to the competing formation of acetal (Figure 29). None of the other stoichiometric spinel batches show high acetal yields (Table 9). The longer reaction time shows that the conversion of the butyraldehyde is still on-going after

24 hours but there is no further increase in butanol yield. There is no quantifiable acetal formation in the first 3 hours of reaction time. In this time span the amount of formed butanol steadily increases, though a lot slower than in the other batches. The conversion of butyraldehyde is a lot slower as well. After three hours of reaction time the formation of acetal begins and in turn the butanol yield stagnates. The conversion of butanal keeps progressing slowly but steadily, but no new butanol is formed. The formed acetal has increased to 9% after 27 hours.

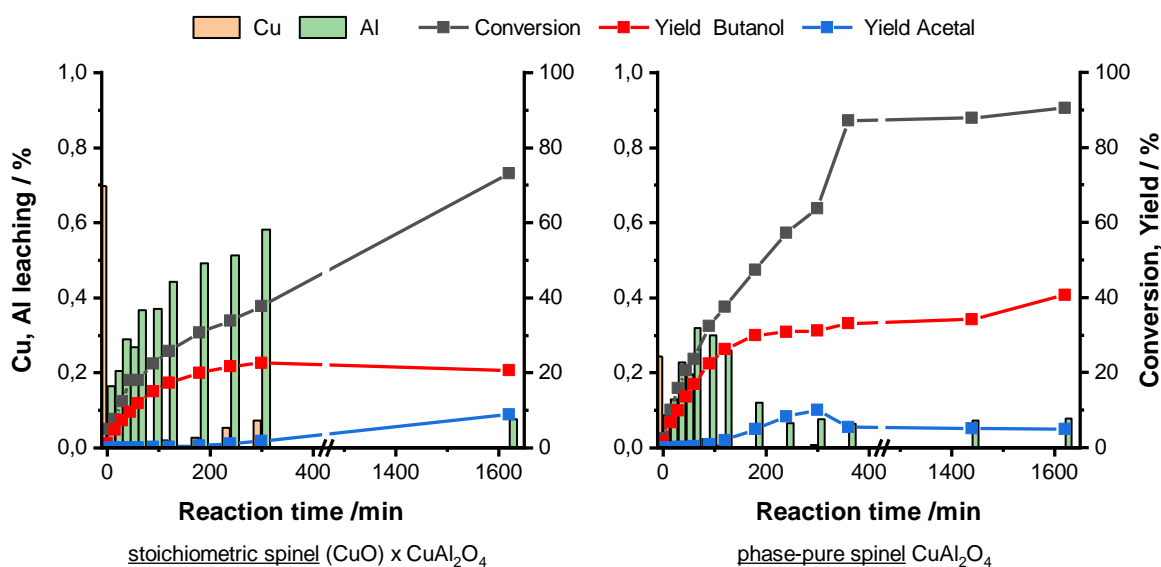


Figure 29: **Increased acetal formation in hexane/ethanol mixture after 24h.** Both, stoichiometric and phase-pure spinel catalyst, show decreased butanol yield when propanoic acid is present. The two catalysts show different progression in acetal formation, but both end with a stagnating formation of butanol and quantifiable amounts of acetal in the resulting liquid composition.

The phase-pure spinel, in contrast to the stoichiometric spinel, does not show continuous acetal formation but a steeper increase in acetal early in the reaction (10% acetal yield after 5 hours) and afterwards a decrease and stabilization of the present acetal amount (around 5% acetal). The butanol formation keeps increasing over the whole observed reaction time, but the increase after the first three hours is very small (30% after 3 hours vs 34% after 24 hours). In the remaining three hours the butanol unexpectedly increases again to about 40%. Nonetheless, this batch reaches nearly double the butanol yield compared to its stoichiometric counterpart. The butyraldehyde conversion progresses noticeably faster than in the stoichiometric batch, the conversion curve fits well with the curve of the shorter experiments in the same solvent mixture (Figure 23). The progression of the analyzed parameters overall fit very well with the shorter-term experiment values, so a comparison of those values with the ones achieved in longer experiment runs seems appropriate.

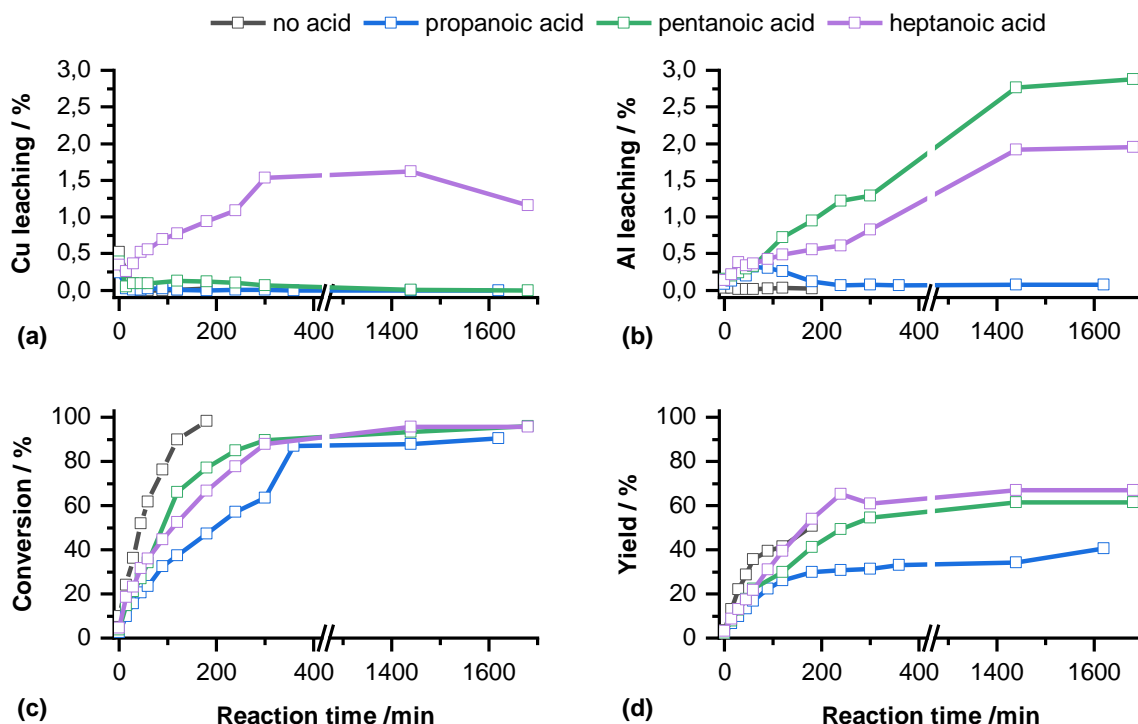


Figure 30: **Phase-pure spinel catalyst - Leaching progression over 24h in hexane/ethanol mixture with three different carboxylic acids as additives (8 mol-%):** (a) Cu leaching, (b) Al leaching, (c) conversion of butyraldehyde, (d) butanol yield. during the hydrogenation of butanal. There is an axis break between 400 and 1150 min to simplify the depiction of the longer time frame. There were no samples taken during this time period.

The phase-pure spinel batches show a logical progression of the previously observed trends when analyzing samples after longer reaction times. The most different behavior can be seen in the propanoic acid batch which has been discussed in the previous paragraph already. Copper leaching is not an issue for any of the batches apart from the heptanoic acid experiment. As seen already in Figure 24a there is a very low amount of copper leaching during the whole observed reaction process. This is also true after 24 hours, though the copper leaching reaches slightly higher overall amounts compared to the shorter experimental series. The heptanoic acid experiment in Figure 30 shows a steady increase in leached copper in the first 5 hours but the samples after 24 hours show that the copper amount stabilizes and might even decrease again with time. Thus, the overall amount of copper lost due to leaching does not appear to be a long-term factor in this case, in contrast to its behavior in pure hexane (see Figure 27).

All batches show similar low aluminum leaching in the first two hours of the reaction (about 0.5 %). The behavior changes after that, with the propanoic acid batch leaching going to zero whereas the other two batches steadily increase up to about 2 and 3 % aluminum leached after 24 hours. This behavior again fits with the observed trends in Figure 24. The increase in

aluminum leaching coincides with a slower hydrogenation of butyraldehyde to butanol. Reassuringly, the aluminum leaching of both the pentanoic and heptanoic acid batch seem to stabilize at the previously mentioned values and does not increase between 24 and 27 hours of reaction time. The overall leached aluminum amount is (as seen before in other batches) higher for the phase-pure spinel compared to the stoichiometric spinel.

The educt conversion and product yield of the pentanoic and heptanoic acid batch progress nearly identical, with the pentanoic acid batch showing slightly faster conversion progression whereas the heptanoic acid batch achieves a higher total yield (see Table 9). The conversion trends of both batches show the same behavior as seen previously in the short-term experimental series, but the yield with the pentanoic acid batch is much higher compared to the correlating previous batch (34.5 vs. 54.5 % yield butanol after 5 hours). Also, both batches don't show the "dip" in butanol yield which was present for both in the long-term experiments using hexane (compare Figure 27).

Table 9: Leached Cu and Al in solution, conversion of butyraldehyde and butanol yield in %-overall after 24 hours or more of reaction time in a 10:1 mixture of hexane and ethanol as a solvent.

% overall	Sample [min, h]	leached Cu*	leached Al*	Conversion Butanal ⁺	Yield Butanol ⁺	Yield Acetal ⁺
Stoichiometric spinel (CuO) · CuAl ₂ O ₄						
No acid	300 min	0	0.07	99.67	60.61	0.14
Propanoic acid	27 h	0	0.08	73.13	20.65	8.84
Pentanoic acid	26 h	0	1.15	96.21	62.24	0.42
Pentanoic acid	28 h	0	1.10	96.22	62.37	0.45
Heptanoic acid	27 h	0	0.70	96.34	64.72	0.30
Phase-pure spinel CuAl ₂ O ₄						
No acid	180 min	0.02	0.02	98.28	50.80	0.10
Propanoic acid	27 h	0	0.08	90.56	40.62	4.90
Pentanoic acid	28 h	0	2.88	96.01	61.41	0.71
Heptanoic acid	28 h	1.16	1.95	95.85	66.92	0.19

* analyzed by ICP-OES (if the value is given as 0 it was below the limit of quantitation of the instrument)

+ analyzed by gas chromatography

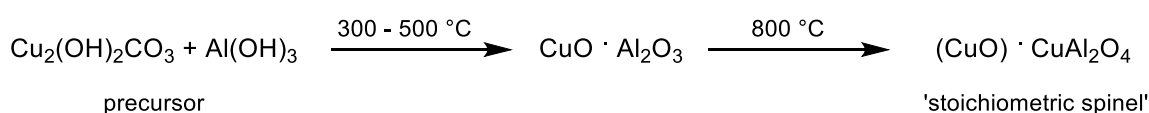
2.4.7 Synthesis and characterization of the catalysts

In order to understand the role of preparation and composition of the copper aluminate spinel catalysts on leaching behavior, three different types of catalysts were prepared:

- (i) the phase-pure spinel CuAl_2O_4 , where CuO residues always remaining on the surface of copper aluminate spinel after preparation were removed by an optimized copper leaching procedure,
- (ii) the “original” spinel forming during synthesis, the so-called stoichiometric spinel $(\text{CuO}) \cdot \text{CuAl}_2\text{O}_4$ after calcination (having a slight excess of CuO on the spinel surface), and
- (iii) the copper oxide-copper aluminate spinel, $\text{CuO} \cdot \text{CuAl}_2\text{O}_4$, analog to the previously established Cu-Cr Adkins catalyst, $\text{CuO} \cdot \text{CuCr}_2\text{O}_4$, which contained a stoichiometric excess of CuO, practically supported on copper aluminate.

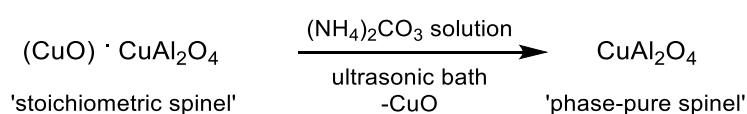
Synthesis by Co-precipitation

All three spinel variants were synthesized by co-precipitation, using stoichiometric amounts of aluminum nitrate and copper nitrate dissolved in water as a feed solution. The co-precipitation takes place in water with sodium carbonate solution as a precipitating agent. The detailed synthesis steps and weight amounts can be found in the Experimental Section (Chapter 6). All precursors were washed, dried at 120 °C over night and calcined at 800°C to form the spinel lattice (Equation 6).



Equation 6: Formation of the Cu-Al spinel by calcination at 800 °C (intermediate formation of $\text{CuO} \cdot \text{Al}_2\text{O}_3$ at temperatures below 700 °C)

The preparation of $\text{CuO} \cdot \text{CuAl}_2\text{O}_4$ and the stoichiometric spinel is finished after the calcination step (followed by reductive activation just before the catalytic reaction). The phase-pure spinel requires an additional synthesis step removing the intermittent surface copper oxide layer, with CuAl_2O_4 remaining (Equation 7).



Equation 7: Leaching step to form the “phase-pure” CuAl_2O_4

All catalysts are sieved prior to activation and the fraction between 100 and 300 μm is used in the catalysis and leaching experiments. The elemental composition of the catalysts determined by ICP-OES after dissolution in concentrated phosphoric acid is given in Table 10.

Table 10: Elemental composition of Cu-Al spinels, determined by ICP-OES.

Catalyst	w_{Cu} (wt.-%)	w_{Al} (wt.-%)
$\text{CuO} \cdot \text{CuAl}_2\text{O}_4$	50 - 51.5	18 - 19
$(\text{CuO}) \cdot \text{CuAl}_2\text{O}_4$	35.5 - 37	27,5 - 29
CuAl_2O_4	33 - 34.5	30 - 32

BET surface and Cu surface calculation by chemisorption

In contrast to “classic” supported catalysts used in catalysis, all three Cu-Al spinels have a comparatively low copper surface area due to their nature as a bulk catalyst composed of a spinel lattice. The copper surface was determined by N_2O chemisorption. The (activated) phase-pure spinel shows a copper surface area of $10.5 \text{ m}^2\text{g}^{-1}$. This is in good agreement with values obtained in other studies, ranging between 9 and $11 \text{ m}^2\text{g}^{-1}$.^[31, 47] The stoichiometric spinel is in a similar range whereas the $\text{CuO} \cdot \text{CuAl}_2\text{O}_4$ shows a slightly higher Cu surface area around $15 \text{ m}^2\text{g}^{-1}$. This is to be expected because of the additional CuO on the spinel surface compared to the other two spinels. The BET surface area found was very low with $18 \text{ m}^2\text{g}^{-1}$. Other works reported BET areas ranging from 50-100 m^2g^{-1} .^[27, 47, 60] This is an indication that the synthesis conditions (molar ratio of Cu:Al, calcination temperatures, calcination time) play a critical role when it comes to the BET surface area determination. As Ahmed et al. report, the spinel formation has a large influence on the BET surface area, losing up to $100 \text{ m}^2\text{g}^{-1}$ between the calcination temperatures of 700° and 900°C .^[60] With a calcination temperature of 800°C in our spinel synthesis, this is exactly the temperature range when the BET surface area changes drastically due to the diffusion of CuO and formation of the spinel lattice. This could be a possible explanation for the wide range of reported values.

Temperature-programmed reduction

Temperature-programmed reduction experiments in H_2 (see Figure 31) fit well with the results reported in literature^[36, 39, 46]. The copper aluminate spinels show two distinct peaks, one in the range of $150\text{-}200^\circ\text{C}$ and a second broader peak between $350\text{-}400^\circ\text{C}$. According to literature, the first peak corresponds to the reduction of surface Cu(II) to Cu(0) whereas the second peak shows the reduction of copper within the spinel lattice.^[46] This fits very well when comparing the stoichiometric and the phase-pure spinel: the higher amount of CuO on the surface results in a larger, narrower reduction peak shifted to lower temperatures, highlighting the differences

between stoichiometric and phase-pure spinel. The TPR results suggest that even the phase-pure spinel retains a small amount of more-easily reduced surface Cu(II). If this is residual CuO or due to a deformation of the upper surface layer due to the previous leaching steps is not clear yet. The second peak associated with the reduction of copper from deeper within the spinel lattice is nearly uniform for both spinels.

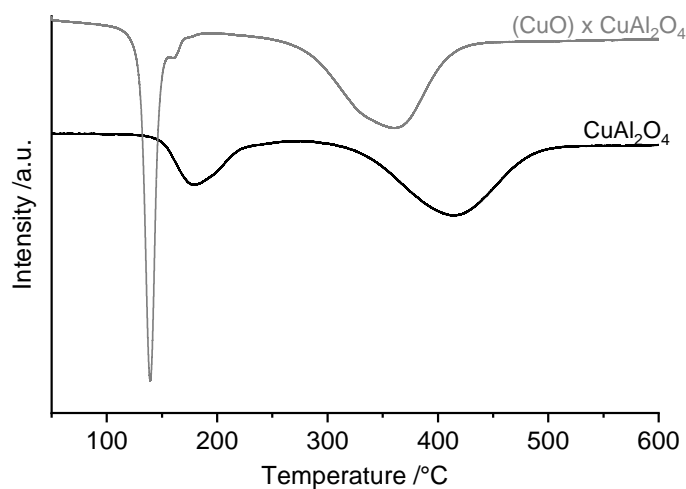


Figure 31: Reduction profile of stoichiometric^[47] and phase-pure spinel.

Phase composition investigated by powder X-Ray diffraction

The differences in the structure and composition of the three Cu-Al spinels can also be observed using powder X-ray diffraction (p-XRD) measurements as well as Raman spectroscopy. Whereas the p-XRD investigations are more representative of the bulk composition of the sample, using a Raman microscope can distinguish between different sub-species which make up the precursor and catalyst sample.

The measurements give a good indication and determination of the present copper species (elemental copper, copper oxide species, copper aluminate spinel) and present an idea of the bulk composition of the measured powder sample. The main phases are assigned according to references from the Powder Diffraction FileTM database PDF-2 (2004).^[61]

Adkins analog - CuO · CuAl₂O₄

The CuO · CuAl₂O₄ spinel is prepared as an analog to the established Adkins hydrogenation catalyst which consists of Cu(II)oxide on a copper chromite support. The copper aluminate equivalent results in CuO · CuAl₂O₄ which corresponds to a stoichiometric Cu:Al ratio of 1:1. Figure 32 shows the p-XRD diffractograms of the resulting (a) precursor, (b) calcined spinel and (c) catalyst after activation in hydrogen.

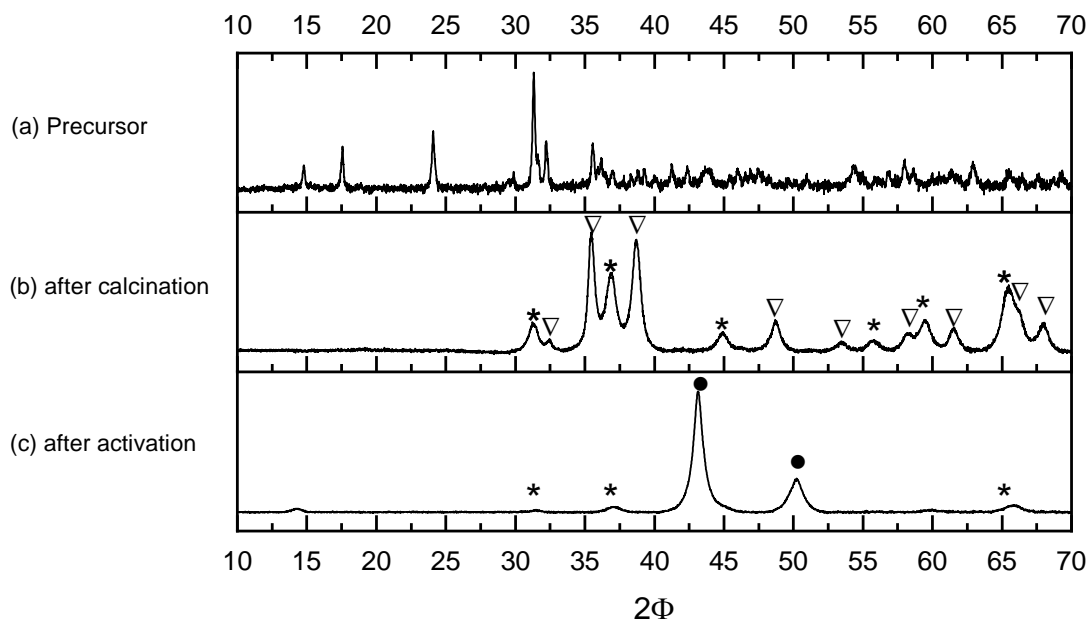


Figure 32: p-XRD diffractogram of the $\text{CuO} \cdot \text{CuAl}_2\text{O}_4$ spinel during synthesis and after activation in hydrogen. (a) dried precatalyst after co-precipitation of copper- and aluminum nitrate solution in water. The reflexes are consistent with a malachite-like structure. (b) catalyst after calcination at 800°C . The diffractogram shows clear reflexes of CuAl_2O_4 and CuO without additional phases. The copper oxide reflexes dominate the diffractogram. (c) catalyst after activation in hydrogen flow and slowly heating to 300°C .

The main reflexes of CuAl_2O_4 (★), CuO (▽) and Cu^0 (●) are marked in the plot, according to the Powder Diffraction File™ database PDF-2 (2004).^[61]

The washed and dried precursor of $\text{CuO} \cdot \text{CuAl}_2\text{O}_4$ shows the main reflexes of a malachite structure $\text{Cu}_2(\text{CO}_3)(\text{OH})_2$, as can be expected. Another copper hydroxide carbonate configuration would be an azurite structure, $\text{Cu}_3(\text{CO}_3)_2(\text{OH})_2$. The formation of azurite can happen at pH 6-7 but it requires a higher carbonate concentration compared to malachite formation. Azurite is also less stable in air and gets pseudomorphically replaced by malachite due to the replacement of CO_2 with H_2O over time.^[62] At pH 6-7 aluminum precipitates as amorphous $\text{Al}(\text{OH})_3$ and cannot be detected by XRD.^[63]

After calcination (Figure 32b) the most prominent reflexes belong to copper(II) oxide, easily identifiable at 35.5° and 38.7° and 48.9° . Apart from CuO , the copper aluminate spinel can also be found in the diffractogram, marked by an ★ in the plot. The reflexes in the region above 50° tend to overlap with the reflexes of the copper(II) oxide situated there, but they can still be separated well enough to assign both mineral phases.

Figure 32c shows the CuO-spinel catalyst after activation in hydrogen, slowly heating it under hydrogen flow to 300 °C. All the previously present copper(II) oxide has been reduced to Cu(0), the main reflexes are marked by •. There are very weak reflexes left at 31.3 °, 36.8 ° and 65.3 ° corresponding to the main features of CuAl₂O₄ but the diffractogram overall is dominated by the formed metallic copper particles.

The subsequent two catalysts both have the theoretical stoichiometric copper: aluminum ratio of 1:2. They are formed from an identical precatalyst.

Stoichiometric spinel - (CuO) · CuAl₂O₄

The washed and dried precursor of the stoichiometric spinel shows a malachite structure, which is very similar to the CuO · CuAl₂O₄ precursor (see Figure 32a and Figure 33a). The difference in Cu:Al ratio does not show in the precursor composition as can be differentiated by p-XRD.

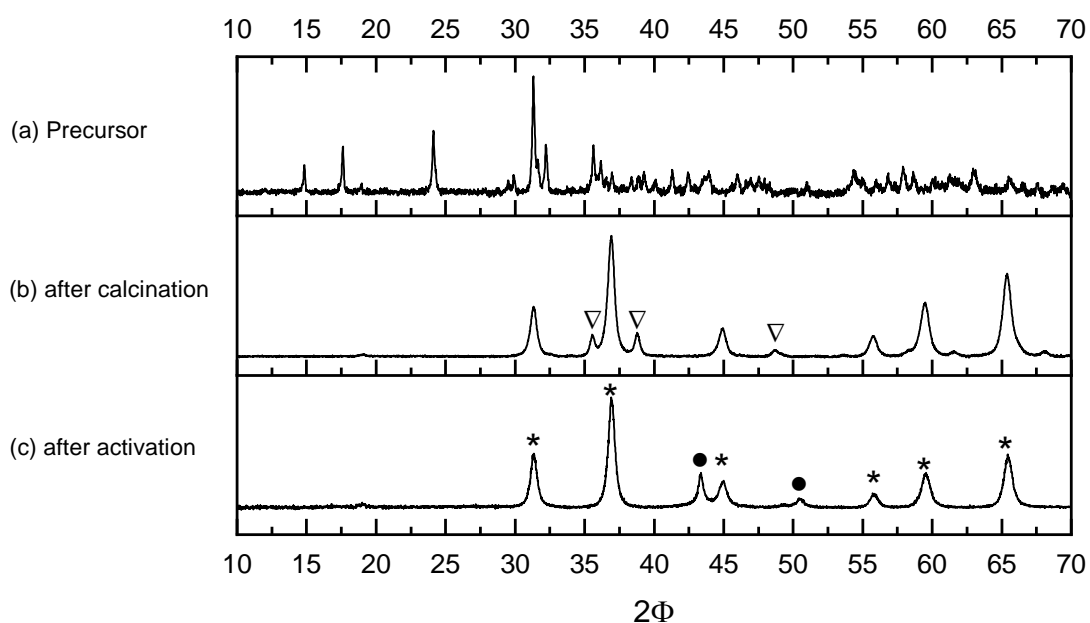


Figure 33: p-XRD diffractogram of the stoichiometric (CuO) · CuAl₂O₄ spinel during synthesis and after activation in hydrogen. (a) dried precatalyst after co-precipitation of copper- and aluminum nitrate solution in water. The reflexes are consistent with a malachite-like structure (b) catalyst after calcination at 800°C. The diffractogram shows clear reflexes of CuAl₂O₄, but also includes smaller reflexes of CuO which build up on the catalyst surface during synthesis. (c) catalyst after activation in hydrogen flow and slowly heating to 300 °C. The Cu-Al spinel structure is still clearly visible. The CuO present before activation has been reduced to Cu⁰, which gives visible reflexes at 43.25° and 50.38°.

The main reflexes of CuAl₂O₄ (★), CuO (▽) and Cu⁰ (●) are marked in the plot, according to the Powder Diffraction File™ database PDF-2 (2004).^[61]

After calcination, the intensities and reflex positions of the copper aluminate spinel are very similar to the Adkins analog, with a slight shift towards higher angles for the stoichiometric and the phase-pure spinel. This can suggest a decrease in the spinel unit cell size compared to the Adkins equivalent $\text{CuO} \cdot \text{CuAl}_2\text{O}_4$ or a change in stress within the spinel lattice due to the change in Cu to Al ratio. The copper(II) oxide reflexes can be clearly identified but are no longer the dominant phase. The Cu-Al spinel reflexes are still clearly visible in the activated p-XRD sample of the stoichiometric spinel. The reflexes of CuO have vanished and metallic copper is present in the diffractogram but to a lesser amount than in the CuO-spinel.

Phase-pure spinel CuAl_2O_4

The washed and dried precursor of the phase-pure spinel shows the same malachite structure as the stoichiometric spinel, because they are both prepared from precursors with identical composition (see Figure 33a and Figure 34a).

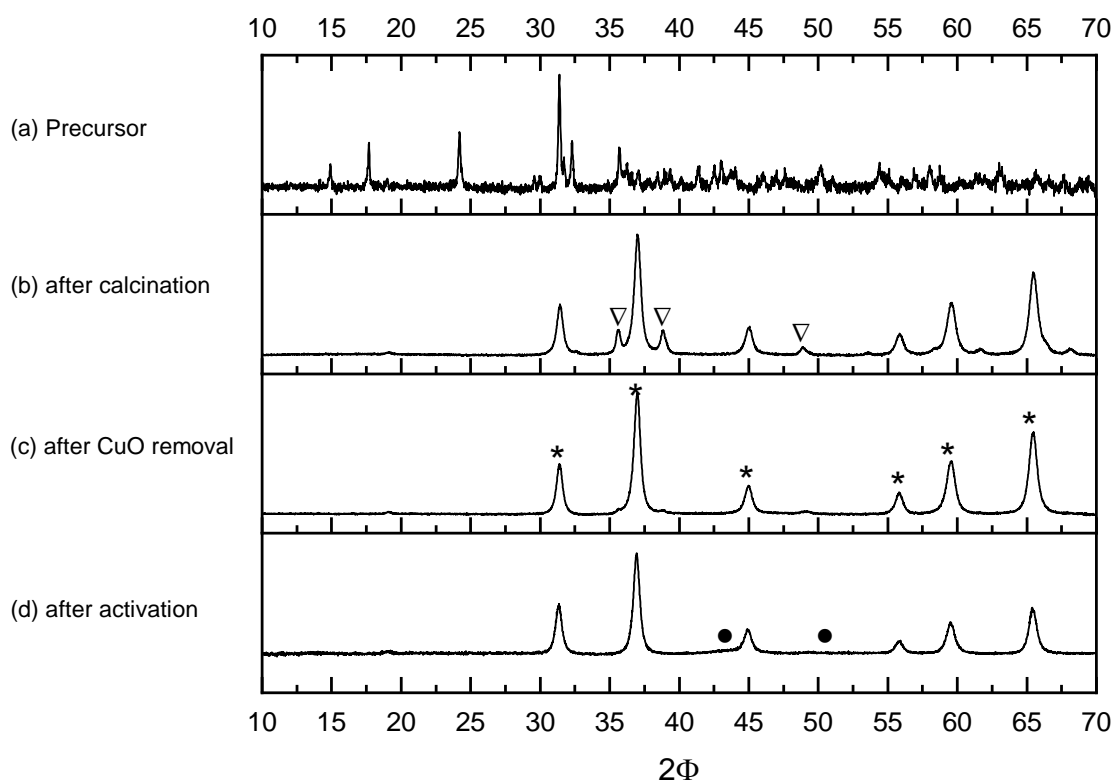


Figure 34: p-XRD diffractogram of the phase-pure CuAl_2O_4 spinel during synthesis and after activation in hydrogen. (a) dried precatalyst after co-precipitation of copper- and aluminum nitrate solution in water. The reflexes are consistent with a malachite-like structure. The precursor is the same composition as used for the stoichiometric spinel (see Figure 33) (b) catalyst after calcination at 800°C . The diffractogram shows clear reflexes of CuAl_2O_4 (\star), but also includes smaller reflexes of CuO (∇) which build up on the catalyst surface during synthesis. (c) catalyst after removal of surface copper(II)oxide. The reflexes of CuO are no longer visible, only the CuAl_2O_4 pattern remains. (d) catalyst after activation in hydrogen flow and slowly heating to 300°C . The Cu-Al spinel structure is still clearly visible. In contrast to Figure 33 there are no reflexes of Cu^0 (\bullet) visible in the diffractogram. The main reflexes of CuAl_2O_4 (\star), CuO (∇), Cu (\bullet) are marked in the plot, according to the Powder Diffraction File™ database PDF-2 (2004).^[61]

The p-XRD of the calcined spinel is also similar to the diffractogram of the stoichiometric spinel due to the identical catalyst synthesis up to this point. In this case, the calcined spinel in Figure 34b even shows higher copper(II)oxide reflexes hinting at slightly more CuO on the surface than in Figure 33b. The formation of the copper oxide surface layer is an unwanted side-product during the calcination process which has to be removed to get a catalyst containing only copper aluminate spinel (P-Sp). After treatment with ammonium carbonate solution and drying overnight, the p-XRD shows only reflexes belonging to CuAl_2O_4 (Figure 34c). The previously present CuO (marked with ∇) has been completely removed from the surface. This is also illustrated quite nicely in the p-XRD of the activated catalyst (Figure 34d). In contrast to the activated stoichiometric spinel, there are no visible Cu^0 reflexes after activation. The formed Cu^0 after activation it is too finely distributed to be visible in the p-XRD.

Phase composition investigated by Raman spectroscopy

The bulk composition of the different spinel phases can be investigated well by p-XRD. A more detailed investigation of existing phases within the overall sample can be accomplished by Raman spectroscopy combined with a microscopic module (Raman microscopy). This allows the identification of subspecies within the sample whereas the XRD measurements mostly show the main components of the overall sample. The microscope also allows a more detailed visual impression of the powder sample (color, composition).

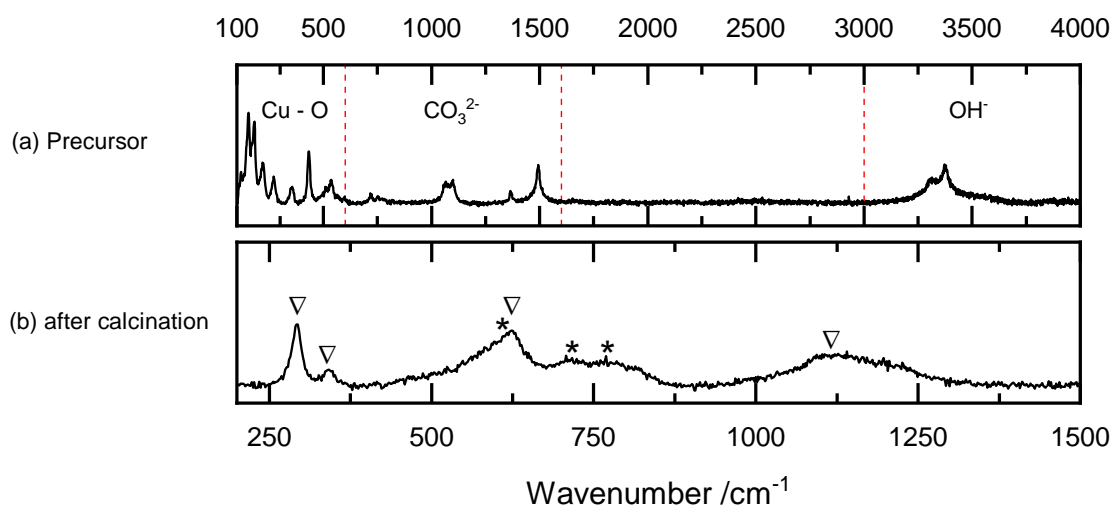


Figure 35: Raman spectra of the $\text{CuO} \cdot \text{CuAl}_2\text{O}_4$ precursor and the calcined catalyst. (a) region 100 - 4000 cm^{-1} . The precursor fits with malachite spectra found in literature; see Table 11. It can be subdivided into three parts: the lattice modes of Cu-O bands in the lower wavenumbers, the subsequent carbonate bands, and the hydroxyl vibrations found in the higher wavenumber regions above 3000 cm^{-1} . There is no additional precursor phase (such as azurite) visible in the Raman spectrum. (b) region 200 – 1500 cm^{-1} . The Raman spectrum of the calcined catalyst is dominated by the characteristic bands of copper(II)oxide (∇) around 290 cm^{-1} , 340 cm^{-1} and 625 cm^{-1} as well as broad bands belonging to the CuAl_2O_4 spinel phase (\star). The main peaks of CuAl_2O_4 (\star) and CuO (∇) are marked in the plot.

Raman spectra of the precursor affirm the observation by p-XRD that malachite makes up the main copper component of the precursor. Solid flakes of $\text{CuO} \cdot \text{CuAl}_2\text{O}_4$ precursor (before milling and sieving) give a good quality Raman spectrum of malachite where the main peaks can be easily identified and fit well with peaks described in literature. ^[64-68] The spectrum covers a large number of wavenumbers ($100\text{--}4000\text{ cm}^{-1}$), with three distinct areas containing the vibrational groups corresponding to Cu-O, CO_3^{2-} and OH^- bonds (Figure 35).

Table 11: Raman peak position (given in cm^{-1}) of malachite species as found in precursor phase (this work) and literature. The Raman peaks of the precursor fit well with malachite Raman data found in literature, confirming it as the main precursor phase. There is a slight shift towards higher wavenumbers for the 1:2 ratio precursor compared to the 1:1 ratio, but overall the values fit well with malachite. The slight differences of peak positions in literature can be explained by differences in excitation wavelength and experimental setup as well as the use of natural and synthetic samples.

Precursor (Cu:Al ratio)		Literature (Malachite)				
1:1 $\text{CuO} \cdot \text{CuAl}_2\text{O}_4$	1:2 CuAl_2O_4	RRUFF ^[68] R050508	Frost ^[65] (2002)	Bouchard ^[64] (2003)	Buzgar ^[66] (2009)	Gao ^[67] (2020)
154	156	154	151	154		153
181	183	176	176	180		178
219	222	220	217	219	215	220
271	274	268	267	270	269	270
			320			
356	354	349	349	355	354	(353)*
433	434	432	429	434	434	(432)*
509	510		514	512		511
537	536	536	531	538	536	533
598		594	596		596	
718	716	721	717	721	722	719
752	751	750	752	753	755	755
			801			
			816		820	
1066	1062	1063	1058	1067	1059	1066
1099	1093	1094	1096	1100	1097	1093
1365	1368	1367	1364	1367	1368	1368
				1462	1462	
1494	1492	1495	1492	1493	1495	1495
3315		3311	3386	3308	3310	3322
3373	3377	3381	3468	3378	3382	3382

* the peak positions were recalculated from Figure 1 in Gao and Yuan^[67], due to mislabeling in the graphic (given peak position does not fit in correlation to x-axis). Thus, both peaks have a larger error margin compared with other peak positions given in Table 11.

The main number of observable peaks is located in the lower region of the Raman spectrum between 100 cm^{-1} and 600 cm^{-1} . The peaks describe the different lattice modes of Cu-O. The internal modes of CO_3^{2-} are observed in the region between 700 cm^{-1} to 1600 cm^{-1} whereas the O-H stretching modes are located in the far region of the Raman spectrum around 3200 cm^{-1} to 3600 cm^{-1} .^[65] No other Raman-active precursor phases could be identified.

The Raman spectrum of the 1:2 Cu:Al precursor phase also shows a malachite spectrum, with a broader signal in the OH⁻ region, hinting at a slightly higher water content remaining in the sample (Figure 36). This is possible due to different storage times of the samples before measuring but does not impair the quality of the spectrum. The relation of the peak intensities to each other can also slightly differ due to the baseline correction of the spectra, though the aim is to use the same measurement conditions and baseline correction for related spectra. Small differences can still occur but do not impede the aspired information sought from the measurements. The peak positions themselves are not affected and fit well with literature data.

The exact positions of the bands differ slightly from publication to publication due to differences in measurement equipment and measurement conditions. Table 11 gives an overview of the main Raman peaks of malachite from literature. The peak positions fit well with the Raman data obtained from the synthesized precursor samples.

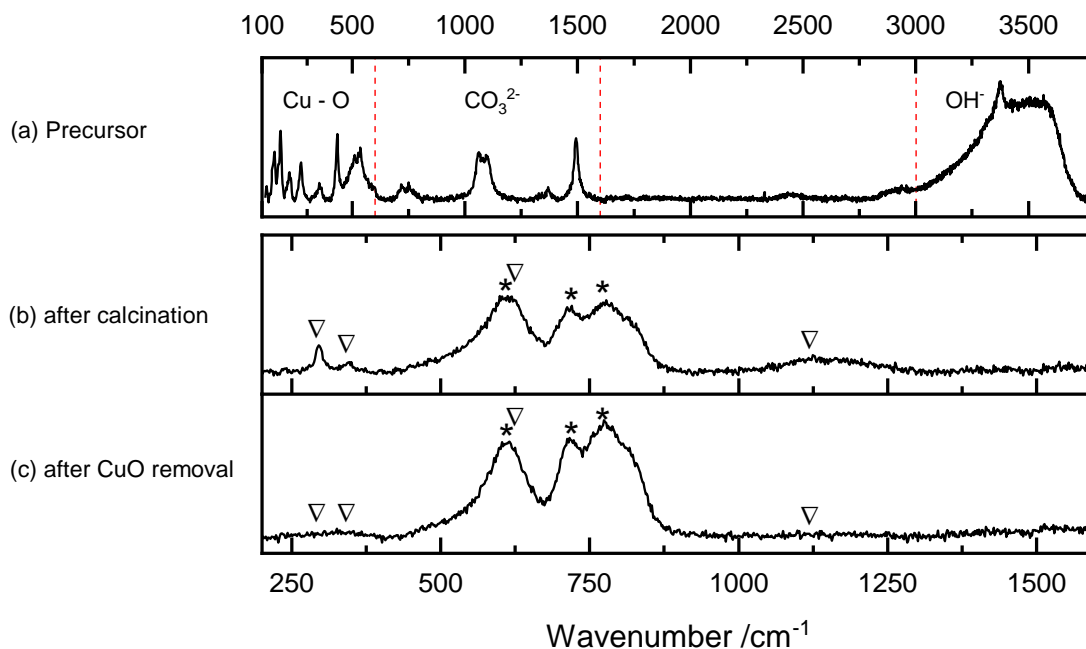


Figure 36: Raman spectra documenting the synthesis route of the phase-pure spinel CuAl_2O_4 : (a) precursor phase (malachite), (b) the Raman spectrum after calcination is dominated by the broad peaks associated with the CuAl_2O_4 spinel (\star) as well as smaller peaks matching CuO (∇). (c) The Raman spectrum of the calcined spinel catalyst after treatment step with $(\text{NH}_4)_2\text{CO}_3$ solution shows only the broad peaks of the spinel phase. The previously present surface copper(II) oxide has been removed.

The calcined spinel of $\text{CuO} \cdot \text{CuAl}_2\text{O}_4$ is dominated by those copper(II) oxide peaks, due to the larger amount of copper oxide present in the sample (Figure 35b). The spinel signals (marked with an \star) are still present, but less intense than in the calcined CuAl_2O_4 catalyst. The comparison of both catalysts after calcination also shows that the overlapping signal around $600\text{--}650\text{ cm}^{-1}$ can still yield information.

The CuO dominated overall spectrum in Figure 35b shows a shift of the peak to 630 cm^{-1} whereas Figure 36b shows a broadening and shift to lower wavenumbers at 610 cm^{-1} , indicating a larger influence of the spinel signal. After the removal of the remaining surface copper oxide to get finished phase-pure spinel, the Raman spectrum only shows the three broader band features between $600\text{--}800\text{ cm}^{-1}$ associated with the spinel lattice (Figure 36c). Luo et al. found additional signals at 1379 and 1402 cm^{-1} but those could not be verified in spinel samples synthesized in this thesis.^[46] The other peak positions found in Luo et al. fit well. The Raman measurements of the mineral thermaerogenite (naturally occurring CuAl_2O_4) reported by Pekov et al. note only two main peaks at 590 cm^{-1} and 762 cm^{-1} . Since this is a naturally occurring sample the small shift of peak position compared to synthetically prepared laboratory samples is expected. Other spinel samples with different cations from literature show comparable spectra with some shifts in peak position due to the different cation sizes (Table 12). Additionally, D'Ippolito et al. described a broadening of the Raman bands with a higher degree of inversion of the spinel.^[69] This fits with the broader bands found in the CuAl_2O_4 due to its nature as a partially inverse spinel.

Since the Raman instrument is coupled to a microscope with magnification up to 50x it is possible to analyze small particles within the sample separately. A lower magnification allows for an average spectrum of the sample because the excited area will be bigger and offer a mean Raman spectrum of all catalyst phases within this area. A higher magnification allows the identification of smaller particles which would possibly not be resolved using a lower magnification or p-XRD.

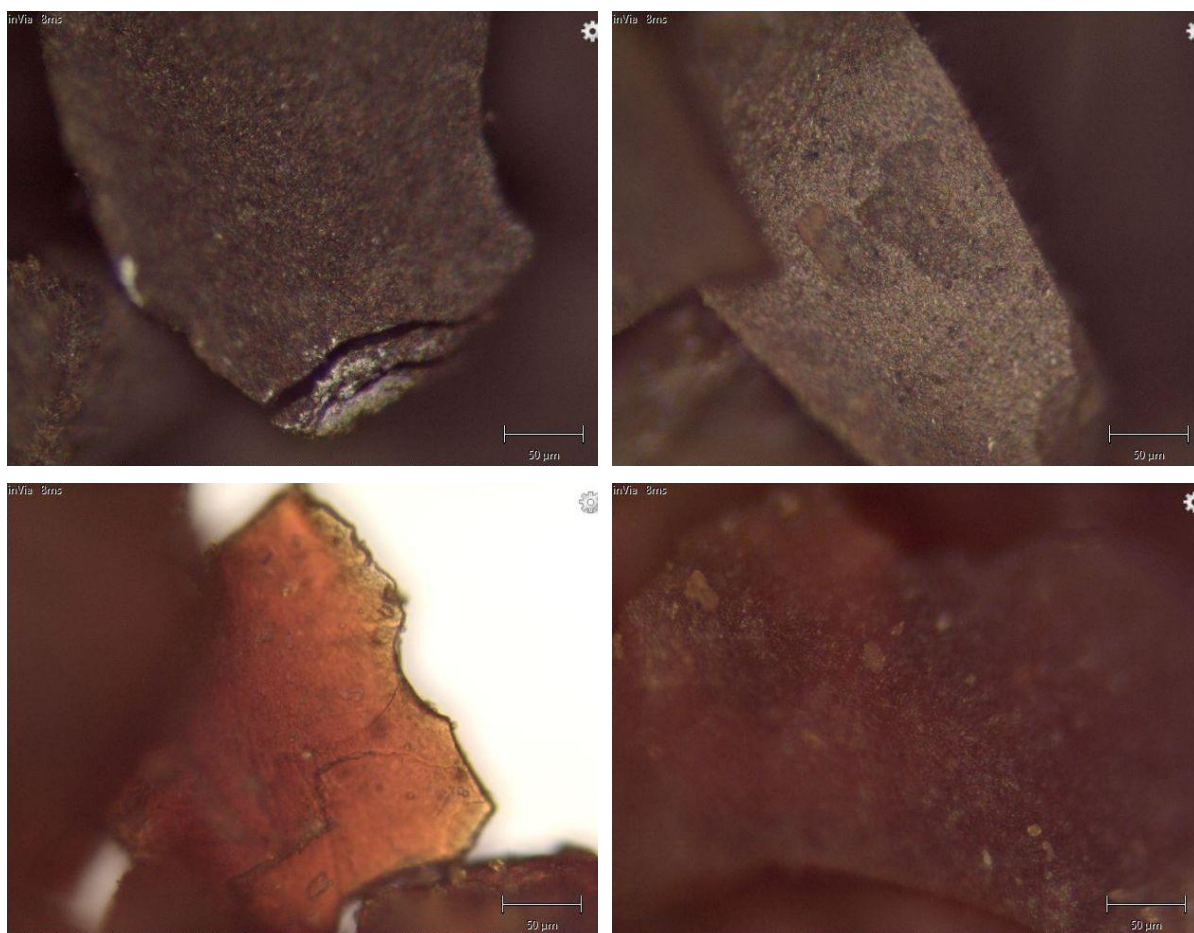


Figure 37: Microscopic images (magnification 20x) of the calcined spinel phases with particle sizes between 100 – 300 μm . (top-left) $\text{CuO} \cdot \text{CuAl}_2\text{O}_4$, (top-right) stoichiometric spinel $(\text{CuO}) \cdot \text{CuAl}_2\text{O}_4$, (bottom row) phase-pure spinel CuAl_2O_4 . The phase-pure spinel has a more reddish color while both other catalyst powders appear dark-brown to black. The darker spots on the stoichiometric spinel showed higher CuO signals in the Raman spectrum whereas the different colored regions within the phase-pure spinel all showed similar CuAl_2O_4 signals. The dark and light region of the $\text{CuO} \cdot \text{CuAl}_2\text{O}_4$ sample pictured (top-left) also showed a similar Raman spectrum despite its difference in appearance.

These small-scale investigations might not necessarily be relevant for the bulk composition of the catalyst but can give additional information on the purity of the material as well as newly formed species, for example after a catalysis run. As all samples are measured as powders it is important to measure enough different points of the sample to get a reliable result of the overall composition. All spectra shown have been verified by measuring the same sample many times in different positions to make sure that the spectrum is representative and not an outlier.

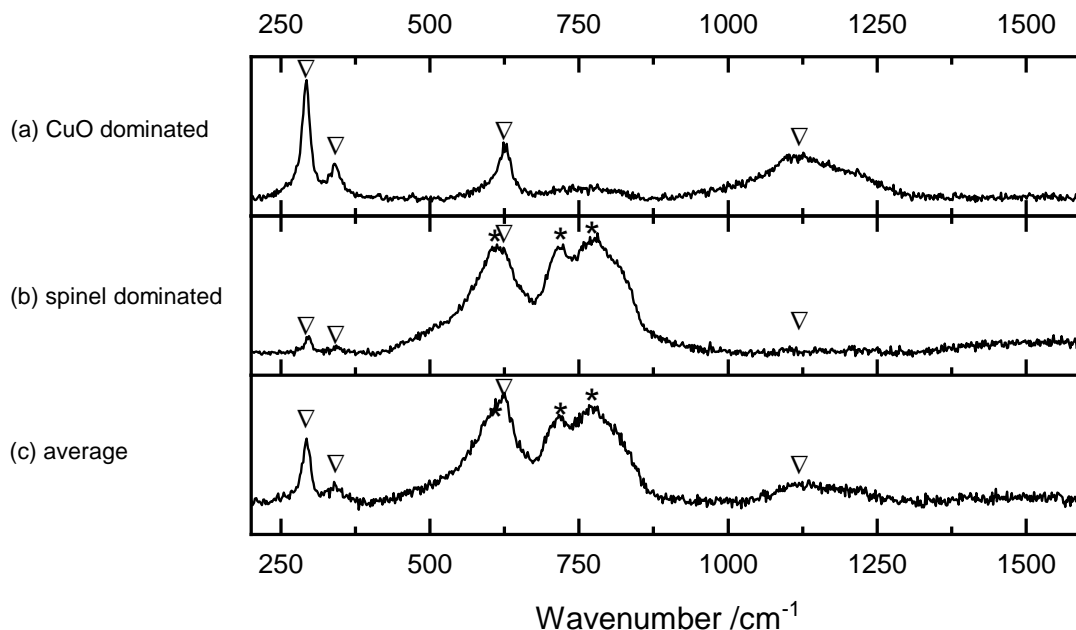


Figure 38: Raman spectra of representative spots within a stoichiometric spinel.

Figure 38 shows three spectra which are representative of the type of Raman spectra most commonly found during measurements of the various calcined Cu-Al spinel species. The main peak positions in comparison to literature values ^[46, 68-70] can be found in Table 12 (spinel samples) and Table 13 (copper oxide). As can be expected from its chemical formula, the spectra are either dominated by CuO, CuAl₂O₄ or a mixture of both signals. Especially in the stoichiometric spinel (CuO) · CuAl₂O₄ all three spectra can often be found in the same powder sample, depending on the chosen excitation spot of the sample. Phase-pure spinel catalysts are characterized by the spinel dominated Raman spectrum but small CuO particles can still be found sporadically. The microscope can help identifying those samples.

Table 13: Raman peak position (given in cm⁻¹) of CuO as found in the calcined Cu-Al spinels prepared (this work) and in literature. The CuO peaks fit well with literature values, small divergences can be explained by the measurement of powder samples opposed to solid, well crystallized samples which lead to broader peaks.

Catalyst phases	Literature (CuO)		
	RRUFF ^[68] R120076	Luo et al. ^[46] (2005)	Debbichi et al. ^[70] (2012)
292	297	290	296
341	345	340	346
624	630	628	631
1117	1115		

Characterization of spent catalyst using p-XRD

Structural characteristics of the catalysts after use in the hydrogenation of butyraldehyde under standard conditions are described in the following. The catalyst was separated from the reaction mixture and dried on air before storage. The catalyst powder itself appears finer but that is due to mechanical milling by the stirring bar.

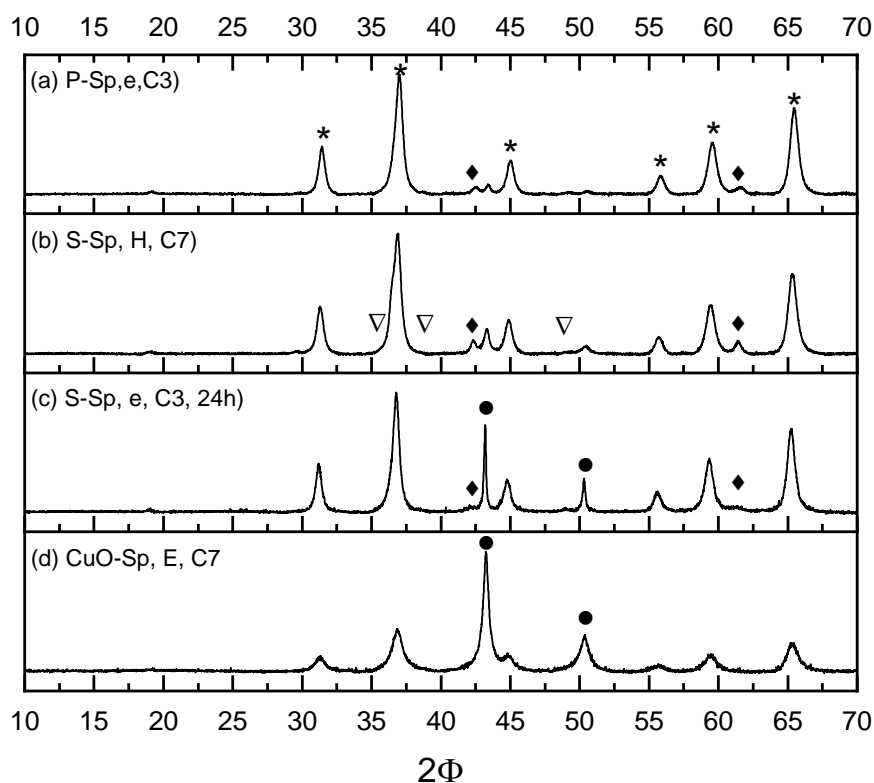


Figure 39: p-XRD diffractogram of (a) phase-pure CuAl_2O_4 spinel and (b)-(d) stoichiometric spinel after reaction, displaying Cu_2O signals (\blacklozenge). The main reflexes of CuAl_2O_4 (\star), CuO (∇) and elemental Cu^0 (\bullet) are marked in the plot as well.

Figure 39 shows chosen examples diffractograms after the catalyst was used in a typical reaction cycle. The most prominent changes that can be identified via p-XRD are the presence of different copper species compared to the fresh catalyst. The catalyst composition of spent catalysts is not identical, but depends on the pre-catalyst used (CuO-Sp , S-Sp or P-Sp) and its reaction conditions.

There is no CuO present in any of the spent catalysts. Some of the spent catalysts show a significant buildup of Cu^0 compared to the fresh catalyst with narrower reflexes (e.g. Figure 39c). Whereas the fresh catalyst is made up of a mixture of Cu-Al spinel and CuO (Cu^0 after activation), the spent catalyst shows signals of Cu_2O and Cu^0 . The Cu-Al spinel signature remains clear in the spent catalyst, there is no significant shift or broadening of signals. This indicates that the spinel lattice has not changed significantly enough due to leaching to be

affected in the XRD. The presence of Cu_2O does not seem dependent on a copper oxide surface layer on the original catalyst composition, it can be found in most spent catalyst. At room temperature the oxidation of a metallic copper surface first forms Cu_2O , CuO starts to form at higher temperatures or with a significantly longer oxidation time^[71]. That means the amount of cuprous oxide found in the spent catalyst can give an idea how much metallic copper was on the spinel catalyst at the end of the reaction. If the sample was measured soon after the experimental run then the metallic copper itself can be found in the p-XRD. Also, in the case of CuO -spinel, the presence of a lot more metallic copper from the beginning also aids the presence of an identifiable metallic copper phase on the spent catalyst.

The presence of Cu_2O can also be verified by Raman spectroscopy (Figure 40 and Table 14). This also allows for the detection of smaller amounts of Cu_2O which cannot be detected by p-XRD (not enough signal intensity compared to noise signal). In exchange Raman spectroscopy cannot be used for the detection of metallic copper (not Raman active), or only indirectly by the absence of a identifiable Raman spectrum. Additionally, Raman spectroscopy is a very good method to check for possible "coking" occurring during the experiments since carbon is very easily identified by Raman. Extended coking can be another reason for catalyst deactivation by blocking the catalytic sites. This was sporadically the case, but not a regularly occurring problem. The third Raman spectrum in Figure 40 shows, in contrast to all XRD measurements, a mixture of Cu_2O and CuO . This documents the previously mentioned possibility of CuO formation from metallic copper (or the subsequently formed cuprous oxide) at higher temperatures or long reaction times. The measurement took place a year after the catalyst was used in an experiment whereas all XRD measurements took place closer to the experimental use.

The spent catalysts investigated all retained their clear spinel patterns in p-XRD and Raman, suggesting an intact spinel lattice. There was no significant shift in position or peak broadening observed. The presence of small particles of cuprous oxide was identified by Raman microscopy, using a 50x magnification. The total amount only sometimes was enough to be identifiable in the corresponding p-XRD measurements. There is no clear trend when a higher amount of Cu_2O was formed in regards to catalyst performance.

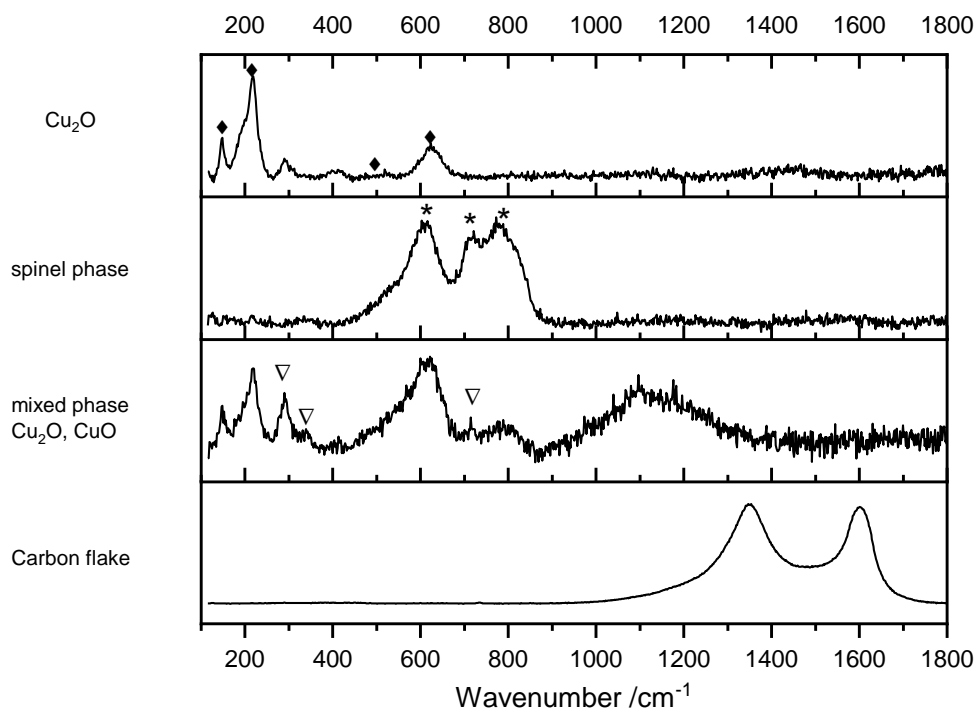


Figure 40: Raman spectra found in spent catalyst samples.

 Table 14: Raman peak positions (given in cm^{-1}) of Cu_2O as found in the spent Cu-Al spinels prepared in this work and in literature. The Cu_2O peaks fit well with literature values, small divergences can be explained by the measurement of powder samples opposed to solid, well crystallized samples.

Catalyst phases	Literature (Cu_2O)			
	RRUFF ^[68]	Cu_2O ref measurement	Bouchard ^[64]	
Cu_2O MJA-3-nR_4	R140763		(2003)	Deng (2016)
146	145	148	148	
218	218	218	218	218
289	306	303		
405	407	413		
	488	481	495	523
623	622	625	638	623

2.5 Conclusion

Discussion of trends in copper and aluminum leaching during butyraldehyde hydrogenation.

Most relevant general trends of leaching shall be discussed first. Some of the starting hypotheses could in fact be confirmed rather clearly. The influence of the large variety of parameters will be discussed concerning consequences for copper and aluminum leaching and catalytic performance (activity, selectivity), all as function of reaction progression. Under high hydrogen pressure (65 bar) and increased temperature (120 °C) in all experiments performed, as expected, copper is dissolved into the reaction solution only in trace amounts (less than 1 % of total copper present). Qualitatively, copper species have not been lost into solution from the pre-reduced catalytically active copper(0) nanoparticles. This was expected for the non-polar solvent hexane, being a very poor solvent for metallic species (complexes) formed by potential leaching. Concerning catalysis, no correlation of these trace amounts of copper dissolved with catalytic performance could be observed in standard experiments.

Qualitatively and roughly quantitatively this holds for all three catalyst modifications investigated (Figure 6):

- (i) the copper oxide-copper aluminate spinel, $\text{CuO} \cdot \text{CuAl}_2\text{O}_4$ (Adkins analogue), which contained an excess of CuO (respectively metallic copper particles after activation) supported on copper aluminate;
- (ii) the so-called stoichiometric spinel $(\text{CuO}) \cdot \text{CuAl}_2\text{O}_4$ (always having a slight excess of CuO on the spinel surface) after calcination, and
- (iii) the phase-pure spinel CuAl_2O_4 , where CuO residues on the surface of copper aluminate spinel after preparation were removed by an optimized copper leaching procedure (leaching led to slight lack of copper relative to exact spinel stoichiometry).

That means, these three catalysts have a rather identical support – CuAl_2O_4 – but differ in the amount (“Cu:Al ratio”) of CuO (pre-catalyst) or copper(0) particles on this support. For catalytic activity (number of active copper species) as well as for leaching, there would be more copper available on the surface for the Adkins analogue than for the stoichiometric and again for the phase-pure spinel catalyst.

Differences in leaching of copper are however very small to negligible for all three catalysts under the standard conditions used. Variations are directly connected to the slight partial re-oxidation of copper(0) during catalyst transfer (contact to air, reproducibility of the transfer procedure). Of course, oxidized copper is more easily dissolved into solution than reduced copper (the latter probably not at all), and notably: it can be re-reduced under the standard conditions (hexane, no additives and ligands, hydrogen, temperature). As underlined by further experiments, both, leaching of copper(0) as well as re-reduction will be substantially modified by a

variation of reaction parameters, also by those which are of relevance in technical processes. It is interesting to note that copper leaching at the beginning of the reaction (up to one hour) is highest for the stoichiometric and phase-pure spinel (Figure 4). Probably it is the copper(II) of the spinel lattice that can be partially and more easily dissolved, possibly due to better accessibility, than in the Adkins analogue (excess of copper on the outer surface). However, this leached copper is re-reduced and re-deposited onto the support completely after less than one hour of reaction time).

All three catalysts are active in the hydrogenation of butyraldehyde and no correlation of copper leaching and activity can be identified. The differences in activity can be explained by the varying amounts of metallic copper (total surface area) in the catalysts (Cu:Al ratio). Thus, the Adkins analogue reaches complete conversion in less than two hours, whereas phase-pure copper aluminate spinel needs nearly 5 hours. For a detailed analysis, more determination of the copper(0) surface area by chemisorption would be necessary, that is however out of the scope of this study. The results are, however, in good agreement with analogous reports of Dörfelt et al.^[31] Also rather similar for all three catalysts is the low selectivity to butanol (below 60 %, Figure 6), which is different to 100 % selectivity in the pure gas phase reaction and will be discussed later^[47, 72].

Beyond all previous expectations, aluminum leaching is non-negligible. This confirms the first surprising observations by C. Dörfelt.^[27] In addition, aluminum leaching is found to be clearly different for the three catalysts investigated. Remarkable leaching of aluminum is observed for the Adkins analogue, starting directly after the heating phase ($t=0$) and continuously increasing with reaction progression (up to more than 2 % of total aluminum in the catalyst). The values for the pure copper spinel catalysts are clearly lower (< 0.5 % or nearly zero for P-Sp). The strongest increase in Al leaching occurs during the fastest substrate conversion (for CuO-Sp), a correlation which cannot easily be explained because aluminum is not taking part in the reaction. One might assume that changes in the composition of the reaction mixture (e.g. increase of butanol concentration) is related to this observation (see also later: influence of solvent and additives). It seems to be more difficult to dissolve aluminum from pure spinel catalysts S-Sp and P-Sp. Possibly, an excess of copper(II) available at the surface of CuO-Sp can compensate the loss of lattice aluminum and stabilize the catalyst.

The presence of carboxylic acids in the reaction mixture is found to be decisive for metal leaching. Their presence relativizes several of the observations described for standard reaction conditions without acids. Leaching data from all three catalysts is available for heptanoic acid as additive (Figure 7). Both copper and aluminum leaching into solution increase substantially in the presence of 8 mol-% heptanoic acid. This rather high concentration had been chosen in order to attain clear effects avoiding discussion of trace effects of limited reproducibility (acid impurities in industrial feeds are in general only 2 %). It could be expected that copper(II) and

aluminum(III) complexes can be (thermodynamically) stabilized in solution due to better solubility leading to an increased leaching into solution. However, the reduction potential of copper(II) in solution has also changed to such an extent that at least copper, once oxidized, cannot be re-reduced in contrast to standard conditions without addition of carbonic acid. Leaching of 1-2 % (P-Sp, CuO-Sp) and even up to 6 % (S-Sp) of the total copper amount over the whole reaction time confirm this. Also, aluminum leaching increases remarkably compared to the absence of heptanoic acid. The catalytic performance (activity and selectivity) decreases for all catalysts. The loss of copper, modified reduction conditions and potential side reactions are explanations. The partial loss of copper is less relevant for the activity of the Adkins analogue, where copper is present in large excess on the spinel support in contrast to S-Sp and P-Sp. Thus, the performance of this catalyst is only moderately diminished by the copper loss with heptanoic acid.

The two “pure” spinel catalysts (S-Sp, P-Sp) without additional copper amount on the surface showing the most drastic effects with variation of the reaction conditions and were used for the evaluation of further parameters for leaching and catalytic performance. First, the influence of the carbon chain length of the carboxylic acid was studied in hexane as solvent for these two catalysts (Figure 8 and Figure 9). The experimental series with different carboxylic acids confirms the trends already observed for heptanoic acid: in all cases, catalytic activity and selectivity are reduced compared to acid free substrate.

To a first approximation, there is no direct correlation between copper amount in solution and activity and selectivity, i.e. copper complexes in solution do not influence butanal conversion. Copper leaching increases less pronounced for shorter acid chain lengths, what is not surprising due to worse solubility of the corresponding complexes in non-polar hexane. Substantial copper leaching is only observed with heptanoic acid, but catalytic performance was decreased for all acids. It is possible that the formation of the particularly sparingly soluble copper carboxylates re-deposited as solids, are lost as an active species and even block active copper sites, resulting in a less active catalyst.

Most critical for catalyst stability is the increased aluminum leaching when carboxylic acids are present, most pronounced for the phase-pure spinel. In all cases, aluminum leaching increases continuously with reaction progression when acids are present, destabilizing the catalyst.

Variation of the solvent influenced the leaching of copper and aluminum remarkably. Toluene – most similar to hexane – showed, not surprisingly, very similar results and confirmed former observations. Surprising and not easy to explain is the observation that the presence of (pentanoic) acid led to better catalytic performance in toluene compared to hexane. Again, the presence of acid in the feed led to increased copper and aluminum leaching, however less pronounced than in hexane. This trend continues for more polar solvents. Generally, leaching of copper as well as of aluminum decreased clearly with more polar solvents (dioxane, ethanol).

This is also true in the presence of carboxylic acids. A possible interpretation is that the dissolved metal complexes (Cu(II), Al(III)) formed in solution are uncharged, thus being less soluble in polar solvents compared to hexane. Unfortunately, we do not have information on the nature of the complexes in solution, but only on the total metal content from the ICP-OES analyses. An interesting result is the continuous increase of copper and aluminum leaching after complete conversion of the substrate in the presence of heptanoic acid (Figure 7). One could speculate that this is related to the increased amount of product, i.e. butanol and its contribution to metal ion solubility.

The most pronounced effect is the strongly increased rate of conversion of butyraldehyde with ethanol as solvent compared to the standard catalysis in hexane (Figure 13 and Figure 14). This is even true for the presence of carboxylic acids. The selectivity however depends very sensitively on the nature of the carboxylic acid added. This is due to the formation of the diethyl acetal as side reaction, which is catalyzed under acidic conditions. In the most extreme case with pentanoic acid as additive, practically no butanol is formed but the acetal is dominating as product (Figure 16). Since the substrate butyraldehyde is very often contaminated with varying small amounts of acids (in lab as well as industrial scale), reproducibility will be limited and ethanol as solvent represents a very interesting but also risky solvent for these reactions.

The solvent effects on metal leaching during butyraldehyde hydrogenation were confirmed by analogous effects with solvent mixtures of hexane with 10 % of toluene, 1,4-dioxane and ethanol. Catalytic performance and stability have been improved for the solvent mixtures, when the added solvent had higher polarity. Most interesting was again the addition of ethanol. Already small the amounts of ethanol decreased leaching of copper and aluminum significantly in comparison to pure hexane. Catalytic performance increased substantially too. The latter result was again accompanied by acetal formation as side reaction when propionic acid was added to the solvent mixture (in contrast to pure ethanol, where pentanoic acid led to selectivity break down). This underlines systematic correlation between solvent polarity, solubility and acid concentration dependent on chain length. The phase-pure spinel is generally more susceptible to aluminum leaching (than S-Sp and also CuO-Sp) under identical conditions.

Long-term experiments on leaching are of interest for the stability of the catalysts, in particular. Aluminum represents a component of the support and/or binder material with industrial applications in continuous processes with fixed bed flow reactors (e.g. trickle bed). The trends discussed for the batch experiments are in principle also confirmed by the long-term experiments performed over 24 hours (Figure 26). More specifically, copper leaching into hexane plays only a role in the presence of heptanoic acid, but in this case, it can increase up to 15 % of the total copper content of the catalyst after 1 day. Aluminum leaching increases continuously over the whole time in the presence of any acid tested reaching up to 6 % of total aluminum during 1 day, thus being in fact a serious danger for potential (shaped) catalyst stability. Addition of

10 % ethanol to hexane can help to suppress copper (nearly completely) and aluminum leaching (below 1%) substantially with a drastic increase in activity and selectivity at the same time (Figure 28). Leaching in hexane/ethanol is slightly more pronounced for the phase-pure catalyst, which shows in general lower stability. The catalytic performance increase by ethanol is however again accompanied by serious sensitivity of selectivity to reaction parameters as described for reactions in pure ethanol (acetal formation). Nevertheless, the huge number of information gives us ideas and variables to control leaching if necessary in a knowledge-based approach for comparable copper catalyzed hydrogenation reactions.

**Leaching of palladium
atoms from small cluster
models during *Heck*
reactions**

3.1 Introduction and Motivation

Leaching is a phenomenon that occurs in different types of reaction. The previous chapter described a leaching process with a focus on the deactivation of the catalyst. In contrast, other types of reactions can incorporate the leaching of catalyst species as an active part of the catalytic reaction itself. One such example is the *Heck* reaction using supported palladium catalysts. Here, dissolution of active metal species can also result in an even more efficient homogeneous catalytic cycle with increased reaction rates.

The results presented in the following chapter examine specific parameters of such leaching processes by close correlation of targeted experiments with computational model results. Leaching processes at solid-liquid interfaces are very complex as they involve solid surfaces, solvent, substrates and additives. It seems reasonable to reduce the complexity by addressing selected parameters and elementary steps. The questions (i) which reaction parameters (components) favor palladium leaching and (ii) under which reaction conditions leaching may be preferably observed are discussed. Temperature-programmed experiments correlating dissolved palladium and catalytic activity on the one hand side and experiments with variation of reactant composition (optional with and without aryl halide, alkene, additional bromide ions) - again as function of temperature and time - were carried out for these reasons. The role of all individual components of typical *Heck* reactions are addressed. Further, supported Pd-nanoparticle catalysts are compared to isolated Pd-complexes immobilized on a support and their different leaching behavior is presented in the context of the catalytic reaction cycle. Additionally, a more-demanding (aryl chloride) and less-demanding substrate (aryl bromide) is briefly discussed in regard to their Pd leaching progression, using supported Pd-complexes as a catalyst.

The leaching results described in the following chapter have been published in ^[73] and ^[74].

3.2 Theoretical background

All heterogeneously catalyzed reactions in liquid phase are potentially associated with the question of (partial) dissolution or leaching phenomena. Leaching of the active metal may cause a loss in catalytic activity and lead to contaminated products, especially in continuous-flow operation. On the other hand, dissolution of active metal species can also result in an even more efficient homogeneous catalytic cycle with increased reaction rates, bridging the gap between heterogenous and homogeneous catalysis.

This effect has been observed for palladium catalyzed C–C coupling reactions of *Heck*^[21] and *Suzuki*-type.^[75] Since their discovery in the 1960s and 1970s, cross coupling reactions reached high importance due to their application in the synthesis of complex natural as well as agricultural and pharmaceutical products. These reactions enable the connection of two molecules by the formation of C-C, C-N or C-S bonds.^[76, 77] In order to facilitate continuous processes and easy catalyst separation, many studies focused on the development of solid palladium catalysts for cross coupling reactions.^[76, 78-80] One of the most versatile cross couplings is the *Heck* reaction, which describes the palladium-catalyzed arylation of an olefin using aryl halides or triflates.^[77, 81, 82] Focusing on *Heck* reactions, the question of how the reaction is catalyzed starting from solid Pd drew much attention initially. In principle, the two discussed possibilities were that either the reaction is catalyzed by a “truly heterogeneous” surface mechanism or that dissolved palladium, which is generated by metal leaching, catalyzes the reaction following the homogeneous reaction mechanism. Consequently, several contributions and reviews have addressed this topic.^[22-24, 79, 83]

The general conclusion is that despite the possibility of a surface mechanism cannot be excluded completely, the homogeneous pathway is evident for several systems such as palladium nanoparticles as well as supported palladium oxide catalysts and that the active species are at least temporary coordinately unsaturated dissolved Pd(0) species.

For these reactions, a variety of authors did not regard leaching primarily as a negative phenomenon, but proposed Pd leaching as a prerequisite for high catalytic activity.^[24, 84-87] However, several studies also reported that *Heck* and in particular Suzuki coupling reactions occur at the surface of solid Pd as truly heterogeneous reaction with a classical surface mechanism; for a review see Ref. ^[23] While leaching of Pd into solution (and re-deposition) has been proven in many experiments, relevant parameters and mechanisms of leaching remain often unclear in detail.

The tests, which are applied mostly for the differentiation of homogeneous or heterogeneous catalyzed reactions, are hot filtration or split tests, selective poisoning of supported palladium as well as three-phase tests. However, the interpretation of the results derived from such tests

can be difficult. In many cases, it is only possible to examine the situation at a particular time during the reaction. In order to improve the understanding of the dynamic leaching process under reaction conditions, the contemporaneous determination and correlation of the conversion of the aryl halide with the amount of leached palladium, using solid palladium catalysts, was established. It was demonstrated that palladium is dissolved simultaneously with the start of the reaction, the highest reaction rate matches the highest palladium concentration in solution and palladium is re-deposited on the support again after the reaction is completed. Therefore, it was concluded that solid palladium catalysts act as reservoirs for active Pd(0) species in solution.^[25, 26, 85, 87-91]

Especially in the case of *Heck* reactions, the matter of how the reaction is catalyzed starting from solid Pd drew much attention. Several contributions and reviews addressed this topic^[22-24, 79, 83], proposing in particular the generation of active species in solution through oxidative addition of the aryl halide to Pd particles.^[23] Ananikov et al. discussed the simultaneous existence of several active species in solution (dissolved palladium complexes, clusters and nanoparticles etc.) and their interconversions as a “cocktail of catalysts”.^[92] De Vries examined the catalytic relevance of the formation of palladium colloids and anionic palladium species in solution at higher temperatures.^[24] In several experiments, the rate of conversion correlated with the concentration of dissolved palladium species.^[73, 85, 89] Analogous concepts of palladium leaching exist for Suzuki-Miyaura type cross-coupling reactions.^[93-95] The catalysts and reaction mixtures were monitored *in situ* during the *Heck* reaction by means of EXAFS by Kleist et al.^[96] showing that the catalyst changed from solid to dissolved species as the substrate is converted. Analogous observations were reported in NMR studies by Smirnov^[97] and with a nanoporous membrane reactor by Gaikwad et al.^[98]

A detailed understanding of how potential elementary steps may contribute to palladium leaching during carbon-carbon coupling reactions was obtained by theoretical studies of Polynski and Ananikov^[99], Ramezani-Dakhel^[100], Proutiere^[101], and Chang et al.^[102] The DFT investigations report the dissolution into the liquid phase, e.g. as function of the palladium particle size as well as the possibility of Pd leaching from solid Pd surfaces into the gaseous phase by means of CO chemisorption. A review of theoretical studies on aspects of carbon-carbon bond formation has been published by Xue and Lin 2010.^[103]

Examples of catalysts with immobilized palladium complexes or molecular palladium species for the *Heck* coupling reaction already exist, but unfortunately most studies lack detailed experimental-based proposals concerning the mechanism and therefore the cause for the partly high activities.^[104-109] The more recent finding of extraordinarily high catalytic activity of grafted Pd methyl complexes on silica for the selective conversion of aryl chlorides opens the possibility of more detailed mechanistic investigations.^[110]

3.3 Results and discussion

The basis of this study is the systematic comparison of different supported palladium pre-catalysts for the *Heck* reaction, focusing on the correlation between activity and palladium leaching. As catalytic systems, supported palladium (oxide) particles as well as supported isolated palladium surface complexes were chosen. Palladium oxide particles immobilized on various supports are well known for their application in C-C coupling reactions and can be regarded as standard or reference systems.^[26, 89]

3.3.1 Synthesis and characterization of the catalysts

Supported Pd particle catalysts

Two palladium catalysts with supported nanoparticles of different loading were studied in the leaching experiments described below: (i) a commercially available catalyst from Evonik with 5 wt.-% Pd deposited on a charcoal support (1120 m²/g BET surface) and (ii) 1 wt.-% Pd deposited on silica (Aerosil 200, Evonik), synthesized by controlled deposition precipitation based on the study of Pearlman.^[111] A detailed synthesis description is given in the Experimental section (Chapter 6.2). The metal loading was confirmed by elemental analysis and the average particle sizes are 3 nm (Pd/C) and 2 nm (Pd/SiO₂).

Isolated Pd complexes grafted on SiO₂ support

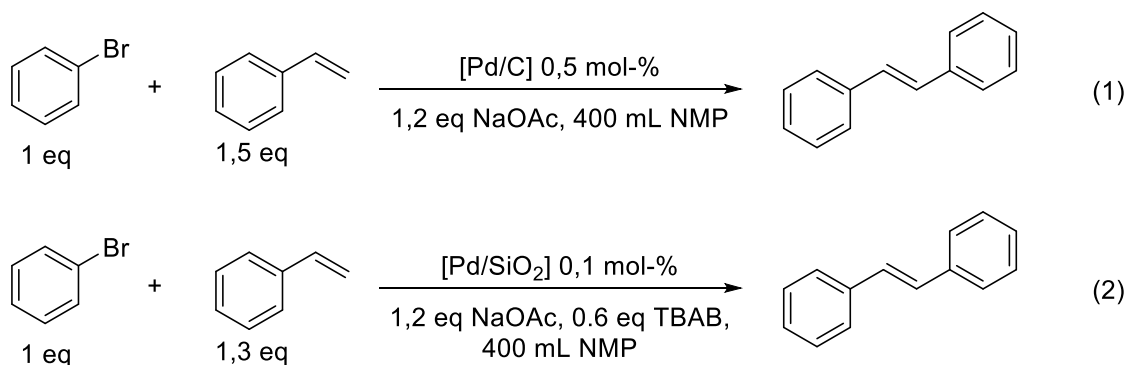
The catalyst PdMe(tmeda)/SiO₂ was used as prepared by C. Gnad^[112], a detailed description of the synthesis can be found in literature.^[110, 113-115] An abridged version, for better understanding of the presented leaching results, is given in the Experimental section (Chapter 6.2). The synthesis route yields solid catalysts of isolated Pd surface complexes with molecular metal centers. Metal loading and stoichiometry of the surface complexes (molar ratio of Pd:C:H:N/P) were confirmed by elemental analysis. IR spectroscopy allowed the assignment of well-defined bands to the symmetric and asymmetric vibrations of the C-H bonds of the tmeda and methyl ligands of the surface complex. TPD studies confirm that no other organic species besides the ligands coordinated by palladium are present. NMR spectroscopy confirms the molecular character of the metal center and the successful bonding of the complexes to the support.

3.3.2 Targeted variation of parameters concerning Pd leaching during *Heck* reactions

In a first step the leaching behavior of the supported Pd catalysts on charcoal and silica in correlation to the rate of substrate conversion under standard *Heck* reaction conditions is described. Following that, both catalysts are tested in a number of targeted leaching experiments and compared to corresponding DFT calculations by N. Rösch et al. in regards to the mobility of palladium.

Leaching under standard Heck reaction conditions

The overall substrate conversion and leaching progression using the supported palladium catalysts is tested for the *Heck* reaction of bromobenzene with styrene. The stoichiometric amounts and reaction conditions are given in Equation 8 and described in detail in the Experimental section (chapter 6.2).



Equation 8: Reaction equation and reaction conditions of the investigated *Heck* coupling reactions using (1) Pd/C or (2) Pd/SiO₂ as a catalyst.

The progression of substrate conversion and palladium leaching in correlation to the reaction temperature is given in Figure 41. The left side shows the reaction using Pd/C, the right side the reaction using Pd/SiO₂. These experiments with the complete *Heck* reaction mixture show leaching behavior analogous to previous studies on leaching in *Heck* reactions.^[87] The conversion of bromobenzene (blue curve, Figure 41) starts at temperatures around 140-150 °C, the typical temperature range for converting aryl bromides in *Heck* reactions. The black curve shows the amount of palladium in solution at the given time. The reaction mixture samples were quickly filtrated using a 200 nm syringe filter and palladium content was determined by elemental analysis, employing ICP-MS or photometric concentration determination (see Experimental, chapter 6.2). Both experiments are characterized by the coincidence of the maximum rate of conversion and the maximum of the leaching curve. Catalytically active species are formed by palladium leaching from the solid catalyst, undergoing catalytic cycles and being redeposited on the support when the substrate is consumed.^[87] According to literature, the most common interpretation of the Pd dissolution observed here is that oxidative addition of the aryl bromide leads to the formation of dissolved molecular palladium species.

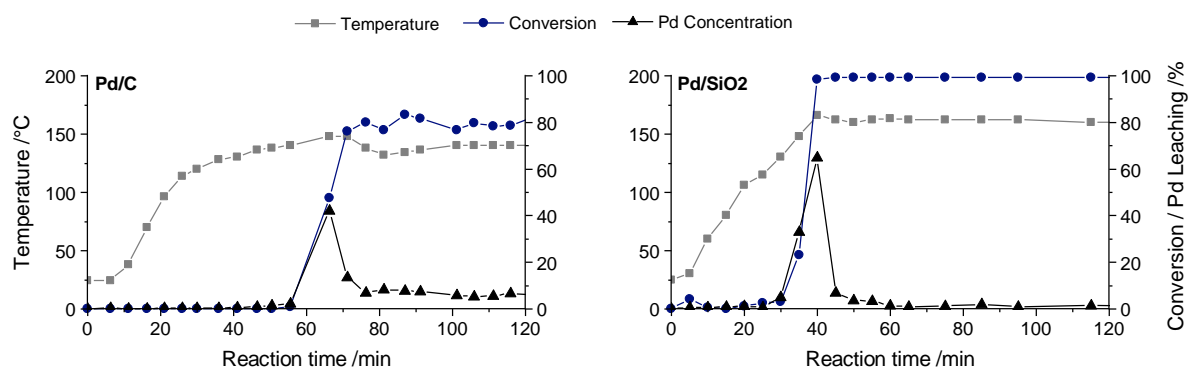


Figure 41: Leaching (black curve) under standard *Heck* reaction conditions as bromobenzene is converted with styrene (blue curve) as a function of reaction time and temperature using Pd/C (left) and Pd/SiO₂ (right) as a catalyst (adapted from [73] and [74]). Reaction conditions: 0.5 / 0.1 mol-% Pd, 1.0 eq substrate, 1.3 eq / 1.5 eq styrene, 1.2 eq NaOAc, - / 0.6 eq TBAB, NMP, 140 °C / 160 °C, air.

Parameter reduction based on DFT calculations

To assess which parameters of the reaction system drive and support the leaching of palladium from solid Pd particles a number of basic DFT calculations have been conducted based on an octahedral Pd-cluster. The model reactions compare the overall energetic situation after leaching one of its Pd atoms in case of (i) Pd cluster + solvent, (ii) Pd cluster, solvent + aryl bromide, (iii) Pd cluster, solvent, aryl halide + additional bromide source and (iv) Pd cluster, aryl bromide + excess of free bromide ions. The calculated free reaction energies G_r (Table 15) show that the model system composed of Pd cluster and solvent cannot support leaching of Pd. The addition of aryl bromide lowers the reaction free energy considerably, indicating that its presence plays a significant role in the leaching step (oxidative addition). The addition of another bromide source (so-called Jeffery conditions^[116]) further lowers G_r , enabling the Pd atom to be more easily detached from its cluster.

Table 15: Reaction free energies G_r for dissolving one palladium atom as a complex from a Pd₆ cluster with various ligand configurations from DFT model calculations.^[74]

Reaction	G_r (150 °C, 1 bar) kJ mol ⁻¹
Pd ₆ + 4 DMF → Pd ₅ + [Pd(DMF) ₄]	517
Pd ₆ + 2 DMF + PhBr → Pd ₅ + [PdBr(DMF) ₂ Ph]	165
Pd ₆ + DMF + PhBr + Br ⁻ → Pd ₅ + [PdBr ₂ (DMF)Ph] ⁻	14
Pd ₆ + PhBr + 2 Br ⁻ → Pd ₅ + [PdBr ₃ Ph] ²⁻	-69

These results of the DFT calculation were used as the basis for targeted leaching experiments, systematically reducing the number of components to observe if the experimental data support the computed leaching predictions. Other reports have done experiments following a similar

top-down approach but did not monitor leaching temperature and time. Sampling in short time intervals allowed a good monitoring of the Pd leaching in the chosen experiments. All experiments were tested with the previously described Pd/C (5 wt.-%) and Pd/SiO₂ (1 wt.-%) to ensure a better general applicability of the drawn conclusions.

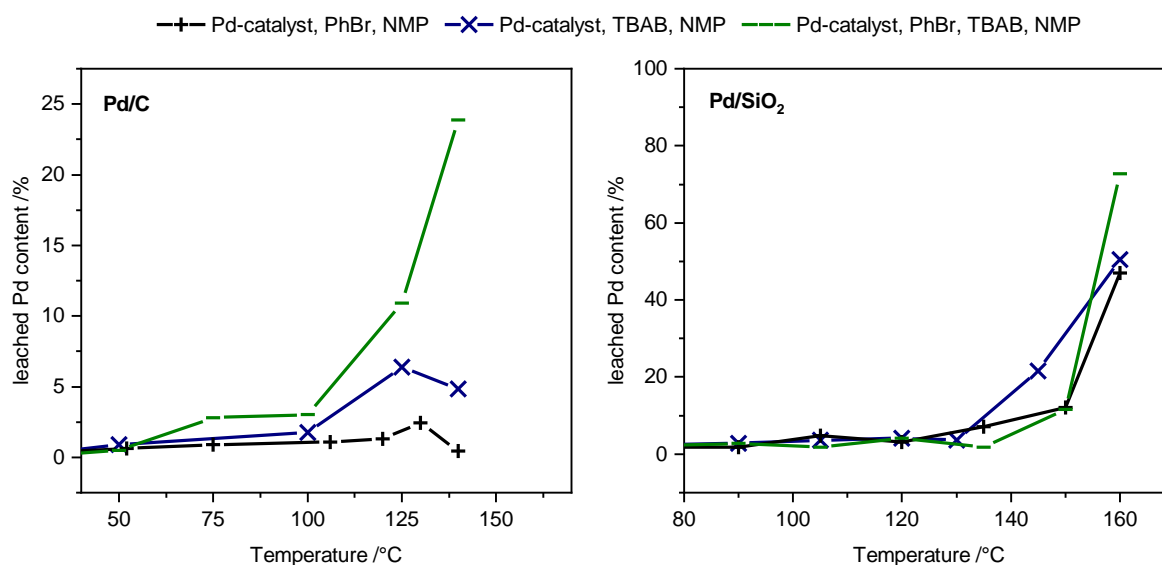


Figure 42: Leaching of palladium from Pd/C (5 wt.-%, left side) and Pd/SiO₂ (1 wt.-%, right side) as function of temperature and reaction time (temperature-programmed experiment). Leaching in 250 mL NMP and 250 mmol bromobenzene (black curve, +), 5 mmol TBAB (blue curve, X) or PhBr + TBAB (green curve, -).

Both catalysts show the same qualitative effects, but the differences in catalyst loading results in a higher percentage of dissolved palladium species in the case of 1 wt.-% Pd/SiO₂ (see different y-axis scaling in Figure 42). This is an expected effect due to the considerably lower Pd loading.

The experiment with bromobenzene (250 mmol), 0.5 mol-% palladium with respect to bromobenzene and N-methylpyrrolidone (250 ml) as standard solvent corresponds to reaction 2 of the DFT calculation. The leaching curves (Figure 42, black curves) show the percentage of total Pd, which has been leached into solution at the temperature given (about 2 % for Pd/C, up to 50 % for Pd/SiO₂). In fact, Pd is leached with PhBr and NMP at temperatures equal to and higher than 120 °C, i.e., the temperature at which the *Heck* reaction (oxidative addition is assumed as rate determining step) started. The blue “leaching curves” show the reaction of the supported Pd nanoparticles with only tetrabutylammonium bromide (TBAB) (5 mmol) and solvent NMP. TBAB is a source for bromide ions which can stabilize Pd in solution by forming palladium bromido complexes. The proposed improved leaching behavior is clearly visible,

both catalysts show higher leached Pd quantities and the dissolution occurs at lower temperatures compared to the previous experiment. The effect is more pronounced for the Pd/C catalyst but present for both tested catalysts. The third experiment was carried out with bromobenzene, TBAB and NMP (green curves). In agreement with expectations and model calculations, there is a significant increase of Pd concentration compared to experiments 1 and 2. In experiment 3, the substrate (able to undergo oxidative addition to the catalyst) is present as well as a source of bromide ions which, as previously mentioned, is known to stabilize palladium species in solution.^[24] In the case of oxidative addition, the C-Br bond needs to be broken before oxidative addition can take place, this explains the higher set-off temperature, when bromide ions/TBAB are not present (as observed for the Pd/C samples).

A different visualization of the experimental data underlines that the dissolved palladium species are not stable at higher temperatures and increased reaction times but (at least partially) re-precipitated, resulting in a reduced Pd concentration. This can be interpreted as effect of “self”-reduction of Pd(II) and missing stabilizing ligands. To illustrate this effect, the experiments using Pd/SiO₂ catalysts were kept isothermally (up to an hour) at reaction temperature.

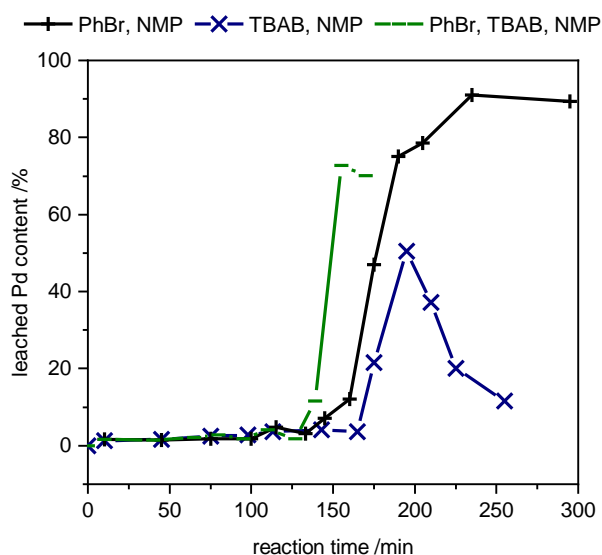
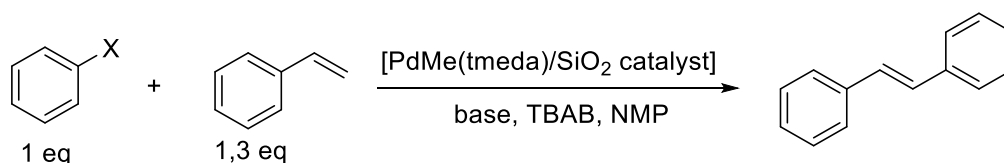


Figure 43: Leaching of palladium from Pd/SiO₂ (1 wt.-%) as function of reaction time (temperature-programmed experiment). Leaching in 250 mL NMP and 250 mmol bromobenzene (black curve, +), 5 mmol TBAB (blue curve, X) or PhBr + TBAB (green curve, -).

3.3.3 Leaching of supported Pd-complexes in *Heck* Reactions of Aryl Bromides and Chlorides

The previous subchapter described the leaching behavior of supported Pd-(nano)particle catalysts under *Heck* reaction conditions. Another specific approach is a catalyst with isolated Pd-complexes immobilized on a support, which shows a different Pd leaching progression. The reaction conditions are given in Equation 9.



Equation 9: Reaction equation and reaction conditions of the investigated *Heck* coupling reactions using PdMe(tmeda)/SiO₂ as a catalyst (X = Br or Cl).

Figure 44 (left) shows the Pd leaching and reaction progression for the conversion of bromobenzene, using supported isolated palladium complexes as a catalyst. The experiment is executed analogously to the conversion of bromobenzene using a supported Pd particle catalyst (compare Figure 41, right). The application of the isolated surface catalyst shows extreme Pd leaching right at the start of the reaction (heating phase). Within 10 minutes almost all palladium is dissolved at temperatures around 100 °C. Nevertheless, the conversion of the substrate does not start simultaneously (or only at a very low rate) in clear contrast to the previously observed reaction progression using supported Pd nanoparticle catalysts. The further increase in temperature shows a drop in Pd concentration at 120 °C to about 75 % Pd concentration. Quickly the Pd concentration increases again to a second maximum which now coincides with the rapid conversion of the substrate. After the reaction is completed, the Pd concentration decreases rapidly.

Although the experiment does not allow the differentiation between different oxidation states of the Pd, several conclusions can be drawn. Driven by the excess of bromide ions in the reaction mixture, it is most likely that the species, which are released from the surface into solution during the heating phase, are bromopalladium(II)-complexes of the kind PdMeBr(tmeda), PdBr₂(tmeda) or similar Pd(II) complexes with coordinating solvent molecules (with or without the tmeda ligand). In contrast to the previously described supported PdO/Pd(0) catalysts, here, the supported Pd is not part of the lattice and does not need to transcend lattice energy to form soluble species.

It seems that the large excess of bromide ions is able to shift the equilibrium to Pd bromide complexes in solution opposed to the strong covalent bond between Pd and surface oxygen.

During the early heating phase, the temperature is not high enough to reduce Pd(II) and the oxidative addition of the aryl halide cannot take place either (requiring Pd(0)). The following decrease in palladium concentration indicates, that the stability of the Pd(II) complexes in solution decreases and Pd is subsequently partially re-deposited, probably as small Pd(0) clusters.

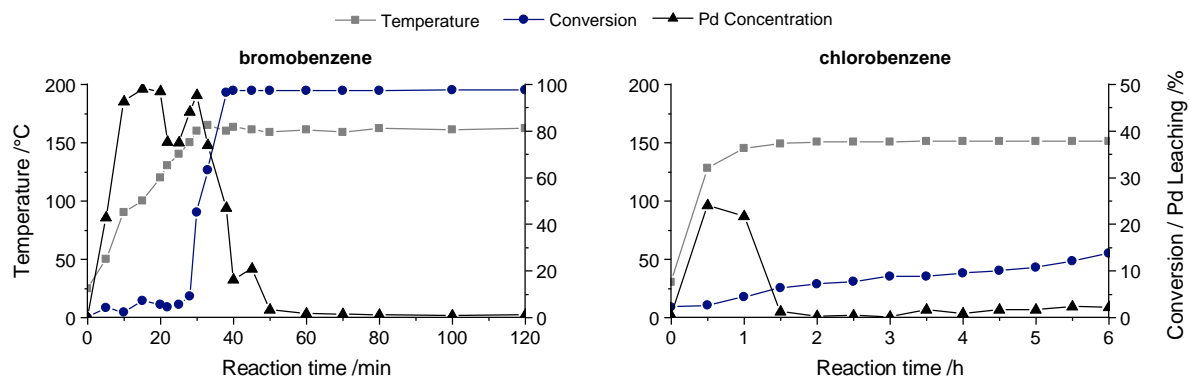


Figure 44: Contemporaneous determination of the conversion of substrate and the amount of palladium in solution with PdMe(tmeda)/SiO₂ as catalyst (adapted from [73]). Please note the differences in axis scaling. Reaction conditions: 0.1 / 0.05 mol-% Pd, 1.0 eq substrate, 1.3 eq styrene, 1.2 eq NaOAc / 0.6 eq Ca(OH)₂, 0.6 eq TBAB, NMP, 160 °C / 150 °C, air.

At the beginning of the reaction ($T = 150\text{ °C}$), around one quarter of the palladium is located on the support whereas three quarters are in solution. Of course, the latter is readily available to enter the catalytic cycle (after reduction of Pd(II) to Pd(0) beforehand). Nevertheless, because of the re-increase of the palladium amount during the reaction, the re-deposited supported palladium species seem to be involved in the catalytic process. It can be assumed that very small metallic palladium species can be generated during re-adsorption processes and still be available for the catalytic reaction, because the temperature range of 130 – 150 °C exactly comprises the onset of the two relevant elementary processes being coupled to each other: reduction of Pd(II) to Pd(0) as well as oxidative addition^[97]. As in the experiment with supported nanoparticles as catalyst, the palladium is re-deposited on the support again after the complete conversion of the bromobenzene (compare Figure 41).

In case of supported palladium (oxide) particles, palladium is partially reduced at the surface prior to its dissolution by oxidative addition of the aryl halide, leaching can be accelerated by the presence of tetrabutylammonium bromide. Pd(0) species can be re-deposited and subsequently re-dissolved (by oxidative addition) if PdMe(tmeda)/SiO₂ is applied, generating supported but for the reaction still available Pd(0) species “in-situ”. The same process cannot be completely excluded for catalysts with supported palladium (oxide) particles, but regarding the

existing leaching experiments (from this work and previous studies^[24-26, 117]) with bromobenzene as aryl halide, it seems rather unlikely. The different kinds of leaching mechanisms and therefore the generation of the active species of both catalytic systems are the cause for the varying performances. This is especially evident towards aryl chlorides as reported in ^[110] with surface complexes clearly outperforming palladium oxide particle catalysts in the coupling of chlorobenzene. The reaction and leaching progression using the PdMe(tmeda)/SiO₂ catalysts with the more-demanding substrate chlorobenzene is shown in Figure 44 (right side). The stability of the C-Cl bond markedly decreases the rate of the oxidative addition, resulting in considerably longer reaction times compared to bromobenzene as a substrate (timeframe of hours instead of minutes).

As previously described for bromobenzene, high amounts of supported palladium complexes are dissolved during the heating of the reaction mixture (50 % palladium leaching after 30 minutes) by complexation with the available bromide ligands. The high palladium concentration in solution during the first hour of the reaction time again underlines that this dissolution process is independent of the oxidative addition of the aryl halide. When the temperature exceeds 130 °C, the palladium concentration in solution is decreasing. Above 150 °C, formation of stilbene starts. Throughout the next several hours, the reaction proceeds slowly (roughly linearly) and the palladium content in solution is increasing to maximum of 5 % of total Pd.

The oxidative addition of chlorobenzene is considerably slower compared to that of bromobenzene. All Pd(0) species in solution are re-deposited (reaction times $t = 2 - 3$ h), because the slow oxidative addition of chlorobenzene cannot compete with the precipitation. Only after some additional induction period, steady increase of the yield shows that the catalyst is able to constantly provide dissolved, active Pd(0) species over several hours of reaction time. Due to the demanding oxidative addition of chlorobenzene and the competing accelerated reduction and agglomeration of Pd at these higher temperatures, the equilibrium between dissolved and supported palladium species is shifted towards the supported species.

3.4 Conclusion

The contemporaneous determination of conversion and palladium concentration during the Heck coupling of bromobenzene and styrene revealed different leaching mechanisms dependent on the applied solid palladium pre-catalyst.

For catalysts with supported palladium particles, the generation of dissolved, active Pd species occurs by reduction at the surface and subsequent dissolution of palladium by oxidative addition of the aryl halide. Pd dissolution is accelerated by bromide ions and substrate molecules. Dissolved palladium is re-deposited to the catalyst surface with increasing temperature and time, and with consumption of the substrates with the progress of the reaction.

Model calculations of reaction free energies balancing educts and products rationalize experimental results on the significance of presence or absence of reactants, additives and solvents for leaching of palladium under typical *Heck* reaction conditions. Oxidative addition of phenyl bromide is decisive for decreasing the dissolution energy, but by far not the only relevant parameter. Additional bromide ions clearly make the leaching process more exergonic. The effect of bromide ions is due to the high stability of the Pd bromide complexes formed.

Pre-catalysts with isolated surface complexes release palladium by complexation prior to its reduction occurring in solution. The active catalyst is formed by re-deposition of these Pd species dissolved at lower temperature "*in situ*", before a second leaching step generates the active species at reaction temperatures. Through this process during an induction period, supported Pd(0) clusters are formed under reaction conditions, which are available for the generation of (renewed) active centers by re-dissolution of palladium via oxidative addition under more demanding conditions. During reactions of chlorobenzene catalyzed by highly active catalysts, a permanent low percentage (< 5 %) of dissolved palladium is present over several hours. No other characteristic correlation of reaction rate and Pd content as with bromides could be observed.

In summary, it can be concluded from the computational and experimental data that leaching of molecular Pd complexes during *Heck* reactions is caused by various parameters and complex mechanisms.

Summary

One of the important causes of deactivation of solid catalysts is the loss of active component due to corrosion or leaching by the reaction medium. Particularly relevant are leaching processes when solid catalysts are applied in a liquid medium. The present thesis examined this dissolution of metals from solid catalysts for two different reaction types in order to better understand the complex leaching processes at solid-liquid interfaces: the copper aluminate spinel catalyzed hydrogenation of aldehydes and carbon-carbon couplings by supported palladium. Deeper understanding could be achieved using a specific experimental approach, in which the metal species dissolved in solution were determined during the reaction as function of reaction time and temperature, dependent on the nature of the solid catalyst, solvent, substrates and additives.

Copper aluminate spinel catalysts with three different copper loadings showed leaching of only traces of copper under strongly reducing conditions (65 bar hydrogen, 120 °C, hexane) during the hydrogenation of butanal to butanol. Oxidized copper(II) species are re-reduced to metallic copper under standard conditions. The amount of leached copper as well as re-reduced copper(0) species are substantially dependent on solvent and additives. Particularly the presence of carboxylic acids – a typical impurity in industrial feeds – causes an increase of the copper content in solution during the reaction. Upon complexation with the carboxylate, copper(II) is stabilized in solution and not easily reduced to Cu^0 again. The amount of copper in solution depends on the carbon chain length of the carboxylic acid and on the solvent (hexane, toluene, dioxane, ethanol) and can reach up to 6 % of the total copper content of the catalyst. The Cu concentration in solution does not correlate with the catalytic activity. Ethanol as solvent and additive can substantially modify the activity and selectivity (acetal formation). Beyond all expectations, aluminum leaching can be remarkable even under standard conditions (up to > 2 % of total aluminum content in the catalyst). Most critical for the stability of the catalyst is the increased aluminum leaching when carboxylic acids are present. Long-term experiments showed that aluminum leaching increases continuously in the presence of any acid tested, reaching up to 6 % of total aluminum content within 24 h, thus being a serious danger for the stability of catalysts. Addition of 10 % ethanol to hexane can help to suppress copper leaching completely and to keep the aluminum leaching below 1 %. The present study contributed ideas and variables to control leaching and catalyst stability in a knowledge-based approach for copper catalyzed hydrogenation reactions.

It is generally accepted in literature now that leaching of palladium from supported catalysts is a prerequisite for catalytic activity in carbon-carbon coupling reactions like the *Heck* reaction, i.e. the reaction is catalyzed by dissolved Pd(0) complexes. The present investigation focusses on the leaching mechanism and the dynamics of dissolution and re-deposition of the palladium

species. In this context, different solid palladium pre-catalysts were compared regarding their activity in the *Heck* reaction and the dissolution process of palladium with demanding aryl bromide and chloride substrates. Depending on the substrate and the pre-catalyst, differing leaching mechanisms have been revealed for supported palladium oxide catalysts and for isolated palladium surface complexes. In a further model study, relevant parameters for the leaching of palladium atoms from small Pd clusters during *Heck* reactions of bromobenzene and styrene have been explored computationally and experimentally. Oxidative addition of bromobenzene and coordination of bromide ions substantially decrease the dissolution energy obtained from DFT calculations. Targeted experiments with Pd leaching from supported catalysts (Pd/C, Pd/SiO₂) as a function of reaction temperature, time and additives agreed very well with the computational results.

Zusammenfassung

Ein wichtiger Aspekt der Desaktivierung von Festkörperkatalysatoren ist der Verlust an aktiver Spezies durch Korrosion oder Leaching. Dies ist besonders bei der Anwendung in der Flüssigphase der Fall. Die vorliegende Arbeit untersuchte diese Herauslösung von Metallspezies aus Festkörperkatalysatoren für zwei verschiedene Reaktionstypen um die komplexen Prozesse besser zu verstehen, die dem Leaching zugrunde liegen. Hierzu wurde die Hydrierung von Aldehyden mittels eines Kupferaluminat-Spinells sowie die *Heck*-Reaktion an einem geträgerten Palladiumkatalysator betrachtet. Im gewählten Ansatz wurde die Metallspezieskonzentration als Funktion der Reaktionszeit und Temperatur, sowie in Abhängigkeit des Katalysatortyps, Lösemittels, Substrats und verschiedener Additive betrachtet.

Drei Kupferaluminat-Spinellkatalysatoren mit verschiedenen Kupferanteilen wurden in der Hydrierung von *n*-Butanal zu *n*-Butanol unter stark reduzierenden Reaktionsbedingungen (65 bar H₂, 120 °C, Hexan) getestet. Sie zeigten nur kleinste Mengen Kupferleaching. Oxydierte Kupfer(II)spezies werden unter diesen experimentellen ‚Standardbedingungen‘ wieder zu metallischem Kupfer reduziert. Die Menge an Kupfer in Lösung und dessen erneute Reduktion sind stark von Lösemittel und Additiven abhängig. Insbesondere die Zumischung von Carbonsäuren – eine typische Verunreinigung im industriellen Feed – sorgt für einen deutlichen Anstieg der Kupferkonzentration in Lösung. Die Komplexbildung als Kupfer(II)-carboxylat ermöglicht eine Stabilisierung der geleachten Spezies in Lösung und verhindert eine erneute Reduktion zu Cu(0). Die Menge an gelöster Kupferspezies hängt insbesondere von der Kettenlänge der Carbonsäure sowie vom gewählten Lösungsmittel ab (Hexan, Toluol, 1,4-Dioxan, Ethanol) und kann bis zu 6 % des im Spinell vorhandenen Kupferanteils in Lösung führen. Die Kupferkonzentration in Lösung korreliert hierbei nicht mit der Katalysatoraktivität. Ethanol als Lösungsmittel oder als Beimischung kann die Katalysatoraktivität deutlich beeinflussen, wirkt sich aber auch in einzelnen Fällen auf die Selektivität aus (Acetalbildung).

Entgegen allen Erwartungen zeigt Aluminium ein erkennbares Leachingverhalten, sogar unter ‚Standardbedingungen‘. Es geht bis zu 2 % des vorhandenen Aluminiumgehalts in Lösung. Das Aluminiumleaching stellt einen kritischen Faktor für die Stabilität des Spinellkatalysators dar, insbesondere bei der Beimischung von Carbonsäuren. Langzeitexperimente zeigen ein kontinuierlich ansteigendes Aluminiumleaching, was innerhalb von 24 Stunden bis zu 6 % gelöste Aluminiumspezies erreicht. Dies ist eine ernstzunehmende Einschränkung für die Stabilität des Katalysators. Die Beimischung von 10 % Ethanol zum Lösungsmittel kann das Leaching von Kupfer nahezu vollständig unterdrücken und das Leaching von Aluminiumspezies deutlich auf Werte < 1 % senken. Die durchgeführte Studie hat systematisch Parameter getestet, die zu einer besseren Beherrschbarkeit des Leachings von Kupferspinell-Katalysatoren in Hydrierreaktionen beitragen.

Es ist inzwischen in der Literatur weitestgehend akzeptiert, dass das Leaching von Palladiumspezies von einem Feststoffkatalysator in die Flüssigphase eine Voraussetzung für dessen katalytische Aktivität in C-C-Kupplungsreaktionen, wie der *Heck*-Reaktion, ist. Das bedeutet die Reaktion wird durch gelöste Pd(0)-Komplexe katalysiert. Der Fokus der durchgeführten Studie lag auf dem zugrundeliegenden Leachingmechanismus und der Dynamik zwischen Lösung- und Wiederabscheidung der Palladiumspezies. Im Rahmen dessen wurden verschiedene geträgerte Pd-Präkatalysatoren hergestellt und in Bezug auf ihre Aktivität in der *Heck*-Reaktion untersucht. Abhängig von Substrat und Präkatalysatorspezies konnten unterschiedliche Leachingmechanismen für geträgerte PdO-Katalysatoren und für Katalysatoren mit isolierten Pd-Oberflächenkomplexen gezeigt werden. In einer weiteren Modellstudie wurden die relevanten Parameter für das Palladium-Leaching von kleinen Pd-Clustern während der *Heck*-Reaktion von Brombenzol und Styrol die relevanten Parameter experimentell und rechnerisch betrachtet. Laut DFT-Rechnungen verringert sowohl die oxidative Addition von Brombenzol als auch die Koordinierung mit Bromidionen die benötigte Energie zur Lösung des Pd erheblich. Gezielte Auflösungs- und Wiederabscheidungsexperimente zum Palladiumleaching von geträgerten Pd-Katalysatoren (Pd/C, Pd/SiO₂) in Abhängigkeit von der Reaktionstemperatur, -zeit und Beimengungen stimmen sehr gut mit den berechneten Ergebnissen überein.

Experimental

6.1 Experimental to chapter 2 – Leaching in Cu-Al spinel catalyzed liquid phase hydrogenation

Synthesis of the catalysts

All chemicals were used without further purification.

Chemical	Supplier	Purification grade
$\text{Cu}(\text{NO}_3)_2 \cdot 3\text{H}_2\text{O}$	VWR Chemicals	GPR Rectapur
$\text{Al}(\text{NO}_3)_3 \cdot 9\text{H}_2\text{O}$	Merck	$\geq 95\%$
Na_2CO_3	VWR Chemicals	Normapur
$(\text{NH}_4)_2\text{CO}_3$	VWR Chemicals	Emsure
NaOH	Grüssing GmbH	99%
H_3PO_4 (85%)	VWR Chemicals	Normapure
Conc. HNO_3	VWR Chemicals	Normapure
Butyraldehyde	Merck	99%
n-Dodecane	Merck	$\geq 99\%$
Hexane	VWR Chemicals	$\geq 99\%$
Ethanol	VWR Chemicals	$\geq 99.5\%$
Toluene	Merck	$\geq 99.8\%$
1,4-Dioxane	VWR Chemicals	GPR Rectapur
Propanoic acid	Merck	$\geq 99\%$
Pentanoic acid	Merck	$\geq 98\%$
Heptanoic acid	Merck	$\geq 99\%$
Octanoic acid	Merck	$\geq 99\%$
Hydrogen	Westfalen	5.0
Helium	Westfalen	4.6
Argon	Westfalen	5.0
Nitrogen	Westfalen	5.0

Preparation feed solution

The Cu-Al spinel catalyst precursor is synthesized by co-precipitation. Stoichiometric amounts of $\text{Cu}(\text{NO}_3)_2 \cdot 3 \text{H}_2\text{O}$ and $\text{Al}(\text{NO}_3)_3 \cdot 9 \text{H}_2\text{O}$ are dissolved in deionized water in a 250 mL volumetric flask to produce the feed solution for the co-precipitation procedure. The stoichiometric amounts weighed in for the three copper aluminate spinel subspecies are given in Table 16

Experimental

Table 16: Amounts weighed in for 250 mL feed solution

Spinel type	Cu(NO ₃) ₂ · 3 H ₂ O	Al(NO ₃) ₃ · 9 H ₂ O
CuO · CuAl ₂ O ₄	36.44 g	56.58 g
Stoichiometric spinel	18.22 g	56.58 g
Phase-pure spinel	18.22 g	56.58 g

Synthesis of Copper aluminate spinel catalyst (CuO · CuAl₂O₄ and stoichiometric spinel)

For the co-precipitation process, 500 mL of distilled water are filled into an 800 mL beaker containing a stirring bar, a pH electrode and a thermometer and placed onto a magnetic hot plate stirrer. The water is heated to 50 °C while stirring with 400 RPM. Upon reaching the target temperature 100 mL of feed solution is fed dropwise into the beaker using a peristaltic pump from *Medorex* with a speed of 5 mL/min. The pH value of the precipitation solution is kept at a constant value of 6.5 by titration with 2M Na₂CO₃. The titration is controlled by a 906 Titrando titrator by *Metrohm*. After the feed solution is fully added to the reaction vessel, the titration is stopped and the reaction mixture kept at 50 °C with stirring at 400 RPM for another hour. After cooling down the resulting precipitate is filtered off, washed by redistribution in 500 mL of deionized water and filtered off again until the electrical conductivity of the filtrate is below 0.5 mS. In most cases this value is reached after 3-4 washing steps. Afterwards the precatalyst is dried at 120 °C overnight and calcined at 800 °C for 8 h with a heating ramp of 5 K/min (stoichiometric and phase-pure spinel) or calcined at 750 °C for 2 h with a heating ramp of 2 K/min (CuO · CuAl₂O₄). The obtained CuO · CuAl₂O₄ and stoichiometric spinel catalyst is then sieved to give particles of a diameter d with $100 \mu\text{m} < d \leq 300 \mu\text{m}$.

Synthesis of phase-pure spinel CuAl₂O₄

The co-precipitation and washing procedure is performed as described in the previous section. After drying at 120 °C overnight the precatalyst is calcined at 800 °C for 8 h with a heating ramp of 5 K/min. After calcination, the surface CuO formed during the synthesis process is removed by an additional leaching step to obtain the phase-pure spinel form CuAl₂O₄. 11 mL of (NH₄)₂CO₃ solution are added to 4 g of the calcined catalyst, mixed and treated for 2 hours in an ultrasonic bath. Afterwards the mixture is heated to 50°C and stirred carefully on a heated stirring plate for an additional 30 min. The mixture is filtered of and washed once with 500 mL of deionized water. The resulting material is dried overnight at 120 °C and then sieved to give particles of a diameter d with $100 \mu\text{m} < d \leq 300 \mu\text{m}$.

Activation of the catalyst

1-1.5 g of catalyst are filled in a U-shaped glass reactor and connected to a top-section with UltraTorr fittings and two valves by *Swagelok* to allow inert transfer. The top section is connected to the gas supply and the reactor placed in a tube furnace. The reactor is flushed with argon for at least 10 minutes to remove all air from the system before the gas supply is switched to hydrogen. The catalyst is slowly heated under H₂ flow to 300 °C with a heating ramp of 1 K/min and held for 1 hour. After that, the gas supply is switched back to argon flow and the reactor is removed from the furnace. After cooling down the valves of the top section are shut and the reactor system can be transferred to the glove box under inert conditions. 350 mg are put in a glass vial inside the glove box to be used for a leaching experiment and enable a close to inert transfer to the reaction vessel (see next section).

Catalyst leaching experiment during hydrogenation of butyraldehyde

The autoclave is assembled under an argon shower to achieve an as inert as possible transfer of the activated catalyst. A standard catalyst leaching experiment consists of 350 mg activated catalyst, 100 mL of the chosen solvent, 8 g butyraldehyde and 1.2 g n-dodecane as an internal GC standard within the reaction mixture. In case of a solvent mixture, 10 mL of the secondary solvent are added to 100 mL of hexane. The liquid components are added to the glass inlet under air, placed inside the bottom part of the autoclave under the argon shower and additionally flushed with argon using a flexible tube for 10 minutes. After removing the tube, the catalyst is added underneath the argon shower and the head of the autoclave quickly fixed on top. The autoclave is connected to the argon supply and flushed while the autoclave assembly is completed to remove as much potential air from the system as possible.

Once the assembly is finished, the autoclave is carefully pressurized with 65 bar hydrogen and slowly heated to the reaction temperature of 120 °C. Upon reaching 120 °C a first sample is taken and stirring (800 RPM) started. Regular sampling throughout the reaction, using a dip tube, monitors the hydrogenation reaction and leaching progression. Stirring is suspended during and restarted once the sampling is finished (normally less than 30s pause). The samples are filtered through a 0.2 µm PTFE syringe filter to avoid secondary leaching from catalyst residue and stored in the fridge. 2 mL of sample are separated for later analysis by ICP-OES and the rest used for GC measurements of the sample composition.

The sampling interval is more frequent in the beginning of the reaction and reduced over time (Table 17).

Table 17: Sampling frequency during leaching experiments. The first sample is taken after the reaction temperature of 120 °C is reached.

Reaction time	Sampling frequency
First hour	Every 15 min
Second hour	Every 30 min
After 2 hours	Every 60 min

The experiment is stopped after 5-6 hours by removing the heating block of the autoclave and cooling down the system using an ice water bath. The autoclave is slowly depressurized via the connected tubing and valves before opening. The remaining catalyst is filtered off and left to dry on air for follow-up analysis of the spent catalyst. The glass inlet and autoclave vessel are emptied and cleaned with acetone.

Sample preparation for analysis

Elemental analysis of the liquid leaching samples and catalyst composition are done by Inductively coupled plasma – optical transmission spectrometry (ICP-OES) using an ICP-OES 700 machine from *Agilent*. The element concentration of the sample should not exceed 50 ppm.

Preparation of liquid samples

The solvent of the leaching samples is left to evaporate overnight inside the fume hood. The remaining organic residue is removed prior to elemental analysis by ICP-OES by heating to 250 °C in a muffle oven with a heating ramp of 50 K/h. After cooling down, 3 mL of concentrated phosphoric acid are added to the sample and treated for 1 hour in an ultrasonic bath. Finally, it is diluted to 10 mL with deionized water and stored in a 15 mL centrifuge tube for ICP-OES analysis.

Preparation of solid samples

40 mg of the powder sample are weighed and stored in a glass vial with snap-on plastic caps. A stirring bar and 2 mL of concentrated phosphoric acid are added to the vial before placing them in an oil bath heated to 90 °C. The plastic caps are pierced in a few spots to allow for gas to escape. The vials are left at 90 °C and mid-range stirring for 15-20 hours until all of the catalyst sample has been dissolved. The sample is transferred to a 50 mL volumetric flask and diluted with deionized water. 1 mL of the resulting sample is removed with an Eppendorf pipette, diluted to 10 mL and stored in a 15 mL centrifuge tube for ICP-OES analysis.

Elemental analysis by Inductively coupled plasma – optical transmission spectrometry

The elemental analysis of the samples is done by ICP-OES measurements, using an ICP-OES 700 from *Agilent* containing an autosampler. The machine uses argon (purity 5.0) for supply

to the plasma, nebulizer and optics interface purge as well as polychromator purge. The tubing system is flushed with 2% nitric acid to remove sample residue in-between measurements. Each sample is measured 5 times (1 mL respectively) and the resulting mean value is displayed as the measurement result. The preferred wavelength for elemental analysis is 324.754 nm (Cu) and 394.401 nm (Al). 5 wavelength per element are measured each time, in case of overlap or interference, the next best wavelength can be used for analysis.

A calibration curve is generated by measuring freshly prepared calibration samples using the "ICP multi-element standard solution IV" from *Merck* Certipur, containing 23 elements (including Cu and Al) in diluted nitric acid with an initial concentration of 1000 mg/L. For leaching samples calibration standard concentrations of 0.25 ppm, 0.5 ppm, 1 ppm and 10 ppm were used for the calibration curve. Solid samples were calibrated against calibration standard concentrations of 1 ppm, 10 ppm, 20 ppm and 50 ppm. In either case a blank sample is measured first, containing deionized water and a drop of the acid used in the preparation of the ICP-OES samples (in this case concentrated phosphoric acid).

Product analysis via gas chromatography

At the specified sampling intervals liquid samples of about 1 mL are filtered through a syringe filter (0.2 μm), transferred into GC vials and later analyzed quantitatively by gas chromatography. The samples are stored in the fridge until measured, an additional preparation step is not necessary.

Gas chromatograms are recorded on an *Agilent G1530A* machine fitted with a FID detector. A HP-1ms GC column (stationary phase: dimethylpolysiloxane, length: 30 m, inner diameter: 0.25 mm, film thickness: 0.25 μm) is used to separate the different components and n-dodecane is used as an internal standard for calibration.

Characterization methods

Analysis by X-Ray diffraction

The powdered catalyst sample is placed onto a flatbed support, inserted into the X-ray machine and measured with an *Empyrean* diffractometer from *PANalytical* ($K_{\alpha}(\text{Cu})$, $\lambda=1.5419$, Ni as $K_{\beta}(\text{Cu})$ -filter) in reflection mode. Diffractograms are recorded in an angle range between 5° and 70° in steps of 0.008° . They are analyzed using the *HighScore Plus* software from *PANalytical* and the Powder Diffraction FileTM database PDF-2 (2004).^[61]

Analysis by Raman spectroscopy

Raman spectra are recorded on an *InVia* Raman Microscope from *Renishaw* equipped with a research-grade microscope by Leica (magnification: 5x, 20x, 50x). Available lasers are a frequency-doubled Nd:YAG laser ($\lambda=532$ nm), HeNe Laser ($\lambda=633$ nm) and a diode laser ($\lambda=785$ nm). Most samples were powder samples with a standard laser intensity of 0.3 mW on the sample and a standard scanning time of 30s with 6 repetitions in case of spinel samples. All lasers were used but predominantly 532 nm. Liquid samples were also tested with slightly different measurement conditions (higher laser intensity, shorter measurement time).

Temperature programmed reduction

Experiments were performed on an *Autochem 2920* device equipped with a thermal conductivity detector. The catalyst is first flushed with Argon (25 mL/min) and heated with a rate of 5 K min⁻¹ to 120 °C and held for an hour. Reductions were carried out under a gas stream of 50 mL min⁻¹ of a 10 % H₂ in Ar. The reaction temperature was increased from room temperature to 800 °C at a rate of 5 K min⁻¹.

Cu-surface measurements

Cu surface was determined by N₂O pulse chemisorption experiments. Catalysts were reduced in pure H₂ (10 mL/min) at 300 °C. The rate was 2 K min⁻¹ and was held for 60 min before cooling to a reaction temperature of 40 °C at a rate of 20 K min⁻¹ and flushed with Helium before pulses of 50 μ L of N₂O were introduced to the gas stream until no difference towards the baseline could be detected or twenty pulses were achieved.

BET surface area determinations

were realized on a *Quantchrome NovaTouch 4XL* Device. The nitrogen adsorption (physisorption) on the samples were conducted at -196 °C. A measurement requires about 100 mg of the sample. Before every measurement the samples must be degassed by 120 °C under vacuum for 3 hours. 40 measuring points are recorded per BET-measurement. For the evaluation of the BET-surface area only those points with a partial pressure between 0.05-0.35 p/p₀ are required. For the BET-surface determination, both absorption and desorption are included in the calculation.

6.2 Experimental to chapter 3 – Leaching of palladium atoms from small cluster models during Heck reactions

Synthesis procedures

All chemicals were used without further purification.

Chemical	Supplier	Purification grade
Bromobenzene	Alfa Aesar	99%
Chlorobenzene	Merck	99%
Calcium hydroxide	Merck	96%
Sodium acetate	Merck	99 %
Tetrabutylammonium bromide	Sigma Aldrich	99%
Diethylene glycol dibutylether	Acros Organics	99%
Styrene	Merck	≥99%
Dichloromethane	Riedl-de-Haen	99.8%
<i>N</i> -methyl-2-pyrrolidone	VWR chemicals	99%
AEROSIL® 200	Evonik	
Palladium chloride	Sigma Aldrich	99%
HCl(aq) 37%	VWR chemicals	
Conc. H ₂ SO ₄	Merck	Emsure
Na(OH)	Grüssing GmbH	99%
Conc. HNO ₃	VWR chemicals	Normapure

Synthesis of silicon dioxide supported palladium oxide particles

AEROSIL® 200 was agglomerated in 150 mL distilled water until a gel is formed. The gel is dried at 70 °C for 3 days, pestled and sieved to a diameter d $100 \mu\text{m} < d \leq 300 \mu\text{m}$. The sieved powder is calcined using a muffle oven from Nabertherm. The calcination protocol is as follows: (1) heating ramp of 1 K min^{-1} to 120 °C, held for 2 hours. (2) heating ramp of 1.3 K min^{-1} to 500 °C, held for 2 hours.

The silicon dioxide supported palladium oxide particles were synthesized by a deposition-precipitation method based on Pearlman.^[111] For 1.0 g of catalyst with a target metal loading of 1.0 wt-% Pd, 0.99 g of the SiO₂ were suspended in 30 mL water. A solution of PdCl₂ in 5% HCl_{aq} was added dropwise under stirring. Subsequently, the pH of the suspension was slowly increased to pH 10 by the addition of 10% NaOH_{aq} using an autotitrator (Metrohm 736 GP Titrino). The resulting solid was filtered, washed several times with water and dried in vacuo. The brown powders were stored at room temperature and in air.

The grafted Pd-surface complexes were synthesized by C. Gnad as described in [112]. The procedure is replicated here for an easier understanding. Further characterization of the catalyst can be found in [110] and [73].

Synthesis of dimethylpalladium(II) complexes (from

Dimethyl(N,N,N',N'-tetramethylethanediamine)palladium(II): 1.5 g PdCl₂ (8.5 mmol, 1.0 eq.) was suspended in 50 mL acetonitrile and was refluxed for 4 h at 85 °C. After cooling down, 1.5 g N,N,N',N'-tetramethylethanediamine (12.7 mmol, 1.5 eq.) was added dropwise and the mixture was stirred at room temperature for 2 h. The yellow precipitate PdCl₂(tmeda) was filtered and washed 2 times with 20 mL diethyl ether. The product was inserted in the following methylation step without further processing. 1.9 g PdCl₂(tmeda) (6.8 mmol, 1.0 eq.) was suspended in 20 mL diethyl ether and was cooled to – 20 °C. 18 mL of a 1.6 M suspension of methyl lithium in diethyl ether (28.6 mmol, 2.2 eq.) was added dropwise. The reaction mixture was slowly warmed to 0 °C and stirred for 1.5 h. A color change from yellow to white indicates complete reaction. Unreacted methyl lithium was quenched by the careful addition of 8 mL cold, deionized water. The water phase was frozen at – 20 °C and the ether phase was separated by filtration. After defrosting, the water phase was extracted 2 times with 20 mL diethyl ether each using the described freezing/defrosting cycles. The ether phases were combined, the solvent removed and the white to slightly grey product dried *in vacuo*.

Synthesis of isolated surface complexes by grafting

The desired amount of the precursor (1.1 eq. referred to the desired occupation of silanol groups) was dissolved in pre-cooled toluene in a *Schlenk*-tube. The solution was filtered onto the desired amount of pre-treated support in another pre-cooled *Schlenk*-tube. The amounts of solvent and SiO₂⁷⁰⁰ were chosen to obtain a solvent:support ratio of 15 mL g⁻¹. The mixture was allowed to react without stirring for 20 hours at temperatures between -30 °C and -40 °C. After that time, the solvent was removed by filtration and the solid was washed twice with two thirds of the original amount of fresh solvent each. After evaporation of toluene residues and drying the material *in vacuo*, a white to pale yellow solid depending on the palladium loading was obtained. The materials were stored under inert conditions below –30 °C.

Elemental analysis

Carbon, hydrogen and nitrogen contents were determined by combustion analysis using an elemental analyzer (Eurovector). Inert sample preparation was carried out in a glovebox charging a tin foil mini weighing-boat with 10 – 15 mg of the sample, which was wrapped into another tin foil weighing boat.

Palladium and phosphorus contents were analyzed by photometry. The samples were boiled with concentrated sulfuric acid under low vacuum to remove organic compounds. In order to

digest the corresponding elements, the residues were treated with concentrated sulfuric and nitric acid. For the quantification of the palladium content, part of the solution was mixed with a freshly prepared solution of nitroso-R salt. In the case of phosphorous, ammonium vanadate solution was used. The contents were determined photometrically by a UV-vis spectrometer (Shimadzu UV-160).

All elemental analyses were conducted by the employees of the microanalytical laboratory at Technical University of Munich.

Catalysis - Heck reaction

The palladium catalyst (0.1 mol-% Pd), 28.3 g bromobenzene (180 mmol), 24.4 g styrene (234 mmol), 17.7 g sodium acetate (216 mmol), 34.8 g tetrabutylammonium bromide (108 mmol), 18.0 g diethylene glycol dibutyl ether and 400 mL NMP were placed in a 1000 mL round bottom flask equipped with a reflux condenser, a septum and an internal thermometer. Every 3-5 minutes, samples of 7 mL were taken with a pre-heated syringe and filtered immediately by a syringe filter (0.2 μ m PTFE membrane).

For the shorter leaching experiments (variation of reaction parameters) the amount of used chemicals was halved and sampling of 4.5 mL occurred at steps of 25 K (corresponds to about 20 min between samples).

In order to determine the palladium concentration in solution during the coupling of chlorobenzene, 0.05 mol% palladium catalyst, 20.3 g chlorobenzene (180 mmol), 24.4 g (234 mmol), 8.0 g calcium hydroxide (108 mmol), 34.8 g tetrabutylammonium bromide (108 mmol), 24.1 g diethylene glycol dibutyl ether and 400 mL NMP were placed in a 1000 mL round bottom flask equipped with a reflux condenser, a septum and an internal thermometer. Samples were taken every 30 minutes.

Elemental analysis by Inductively coupled plasma – optical transmission spectrometry

In order to quantify the palladium content in the filtered fraction, all organic substances were removed by evaporation and decomposition at 450 °C followed by the treatment with peroxy-monosulfuric acid. Palladium was subsequently digested by heating the sample with a mixture of concentrated sulfuric acid, concentrated nitric acid and concentrated hydrochloric acid. After diluting the samples to a proper extent, the palladium concentration was determined by ICP-OES (*Agilent 700*) against a freshly prepared series of calibration samples to calculate the calibration curve. The wavelength Pd 340.458 nm was used for the calculation.

Literature

1. Stringfield, V. T.; Rapp, J. R.; Anders, R. B., Effects of karst and geologic structure on the circulation of water and permeability in carbonate aquifers. *Journal of Hydrology* **1979**, *43* (1-4), 313-332.
2. Novack, C. A.; Anovitz, L. M.; Hussey, D. S.; LaManna, J. M.; Labotka, T. C., Experimental Limestone Dissolution and Changes in Multiscale Structure Using Small- and Ultrasmall-Angle Neutron Scattering. *ACS Earth and Space Chemistry* **2022**, *6* (4), 974-986.
3. Gordon, H.; Haygarth, P. M.; Bardgett, R. D., Drying and rewetting effects on soil microbial community composition and nutrient leaching. *Soil Biology and Biochemistry* **2008**, *40* (2), 302-311.
4. Katagi, T., Soil Column Leaching of Pesticides. In *Reviews of Environmental Contamination and Toxicology Volume 221*, Whitacre, D. M., Ed. Springer New York: New York, NY, 2013; pp 1-105.
5. Mohammadi, M.; Salarirad, M. M., Kinetics of Direct Leaching of Natural Alunite in KOH. *Industrial & Engineering Chemistry Research* **2013**, *52* (40), 14359-14365.
6. Momade, F. W. Y.; Momade, Z. G., Reductive leaching of manganese oxide ore in aqueous methanol–sulphuric acid medium. *Hydrometallurgy* **1999**, *51* (1), 103-113.
7. Santos, A.; Yustos, P.; Quintanilla, A.; García-Ochoa, F., Influence of pH on the wet oxidation of phenol with copper catalyst. *Topics in Catalysis* **2005**, *33* (1-4), 181-192.
8. Jana, R. K.; Singh, D. D. N.; Roy, S. K., Hydrochloric Acid Leaching of Sea Nodules with Methanol and Ethanol Addition. *Materials Transactions, JIM* **1993**, *34* (7), 593-598.
9. Mehta, K. D.; Das, C.; Pandey, B. D., Leaching of copper, nickel and cobalt from Indian Ocean manganese nodules by *Aspergillus niger*. *Hydrometallurgy* **2010**, *105* (1-2), 89-95.
10. Jin, Z.; Ren, J.; Rivera, N. A.; Hower, J. C.; Hsu-Kim, H., Functional Predictor Variables for the Leaching Potential of Arsenic and Selenium from Coal Fly Ash. *ACS ES&T Water* **2023**, *3* (4), 1105-1115.
11. Golwala, H.; Saha, B.; Zhang, X.; Bolyard, S. C.; He, Z.; Novak, J. T.; Deng, Y.; Brazil, B.; DeOrio, F. J.; Iskander, S. M., Advancement and Challenges in Municipal Landfill Leachate Treatment—The Path Forward! *ACS ES&T Water* **2022**, *2* (8), 1289-1300.
12. Cappuyns, V.; Alian, V.; Vassilieva, E.; Swennen, R., pH Dependent Leaching Behavior of Zn, Cd, Pb, Cu and As from Mining Wastes and Slags: Kinetics and Mineralogical Control. *Waste and Biomass Valorization* **2014**, *5* (3), 355-368.
13. Maldonado, V. Y.; Schwichtenberg, T.; Schmokel, C.; Witt, S. E.; Field, J. A., Electrochemical Transformations of Perfluoroalkyl Acid (PFAA) Precursors and PFAAs in Landfill Leachates. *ACS ES&T Water* **2022**, *2* (4), 624-634.
14. Shih, K.; Tang, Y., Prolonged toxicity characteristic leaching procedure for nickel and copper aluminates. *Journal of Environmental Monitoring* **2011**, *13* (4), 829-835.

15. Li, L.; Dong, X.; Dong, Y.; Zheng, Y.-M.; Zhu, L.; Liu, J., Thermal Conversion of Hazardous Metal Copper via the Preparation of CuAl₂O₄ Spinel-based Ceramic Membrane for Potential Stabilization of Simulated Copper-Rich Waste. *ACS Sustainable Chemistry & Engineering* **2015**, 3 (11), 2611-2618.
16. Tang, Y.; Lee, P.-H.; Shih, K., Copper Sludge from Printed Circuit Board Production/Recycling for Ceramic Materials: A Quantitative Analysis of Copper Transformation and Immobilization. *Environmental Science & Technology* **2013**, 47 (15), 8609-8615.
17. Tang, Y.; Shih, K., Stabilization Mechanisms and Reaction Sequences for Sintering Simulated Copper-Laden Sludge with Alumina. *ACS Sustainable Chemistry & Engineering* **2013**, 1 (10), 1239-1245.
18. Hii, K. K. M.; Hellgardt, K., Catalysis in Flow: Why Leaching Matters ORGANOMETALLIC FLOW CHEMISTRY. SPRINGER-VERLAG BERLIN: 2016; pp 249-262.
19. Sádaba, I.; López Granados, M.; Riisager, A.; Taarning, E., Deactivation of solid catalysts in liquid media: the case of leaching of active sites in biomass conversion reactions. *Green Chemistry* **2015**, 17 (8), 4133-4145.
20. Besson, M.; Gallezot, P., Deactivation of metal catalysts in liquid phase organic reactions. *Catalysis Today* **2003**, 81 (4), 547-559.
21. Heck, R. F., Palladium-catalyzed reactions of organic halides with olefins. *Accounts of Chemical Research* **1979**, 12 (4), 146-151.
22. Ananikov, V. P.; Beletskaya, I. P., Toward the Ideal Catalyst: From Atomic Centers to a "Cocktail" of Catalysts. *Organometallics* **2012**, 31, 1595-1604.
23. Biffis, A.; Centomo, P.; Del Zotto, A.; Zecca, M., Pd Metal Catalysts for Cross-Couplings and Related Reactions in the 21st Century: A Critical Review. *Chem. Rev.* **2018**, 118, 2249-2295.
24. de Vries, J. G., A unifying mechanism for all high-temperature Heck reactions. The role of palladium colloids and anionic species. *Dalton Transactions* **2006**, (3), 421-429.
25. Köhler, K.; Kleist, W.; Pröckl, S. S., Genesis of Coordinatively Unsaturated Palladium Complexes Dissolved from Solid Precursors during Heck Coupling Reactions and Their Role as Catalytically Active Species. *Inorg. Chem.* **2007**, 46, 1876-1883.
26. Pröckl, S. S.; Kleist, W.; Gruber, M. A.; Köhler, K., In Situ Generation of Highly Active Dissolved Palladium Species from Solid Catalysts - A Concept for the Activation of Aryl Chlorides in the Heck reaction. *Angew. Chem. Int. Ed.* **2004**, 43, 1881-2.
27. Dörfelt, C. Catalysis and Deactivation Mechanisms of Copper Aluminate Spinel Hydrogenation Catalysts. Technical University Munich, 2017.
28. Bosi, F.; Biagioni, C.; Pasero, M., Nomenclature and classification of the spinel supergroup. *European Journal of Mineralogy* **2019**, 31 (1), 183-192.

29. Zhao, Q.; Yan, Z.; Chen, C.; Chen, J., Spinel: Controlled Preparation, Oxygen Reduction/Evolution Reaction Application, and Beyond. *Chemical Reviews* **2017**, *117* (15), 10121-10211.
30. Baidya, T.; Murayama, T.; Nellaiappan, S.; Katiyar, N. K.; Bera, P.; Safonova, O.; Lin, M.; Priolkar, K. R.; Kundu, S.; Srinivasa Rao, B.; Steiger, P.; Sharma, S.; Biswas, K.; Pradhan, S. K.; Lingaiah, N.; Malviya, K. D.; Haruta, M., Ultra-Low-Temperature CO Oxidation Activity of Octahedral Site Cobalt Species in Co₃O₄ Based Catalysts: Unravelling the Origin of the Unique Catalytic Property. *The Journal of Physical Chemistry C* **2019**, *123* (32), 19557-19571.
31. Dörfelt, C.; Hammerton, M.; Martin, D.; Wellmann, A.; Aletsee, C. C.; Tromp, M.; Köhler, K., Manganese containing copper aluminate catalysts: Genesis of structures and active sites for hydrogenation of aldehydes. *Journal of Catalysis* **2021**, *395*, 80-90.
32. Simon, C.; Zakaria, M. B.; Kurz, H.; Tetzlaff, D.; Blösser, A.; Weiss, M.; Timm, J.; Weber, B.; Apfel, U.-P.; Marschall, R., Magnetic NiFe₂O₄ Nanoparticles Prepared via Non-Aqueous Microwave-Assisted Synthesis for Application in Electrocatalytic Water Oxidation. *Chemistry – A European Journal* **2021**, *27* (68), 16990-17001.
33. Liu, Y.; Qing, S.; Hou, X.; Qin, F.; Wang, X.; Gao, Z.; Xiang, H., Temperature dependence of Cu–Al spinel formation and its catalytic performance in methanol steam reforming. *Catalysis Science & Technology* **2017**, *7* (21), 5069-5078.
34. Pekov, I. V.; Sandalov, F. D.; Koshlyakova, N. N.; Vigasina, M. F.; Polekhovskiy, Y. S.; Britvin, S. N.; Sidorov, E. G.; Turchkova, A. G., Copper in Natural Oxide Spinel: The New Mineral Thermaerogenite CuAl₂O₄, Cuprospinel and Cu-Enriched Varieties of Other Spinel-Group Members from Fumaroles of the Tolbachik Volcano, Kamchatka, Russia. *Minerals* **2018**, *8* (11).
35. Hu, C.-Y.; Shih, K.; Leckie, J. O., Formation of copper aluminate spinel and cuprous aluminate delafossite to thermally stabilize simulated copper-laden sludge. *Journal of Hazardous Materials* **2010**, *181* (1-3), 399-404.
36. Janmanchi, K.; Coppernoll, A.; Katsoulis, D., Two-Step Process for the Synthesis of Dimethyldichlorosilane Using Copper Aluminate Catalysts. *Industrial & Engineering Chemistry Research* **2020**, *59* (8), 3321-3333.
37. Mindru, I.; Gingasu, D.; Patron, L.; Marinescu, G.; Calderon-Moreno, J. M.; Preda, S.; Oprea, O.; Nita, S., Copper aluminate spinel by soft chemical routes. *Ceramics International* **2016**, *42* (1), 154-164.
38. Wang, Z.; Liang, K.; Chan, S.-W.; Tang, Y., Fabrication of nano CuAl₂O₄ spinel for copper stabilization and antibacterial application. *Journal of Hazardous Materials* **2019**, *371*, 550-557.

-
39. Bialas, A.; Niebrzydowska, P.; Dudek, B.; Piwowarska, Z.; Chmielarz, L.; Michalik, M.; Kozak, M.; Kuśtrowski, P., Coprecipitated Co–Al and Cu–Al oxide catalysts for toluene total oxidation. *Catalysis Today* **2011**, *176* (1), 413-416.
40. Tang, Y.; Chui, S. S.-Y.; Shih, K.; Zhang, L., Copper Stabilization via Spinel Formation during the Sintering of Simulated Copper-Laden Sludge with Aluminum-Rich Ceramic Precursors. *Environmental Science & Technology* **2011**, *45* (8), 3598-3604.
41. Guarneros Aguilar, C.; Estrada Moreno, C.; Pacio Castillo, M.; Caballero-Briones, F., Effect of calcination temperature on structure and thermoelectric properties of CuAlO₂ powders. *Journal of Materials Science* **2018**, *53* (3), 1646-1657.
42. Raff, D. K., Butanals. In *Ullmann's Encyclopedia of Industrial Chemistry*, 2013.
43. Tang, Y.; Shih, K.; Chan, K., Copper aluminate spinel in the stabilization and detoxification of simulated copper-laden sludge. *Chemosphere* **2010**, *80* (4), 375-380.
44. Xi, H.; Hou, X.; Liu, Y.; Qing, S.; Gao, Z., Cu–Al Spinel Oxide as an Efficient Catalyst for Methanol Steam Reforming. *Angewandte Chemie International Edition* **2014**, *53* (44), 11886-11889.
45. Batista, A. H. d. M.; Ramos, F. S. O.; Braga, T. P.; Lima, C. L.; de Sousa, F. F.; Barros, E. B. D.; Filho, J. M.; Oliveira, A. S. d.; Sousa, J. R. d.; Valentini, A.; Oliveira, A. C., Mesoporous MAI₂O₄ (M=Cu, Ni, Fe or Mg) spinels: Characterisation and application in the catalytic dehydrogenation of ethylbenzene in the presence of CO₂. *Applied Catalysis A: General* **2010**, *382* (2), 148-157.
46. Luo, M.-F.; Fang, P.; He, M.; Xie, Y.-L., In situ XRD, Raman, and TPR studies of CuO/Al₂O₃ catalysts for CO oxidation. *Journal of Molecular Catalysis A: Chemical* **2005**, *239* (1-2), 243-248.
47. Hiller, M. J. Synthesis, Characterization and Catalytic Performance of Copper-Based Catalysts in the Butyraldehyde Hydrogenation. Technical University Munich, 2023.
48. Plyasova, L. M.; Yur'eva, T. M.; Molina, I. Y.; Kriger, T. A.; Balagurov, A. M.; Davydova, L. P.; Zaikovskii, V. I.; Kustova, G. N.; Malakhov, V. V.; Dovlitova, L. S., Dynamics of structural transformations in the reduction of copper aluminate. *Kinetics and Catalysis* **2000**, *41* (3), 429-436.
49. Zhang, L.; Zhou, M.; Wang, A.; Zhang, T., Selective Hydrogenation over Supported Metal Catalysts: From Nanoparticles to Single Atoms. *Chemical Reviews* **2020**, *120* (2), 683-733.
50. Lan, X.; Wang, T., Highly Selective Catalysts for the Hydrogenation of Unsaturated Aldehydes: A Review. *ACS Catalysis* **2020**, *10* (4), 2764-2790.
51. Mäki-Arvela, P.; Hájek, J.; Salmi, T.; Murzin, D. Y., Chemoselective hydrogenation of carbonyl compounds over heterogeneous catalysts. *Applied Catalysis A: General* **2005**, *292*, 1-49.

-
52. Thakur, D. S.; Kundu, A., Catalysts for Fatty Alcohol Production from Renewable Resources. *Journal of the American Oil Chemists' Society* **2016**, *93* (12), 1575-1593.
53. Kochloefl, K.; Maletz, G.; Hausinger, G.; Schneider, M., Acid Resistant Copper Chromium Oxide Catalysts Used in the Hydrogenolysis of Fatty Acids. In *New Frontiers in Catalysis - Proceedings of the 10th International Congress on Catalysis, Budapest, 19-24 July 1992*, Guczi, L.; Solymosi, F.; TÉTÉNYI, P., Eds. Elsevier: 1993; Vol. 75, pp 2559-2563.
54. Zhang, Z.; Zhou, F.; Chen, K.; Fu, J.; Lu, X.; Ouyang, P., Catalytic In Situ Hydrogenation of Fatty Acids into Fatty Alcohols over Cu-Based Catalysts with Methanol in Hydrothermal Media. *Energy & Fuels* **2017**, *31* (11), 12624-12632.
55. Rao, R.; Dandekar, A.; Baker, R. T. K.; Vannice, M. A., Properties of Copper Chromite Catalysts in Hydrogenation Reactions. *Journal of Catalysis* **1997**, *171* (2), 406-419.
56. Adkins, H.; Connor, R., THE CATALYTIC HYDROGENATION OF ORGANIC COMPOUNDS OVER COPPER CHROMITE. *Journal of the American Chemical Society* **1931**, *53* (3), 1091-1095.
57. *Commission Regulation (EU) No 301/2014*; European Commission: March 25 2014, 2014.
58. Kaitwade, N. Butyraldehyde Market Overview (2022-2032). <https://www.futuremarketinsights.com/reports/butyraldehyde-market> (accessed 17.07.2023).
59. Hahn, H.-D.; Dämbkes, G.; Rupprich, N.; Bahl, H.; Frey, G. D., Butanols. In *Ullmann's Encyclopedia of Industrial Chemistry*, 2013.
60. Ahmed, A. I.; Samra, S. E.; El-Hakam, S. A., Structural and surface aspects of thermally treated copper aluminium mixed hydroxides. *Canadian Journal of Chemistry* **1991**, *69* (10), 1511-1515.
61. Gates-Rector, S.; Blanton, T., The Powder Diffraction File: a quality materials characterization database. *Powder Diffraction* **2019**, *34* (4), 352-360.
62. Vink, B. W., Stability relations of malachite and azurite. *Mineralogical Magazine* **1986**, *50* (355), 41-47.
63. Du, X.; Wang, Y.; Su, X.; Li, J., Influences of pH value on the microstructure and phase transformation of aluminum hydroxide. *Powder Technology* **2009**, *192* (1), 40-46.
64. Bouchard, M.; Smith, D. C., Catalogue of 45 reference Raman spectra of minerals concerning research in art history or archaeology, especially on corroded metals and coloured glass. *Spectrochimica Acta Part A: Molecular and Biomolecular Spectroscopy* **2003**, *59* (10), 2247-2266.
65. Frost, R. L.; Martens, W. N.; Rintoul, L.; Mahmutagic, E.; Kloprogge, J. T., Raman spectroscopic study of azurite and malachite at 298 and 77 K. *Journal of Raman Spectroscopy* **2002**, *33* (4), 252-259.

66. Buzgar, N.; Apopei, A. I., The Raman study of certain carbonates. *Geologie Tomul L* **2009**, 2 (2), 97-112.
67. Gao, J.; Yuan, X., Vibrational Investigation of Pressure-Induced Phase Transitions of Hydroxycarbonate Malachite $\text{Cu}_2(\text{CO}_3)(\text{OH})_2$. *Minerals* **2020**, 10 (3).
68. Lafuente, B.; Downs, R. T.; Yang, H.; Stone, N., The power of databases: The RRUFF project
In *Highlights in Mineralogical Crystallography*, Armbruster, T.; Danisi, R. M., Eds. De Gruyter (O): Berlin, Germany, 2015; pp 1-30.
69. D'Ippolito, V.; Andreozzi, G. B.; Bersani, D.; Lottici, P. P., Raman fingerprint of chromate, aluminate and ferrite spinels. *Journal of Raman Spectroscopy* **2015**, 46 (12), 1255-1264.
70. Debbichi, L.; Marco de Lucas, M. C.; Pierson, J. F.; Krüger, P., Vibrational Properties of CuO and Cu_4O_3 from First-Principles Calculations, and Raman and Infrared Spectroscopy. *The Journal of Physical Chemistry C* **2012**, 116 (18), 10232-10237.
71. Aromaa, J.; Kekkonen, M.; Mousapour, M.; Jokilaakso, A.; Lundström, M. The Oxidation of Copper in Air at Temperatures up to 100 °C *Corrosion and Materials Degradation* [Online], 2021, p. 625-640.
72. Hiller, M.; Köhler, K., Copper-Zinc Oxide Catalysts for Aldehyde Hydrogenation by Direct Reductive Activation of Precursors. *Chemie Ingenieur Technik* **2022**, 94 (11), 1720-1726.
73. Gnad, C.; Abram, A.; Urstöger, A.; Weigl, F.; Schuster, M.; Köhler, K., Leaching Mechanism of Different Palladium Surface Species in Heck Reactions of Aryl Bromides and Chlorides. *ACS Catalysis* **2020**, 10 (11), 6030-6041.
74. Wussow, K.; Abram, A.; Köhler, K.; Chang, C.-R.; Genest, A.; Li, J.; Rösch, N., Leaching of palladium atoms from small cluster models during Heck reactions – An experimental and theoretical study. *Catalysis Communications* **2022**, 165, 106441.
75. Miyaura, N.; Suzuki, A., Palladium-Catalyzed Cross-Coupling Reactions of Organoboron Compounds. *Chemical Reviews* **1995**, 95 (7), 2457-2483.
76. Molnár, A., Efficient, Selective, and Recyclable Palladium Catalysts in Carbon-Carbon Coupling Reactions. *Chem. Rev.* **2011**, 111, 2251-320.
77. Molnár, Á., *Palladium-Catalyzed Coupling Reactions*. Wiley-VHC: Weinheim, 2013.
78. Lamblin, M.; Nassar-Hardy, L.; Hierso, J.-C.; Fouquet, E.; Felpin, F.-X., Recyclable Heterogeneous Palladium Catalysts in Pure Water: Sustainable Developments in Suzuki, Heck, Sonogashira and Tsuji Trost Reactions. *Adv. Synth.Catal.* **2010**, 352, 33-79.
79. Pagliaro, M.; Pandarus, V.; Ciriminna, R.; Béland, F.; Demma Carà, P., Heterogeneous versus Homogeneous Palladium Catalysts for Cross-Coupling Reactions. *ChemCatChem* **2012**, 4, 432-445.

-
80. Polshettiwar, V.; Len, C.; Fihri, A., Silica-Supported Palladium: Sustainable Catalysts for Cross-Coupling Reactions. *Coord. Chem. Rev.* **2009**, *253*, 2599-2626.
81. Wu, X. F.; Anbarasan, P.; Neumann, H.; Beller, M., From Noble Metal to Nobel Prize: Palladium-Catalyzed Coupling Reactions as Key Methods in Organic Synthesis. *Angew. Chem. Int. Ed.* **2010**, *49*, 9047-50.
82. Ziegler, C. B.; Heck, R. F., Palladium-Catalyzed Vinylic Substitution with Highly Activated Aryl Halides. *J. Org. Chem.* **1978**, *43*, 2941-2946.
83. Phan, N. T. S.; Van Der Sluys, M.; Jones, C. W., On the Nature of the Active Species in Palladium Catalyzed Mizoroki–Heck and Suzuki–Miyaura Couplings – Homogeneous or Heterogeneous Catalysis, A Critical Review. *Adv. Synth. Catal.* **2006**, *348*, 609-679.
84. Schmidt, A. F.; Mametova, L. V., Main features of catalysis in the styrene phenylation reaction. *Kinetics and Catalysis* **1996**, 406-408.
85. Zhao, F.; Bhanage, B. M.; Shirai, M.; Arai, M., Heck Reactions of Iodobenzene and Methyl Acrylate with Conventional Supported Palladium Catalysts in the Presence of Organic and/or Inorganic Bases without Ligands. *Chem. Eur. J.* **2000**, *6*, 843-848.
86. Biffis, A.; Zecca, M.; Basato, M., Palladium metal catalysts in Heck C - C coupling reactions. *Journal of Molecular Catalysis A: Chemical* **2001**, *173* (1), 249-274.
87. Köhler, K.; Heidenreich, R. G.; Krauter, J. G. E.; Pietsch, J., Highly Active Palladium/Activated Carbon Catalysts for Heck Reactions: Correlation of Activity, Catalyst Properties, and Pd Leaching. *Chem. Eur. J.* **2002**, *8*, 622-631.
88. Kleist, W.; Lee, J.-K.; Köhler, K., Pd/MOx Materials Synthesized by Sol-Gel Coprecipitation as Catalysts for Carbon-Carbon Coupling Reactions of Aryl Bromides and Chlorides. *Eur. J. Inorg. Chem.* **2009**, *2009*, 261-266.
89. Pröckl, S. S.; Kleist, W.; Köhler, K., Design of Highly Active Heterogeneous Palladium Catalysts for the Activation of Aryl Chlorides in Heck Reactions. *Tetrahedron* **2005**, *61*, 9855-9859.
90. Zhao, F.; Murakami, K.; Shirai, M.; Arai, M., Recyclable Homogeneous/Heterogeneous Catalytic Systems for Heck Reaction through Reversible Transfer of Palladium Species between Solvent and Support. *J. Catal.* **2000**, *194*, 479-483.
91. Zhao, F.; Shirai, M.; Arai, M., Palladium-Catalyzed Homogeneous and Heterogeneous Heck Reactions in NMP and Water Mixed Solvents Using Organic, Inorganic and Mixed Bases. *J. Mol. Cat. A* **2000**, *154*, 39-44.
92. Eremin, D. B.; Ananikov, V. P., Understanding active species in catalytic transformations: From molecular catalysis to nanoparticles, leaching, "Cocktails" of catalysts and dynamic systems. *Coordination Chemistry Reviews* **2017**, *346*, 2-19.
93. Van Vaerenbergh, B.; Lauwaert, J.; Thybaut, J. W.; Vermeir, P.; De Clercq, J., Pd nanoparticle and molecular Pd²⁺ leaching pathways for a strongly acid versus strongly basic

resin supported Pd nanoparticle catalyst in Suzuki coupling. *Chemical Engineering Journal* **2019**, *374*, 576-588.

94. Alfonso Albiñana, P., A new efficient, highly dispersed, Pd nanoparticulate silica supported catalyst synthesized from an organometallic precursor. Study of the homogeneous vs. heterogeneous activity in the Suzuki-Miyaura reaction. *Journal of catalysis* **2018**, *v. 367*, pp. 283-295-2018 v.367.

95. Barreiro, E. M.; Hao, Z.; Adrio, L. A.; van Ommen, J. R.; Hellgardt, K.; Hii, K. K., Spatial, temporal and quantitative assessment of catalyst leaching in continuous flow. *Catalysis Today* **2018**, *308*, 64-70.

96. Reimann, S.; Stötzel, J.; Frahm, R.; Kleist, W.; Grunwaldt, J.-D.; Baiker, A., Identification of the Active Species Generated from Supported Pd Catalysts in Heck Reactions: An in situ Quick Scanning EXAFS Investigation. *Journal of the American Chemical Society* **2011**, *133* (11), 3921-3930.

97. Smirnov, V.; Pröckl, S.; Schmidt, A.; Köhler, K., In situ NMR studies of the mechanism of homogeneously and heterogeneously catalysed Heck reactions of aryl chlorides and bromides. *ARKIVOC* **2011**, *2011*, 225-241.

98. Gaikwad, A. V.; Holuigue, A.; Thathagar, M. B.; ten Elshof, J. E.; Rothenberg, G., Ion- and Atom-Leaching Mechanisms from Palladium Nanoparticles in Cross-Coupling Reactions. *Chemistry – A European Journal* **2007**, *13* (24), 6908-6913.

99. Polynski, M. V.; Ananikov, V. P., Modeling Key Pathways Proposed for the Formation and Evolution of “Cocktail”-Type Systems in Pd-Catalyzed Reactions Involving ArX Reagents. *ACS Catalysis* **2019**, *9* (5), 3991-4005.

100. Ramezani-Dakhel, H.; Mirau, P. A.; Naik, R. R.; Knecht, M. R.; Heinz, H., Stability, surface features, and atom leaching of palladium nanoparticles: toward prediction of catalytic functionality. *Physical Chemistry Chemical Physics* **2013**, *15* (15), 5488-5492.

101. Proutiere, F.; Schoenebeck, F., Solvent Effect on Palladium-Catalyzed Cross-Coupling Reactions and Implications on the Active Catalytic Species. *Angewandte Chemie International Edition* **2011**, *50* (35), 8192-8195.

102. Chang, C.-R.; Zhao, Z.-J.; Köhler, K.; Genest, A.; Li, J.; Rösch, N., Theoretical study on the leaching of palladium in a CO atmosphere. *Catalysis Science & Technology* **2012**, *2* (11), 2238-2248.

103. Xue, L.; Lin, Z., Theoretical aspects of palladium-catalysed carbon–carbon cross-coupling reactions. *Chemical Society Reviews* **2010**, *39* (5), 1692-1705.

104. Chen, L.; Rangan, S.; Li, J.; Jiang, H.; Li, Y., A Molecular Pd(II) Complex Incorporated Into a MOF as a Highly Active Single-site Heterogeneous Catalyst for C–Cl Bond Activation. *Green Chem.* **2014**, *16*.

-
105. Ghorbani-Choghamarani, A.; Rabiei, H.; Arghand, F., Pd- Dithizone Grafted onto Magnetic Nanoparticles and Study of its Catalytic Activity in C-C and C-N Coupling Reactions. *Appl. Organomet. Chem.* **2017**, *31*.
106. Alper, H.; Arya, P.; Bourque, C.; Jefferson, R. G.; Manzer, L. E., Heck Reaction Using Palladium Complexed To Dendrimers on Silica. *Can. J. Chem.* **2000**, *78*, 920-924.
107. González-Arellano, C.; Corma, A.; Iglesias, M.; Sánchez, F., Pd(II)-Schiff Base Complexes Heterogenised on MCM-41 and Delaminated Zeolites as Efficient and Recyclable Catalysts for the Heck Reaction. *Adv. Synth. Catal.* **2004**, *346*, 1758-1764.
108. Phan, N. T. S.; Brown, D. H.; Adams, H.; Spey, S. E.; Styring, P., Solid-Supported Cross-Coupling Catalysts Derived from Homogeneous Nickel and Palladium Coordination Complexes. *Dalton Trans.* **2004**, 1348-1357.
109. Venkatesan, C.; Singh, A., Synthesis and Characterization of Carbometallated Palladacycles over 3-Hydroxypropyltriethoxysilyl-Functionalized MCM-41. *J. Catal.* **2004**, *227*, 148-163.
110. Gnad, C.; Dachwald, O.; Raudaschl-Sieber, G.; Köhler, K., Synthesis of Methyl Palladium Complexes on Silica as Single Site Catalysts Activating C-Cl Bonds in Heck Reactions. *J. Catal.* **2019**, *375*, 257-266.
111. Pearlman, W. M., Noble Metal Hydroxides On Carbon Nonpyrophoric Dry Catalysts. *Tetrahedron Lett.* **1967**, *17*, 1663-1664.
112. Gnad, C. Molecular Palladium Catalysts Supported on Functionalized Oxide Surfaces. Technical University Munich, Munich, 2019.
113. Basset, J.-M.; Psaro, R.; Roberto, D.; Ugo, R., *Modern Surface Organometallic Chemistry*. Wiley-VHC: Weinheim, 2009.
114. Copéret, C.; Chabanas, M.; Saint-Arroman, R. P.; Basset, J.-M., Homogeneous and Heterogeneous Catalysis: Bridging the Gap through Surface Organometallic Chemistry. *Angew. Chem. Int. Ed.* **2003**, *42*, 156-181.
115. Copéret, C.; Comas-Vives, A.; Conley, M. P.; Estes, D. P.; Fedorov, A.; Mougél, V.; Nagae, H.; Nunez-Zarur, F.; Zhizhko, P. A., Surface Organometallic and Coordination Chemistry toward Single-Site Heterogeneous Catalysts: Strategies, Methods, Structures, and Activities. *Chem. Rev.* **2016**, *116*, 323-421.
116. Jeffery, T., Palladium-catalysed vinylation of organic halides under solid-liquid phase transfer conditions. *Journal of the Chemical Society, Chemical Communications* **1984**, (19), 1287-1289.
117. Wussow, K. Palladium Catalysed Heck Reactions and Photoassisted Catalytic Reduction of Nitrogen Oxide by Silver: The Role of Supported Metal Particles, Small Clusters and Molecular Complexes. Technical University Munich, Munich, 2014.

Appendix

7.1 Additional data

Table S1: Overview of the nomenclature used to describe the batch composition of the individual leaching experiments

Spinel type (350 mg)	CuO-Sp CuO · CuAl ₂ O ₄ (Adkins analog)	S-Sp (CuO) · CuAl ₂ O ₄ (Stoichiometric spinel)	P-Sp CuAl ₂ O ₄ (Phase-pure spinel)	
Solvent pure (100 mL)	H (Hexane)	T (Toluene)	D (1,4-Dioxane)	E (Ethanol)
Solvent mixture (100 mL hexane and 10 mL additive)		t (10 mL Toluene)	d (10 mL 1,4-Dioxane)	e (10 mL Ethanol)
Carboxylic acid (8 mol-%)	C3 (Propanoic acid)	C5 (Pentanoic acid)	C7 (Heptanoic acid)	C8 (Octanoic acid)
Others	24h (Sampling after > 24 h reaction time)	T-Series (Sampling during heating phase)	60min (First sample after 60 min reaction time)	

Example: AH-P (S-Sp, e, C3, 24h)

Sample Name: AH-P; batch composition: stoichiometric spinel used as catalyst, solvent mixture of 100 mL hexane and mL ethanol, additive of 8 mol-% propanoic acid and additional samples after 24h of reaction time.

Table S2: Overview of all experiments discussed in the text. The table is subdivided by figure to facilitate the location within the text.

Figure	Catalyst abbreviation	Description
Figure 3	AAB-44	P-Sp, H
Figure 5	AAB-33	P-Sp, H, test without butanal), T-Series
	AAB-61	P-Sp, H, pressurized with Ar), T-Series
	AAB-19	P-Sp, H, T-Series
	AAB-37	P-Sp, H, C8, T-Series
Figure 6	AAB-54	CuO-Sp, H
	AAB-V	S-Sp, H
	AAB-44	P-Sp, H

Appendix

Figure	Catalyst abbreviation	Description
Figure 7	AAB-57	CuO-Sp, H, C7
	AH-I	S-Sp, H, C7
	AH-G	P-Sp, H, C7
Figure 8	AH-V	S-Sp, H
	AH-N	S-Sp, H, C3, 24h
	AH-D	S-Sp, H, C5
	AH-I	S-Sp, H, C7
Figure 9	AAB-44	P-Sp, H
	AH-M	P-Sp, H, C3
	AH-C	P-Sp, H, C5
	AH-G	P-Sp, H, C7
Figure 10	MJA-4	S-Sp, T
	MJA-6	S-Sp, T, C5
Figure 11	MJA-3	P-Sp, T
	MJA-9	P-Sp, T, C5
Figure 12	AAB-60	S-Sp, D, C5
	AAB-63	P-Sp, D, C5
Figure 13	AAB-42	S-Sp, E
	AH-H	S-Sp, E, C5
	AAB-68	S-Sp, E, C7
Figure 14	AAB-68	S-Sp, E, C7
Figure 15	AAB-27	P-Sp, E
	AAB-64	P-Sp, E, C3
	AH-F	P-Sp, E, C5
	AAB-65	P-Sp, E, C7
Figure 16	AH-H	S-Sp, E, C5
	AH-F	P-Sp, E, C5
Figure 18	MJA-1	S-Sp, t
	MJA-5	S-Sp, t, C5
Figure 19	MJA-2	P-Sp, t
	MJA-10	P-Sp, t, C5
Figure 20	AAB-58	S-Sp, d
	AAB-59	S-Sp, d, C5
Figure 21	MJA-7	P-Sp, d
	AAB-67	P-Sp, d, C3
	MJA-8	P-Sp, d, C5

Appendix

Figure	Catalyst abbreviation	Description
Figure 22	AAB-41	S-Sp, e
	AH-P	S-Sp, e, C3, 24h
	AAB-52	S-Sp, e, C5, 24h
	AH-S	S-Sp, e, C7
Figure 23	AH-P	S-Sp, e, C3, 24h
	AH-K	P-Sp, e, C3
Figure 24	AAB-23	P-Sp, e
	AH-K	P-Sp, e, C3
	AH-E	P-Sp, e, C5
	AH-L	P-Sp, e, C7
Figure 26	AH-V	S-Sp, H
	AH-N	S-Sp, H, C3, 24h
	AAB-46	S-Sp, H, C5, 24h
	AH-W	S-Sp, H, C7, 24h
Figure 27	AAB-44	P-Sp, H
	AH-X	P-Sp, H, C3, 24h
	AH-U	P-Sp, H, C5, 24h
	AH-T	P-Sp, H, C7, 24h
Figure 28	AAB-41	S-Sp, e
	AH-P	S-Sp, e, C3, 24h
	AAB-52	S-Sp, e, C5, 24h
	AH-Y	S-Sp, e, C7, 24h
Figure 29	AH-P	S-Sp, e, C3, 24h
	AH-O	P-Sp, e, C3, 24h
Figure 30	AAB-23	P-Sp, e
	AH-O	P-Sp, e, C3, 24h
	AAB-50	P-Sp, e, C5, 24h
	AH-Z	P-Sp, e, C7, 24h

7.2 List of Publications

- Leaching Mechanism of Different Palladium Surface Species in Heck Reactions of Aryl Bromides and Chlorides
Christoph Gnad, Andrea Abram, Alexander Urstöger, Florian Weigl, Michael Schuster, Klaus Köhler, ACS Catalysis (2020), 10 (11), 6030–6041.
<https://dx.doi.org/10.1021/acscatal.0c01166>
- Walter Reppe Revival – Identification and Genesis of Copper Acetylides Cu_2C_2 as Active Species in Ethynylation Reactions
Tobias Bruhm, Andrea Abram, Johannes Häusler, Oliver Thomys, Klaus Köhler, Chemistry – A European Journal (2021), 27, 16834-16839.
<https://doi.org/10.1002/chem.202101932>
- Leaching of palladium atoms from small cluster models during Heck reactions – An experimental and theoretical study
Katharina Wussow; Andrea Abram, Klaus Köhler, Chun-Ran Chang, Alexander Genest, Jun Li, Notker Rösch, Catalysis Communications (2022), 165, 106441.
<https://doi.org/10.1016/j.catcom.2022.106441>
- Leaching of Catalyst Components from Cu-Al-spinel during Hydrogenation reactions
Andrea Abram, Christoph Dörfelt, Michelle Hammerton, Moniek Tromp, Klaus Köhler
In preparation

7.3 Conference contributions

- Walter Reppe Revival – the formation of the active species in the ethynylation of formaldehyde to form 1,4-butyne-1,3-diol
Tobias Bruhm, Oliver Thomys, Andrea Abram, Klaus Köhler
52. Jahrestreffen Deutscher Katalytiker, Weimar, Germany, 13 – 15 March 2019
Poster contribution
- Leaching of Catalyst Components from Cu-Al-spinel during Hydrogenation
Andrea Abram, Christoph Dörfelt, Michelle Hammerton, Moniek Tromp, Klaus Köhler
53. Jahrestreffen Deutscher Katalytiker, Weimar, Germany, 11 – 13 March 2020
Accepted poster contribution, cancelled due to Covid
- Leaching of Catalyst Components from Cu-Al-spinel during Hydrogenation
Andrea Abram, Christoph Dörfelt, Michelle Hammerton, Moniek Tromp, Klaus Köhler
17. International Congress on Catalysis, San Diego, California, USA, 14 – 19 June 2020
Accepted poster contribution, cancelled due to Covid
- Leaching of Catalyst Components from Cu-Al-spinel during Hydrogenation in the Presence of Carboxylic Acids
Andrea Abram, Christoph Dörfelt, Michelle Hammerton, Moniek Tromp, Klaus Köhler
54. Jahrestreffen Deutscher Katalytiker, Weimar, Germany, 16 – 19 March 2021
Poster contribution, Short presentation in Poster Show 2: Catalysis goes liquid!